Tailoring the properties of spray deposited SnO_2 and ZnO thin films for energy applications

Thesis submitted to

Cochin University of Science and Technology

in partial fulfilment of the requirements

for the award of the degree of

Doctor of Philosophy

Under the Faculty of Science

Deepu D.R.

Thin Film Photovoltaic Division
Department of Physics
Cochin University of Science and Technology
Cochin-22

April 2016

Tailoring the properties of spray deposited SnO_2 and ZnO thin films for energy applications

Ph.D thesis in the field of Thin Film Photovoltaics

Author

Deepu D. R.

Thin Film Photovoltaic Division
Department of Physics
Cochin University of Science and Technology
Cochin – 682 022, Kerala, India
email: deepudamodhar@gmail.com

Supervising Guide

Dr. C. Sudha Kartha
Professor (Retd.) & KSCSTE Emeritus Scientist
Department of Physics
Cochin University of Science and Technology
Cochin – 682 022, India
email: csk@cusat.ac.in

April 2016

Department of Physics
Cochin University of Science and Technology
Cochin – 682 022

Dr. C. Sudha Kartha
Professor (Retd.) & KSCSTE Emeritus Scientist

Certificate

Certified that the thesis entitled **"Tailoring the properties of spray deposited SnO_2 and ZnO thin films for energy applications"** submitted by **Mr. Deepu D. R.** is an authentic record of research work carried out by him under my supervision at the Department of Physics in partial fulfilment of the requirements for the award of degree of Doctor of Philosophy of Cochin University of Science and Technology and the work embodied in this thesis has not been included in any other thesis submitted for the award of any other degree. All the relevant corrections and modifications suggested by the audience during the pre-synopsis seminar and recommendations by doctoral committee of the candidate have been incorporated in the thesis.

Cochin - 22
Date:

Dr. C. Sudha Kartha
Supervising Guide

Phone: +91 4842577404. **Email:** csk@cusat.ac.in

Declaration

I hereby declare that the thesis entitled *"***Tailoring the properties of spray deposited SnO_2 and ZnO thin films for energy applications***"* submitted for the award of degree of Doctor of Philosophy of Cochin University of Science and Technology is based on the original work done by me under the guidance of **Dr. C. Sudha Kartha**, Professor (Retd.) & KSCSTE Emeritus Scientist, Department of Physics, Cochin University of Science and Technology, Cochin - 682 022 and this work has not been included in any other thesis submitted for the award of any other degree.

Cochin – 22 **Deepu D.R.**
Date:

Acknowledgement

I would like to express my heartfelt thanks to my guide Dr. C. Sudha Kartha for her valuable guidance and inspiration given throughout my research work. Without her expert advice and help, my work would not have been completed. I also express my sincere gratitude to Dr. K.P. Vijayakumar for his supervision, scientific and technical advice and moral support.

I am thankful to Prof. S. Jayalekshmi, Head, Department of Physics and to all former heads of Physics department for providing the necessary facilities. I am grateful to all the faculty members and office staff of department of Physics and university officials for their helping hands whenever needed.

I am indebted to Dr. Y. Kashiwaba (Iwate university, Japan), Dr. S. Shaji (UANL, Mexico), Dr. K.B. Jinesh (IIST, TVM), Dr. Prabhakar Rao (NIST, TVM) Dr. K. Sreekumar (Dept. of Applied Chemistry, CUSAT) and Dr. K. Rajeev Kumar (Dept. of Instrumentation, CUSAT) for their unconditional support.

The financial assistance from Cochin University of Science and Technology, M/s. Corus group, The Netherlands, and UGC, India is greatly acknowledged.

A big thanks to my family and friends, I couldn't have done it without you.

Deepu D. R.

Contents

Preface

Today's world is more concerned about the energy production, consumption and conservation due to the unstable petroleum prices, global warming etc. The world demands reliable and affordable green renewable energy sources and energy conservation techniques. In this scenario, tackling solar energy has gained more attention and solar photovoltaic has emerged as an inevitable candidate for clean and renewable energy technology. Photovoltaics are pollution free, reliable, quiet, virtually maintenance free and durable at moderate cost. But till date, solar electricity is out of common man's reach due to the high cost of solar cells. Next generation commercial photovoltaic devices will be thin film based. To make it affordable, costly ITO substrates have to be substituted either by another economical TCO material or by a metal substrate. Energy saving is equally important as energy production in the present scenario. TCO materials are generally used in solid state lighting devices, low emissivity windows etc. which in turn reduce the energy consumption.

This thesis is devoted to the development of economical and environment-friendly transparent conducting oxide materials (TCO) for different energy applications. The work mainly focused on tailoring the properties of wide band gap oxide thin films namely SnO_2 and ZnO. Tailored SnO_2 can be used as a low cost alternative to ITO thin films in energy applications, especially in solar cells. The developed ZnO based p-type TCO thin film can be ideal for transparent electronics. Other than TCO applications, this work explored the possibility of creating sub-band levels in ZnO films for the plausible all layer ZnO based solar cells. ZnO-based ion diffusion barrier layer over steel substrate was also studied to use in flexible solar cells.

Chapter 1 begins with an introduction to present trends and future prospects of transparent conducting oxides in thin film solar cells and other energy conserving device applications for the sustainable development of humanity. The basic requirements of TCOs were elaborated in terms of material properties followed by short review of SnO_2 and p type ZnO. The motivation behind the work is also included in this chapter.

Chapter 2 explains the preparation and characterization of undoped SnO_2 thin films by chemical spray pyrolysis (CSP) by systematically varying the deposition conditions. The effect of three different parameters namely substrate temperature, precursor concentration and spray rate is discussed in detail. SnO_2 films were prepared by varying substrate temperature from 375^0C to 500^0C and 425^0C was selected for further studies after measuring sheet resistance and transmission spectra. Precursor concentration was varied from 0.1M to 0.3M and better quality films were obtained with 0.2M solution. To study the effect of spray rate on the properties of sprayed tin oxide thin films, films were deposited by varying spray rate from 3ml/min to 9ml/min and the films prepared at 9ml/min were turned out to be more conducting. XPS analysis of the films revealed the change in composition and a reduction in detrimental oxygen components in the films with spray rate.

Chapter 3 discusses the effect of fluorine dopant sources and concentrations in SnO_2 films by CSP. Exact doping concentrations are not included to protect patent data. Fluorine (F) doped SnO_2 films were prepared by incorporating different concentrations of NH_4F and HF as F source in the precursor solution and found that NH_4F is the best dopant source. FTO films with transmittance between 77 – 95% in the visible region and resistivity of 2.48×10^{-4} Ω.cm were successfully deposited.

To prove the applicability of the deposited FTO films, different all layer spray deposited solar cells were fabricated on FTO substrates with reasonable efficiencies. A transparent thin film heater (TTFH) was also fabricated, which can reach high temperatures at relatively lower voltages with low power consumption. The TTFH could attain 340^0C within two minutes by the application of 20V. The FTO films exhibited high IR reflectance and this FTO-coated glass can be used as low emissivity windows to conserve energy in buildings and vehicles.

Chapter 4 discusses the preparation and characterization of in-situ Ag-doped ZnO films by CSP. Films were prepared by adding different concentrations of Ag dopant sources in the precursor solution. Intrinsic and p-type ZnO films were obtained at 5% and 7% doping concentrations respectively. p-type nature of the 7% Ag-doped ZnO films was identified from Hall measurement and is further confirmed by fabrication of ZnO-based p-i-n homojunction. Intrinsic ZnO was used as the window layer in CIS/CdS solar cells with reasonable improvement in cell parameters.

Chapter 5 deals with the ex-situ doping of metallic Ag and Sn in ZnO thin films. Different quantities of these metals were deposited over spray deposited ZnO films using vacuum evaporation and these films were annealed at 450^0C for two hours to diffuse the metals into ZnO. All the films were n-type in nature without much variation in electrical properties. But the metal incorporated films were darker. Sub-band absorbing levels were identified from the low energy regions of the absorption spectra. On XPS analysis, it was observed that the incorporated metals exist in a metal - metal oxide mixed state in ZnO lattice.

Chapter 6 deals with the deposition of ZnO layers on steel substrates using CSP for flexible solar cell applications. First ZnO layer was deposited at a relatively lower substrate temperature to prevent detrimental ion diffusion from the substrate and a top layer of Al:ZnO was deposited over it at a higher

temperature for reducing the sheet resistance. XPS depth profile analysis of the samples proved the capability of these conducting ZnO layers in preventing ion diffusion from steel substrates. To demonstrate the efficacy of this metal ion diffusion barrier layer, all layer spray deposited CIS/InS solar cells were fabricated on steel substrates with and without ZnO barrier layer. The device fabricated with ZnO barrier layer showed a reasonable improvement in short circuit current density and efficiency.

Chapter 7 summarizes the entire work along with future prospects.

List of Publications

Patents filed

1. Fluorine doped Tin Oxide (FTO) thin films using Chemical Spray Pyrolysis technique (021/PF-PIC/2014/KSCSTE)
2. Zinc Oxide thin film over flexible steel substrate using chemical spray pyrolysis technique

Publications

1. "Effect of molarity on properties of spray pyrolysed SnO_2:F thin films", **D.R. Deepu**, C.S. Kartha, K.P. Vijayakumar, AIP Conf. Proc. 58 (2014) 58–59
2. "XPS depth profile study of sprayed CZTS thin films", **D.R. Deepu**, V.G. Rajeshmon, C.S. Kartha, K.P. Vijayakumar, AIP Conf. Proc. 1591 (2014) 1666–1668
3. "Modification of opto-electronic properties of ZnO by incorporating metallic tin for buffer layer in thin film solar cells", **D.R. Deepu**, J. Jubimol, C.S. Kartha, G. Louis, K.R. Kumar, K.P. Vijayakumar, AIP Conf. Proc.1665 (2015) 120019
4. "All sprayed ITO-free $CuInS_2/In_2S_3$ solar cells", M.V. Santhosh, **D.R. Deepu**, C. Sudha Kartha, K. Rajeev Kumar, K.P. Vijayakumar, Sol. Energy. 108 (2014) 508–514
5. "Spray pyrolysed microporous TiO_2 thin films by optimisation of substrate temperature for "all sprayed" solar cells", M. V Santhosh, **D.R. Deepu**, R. Geethu, K. Rajeev Kumar, C. Sudha Kartha, K.P. Vijayakumar, Semicond. Sci. Technol. 29 (2014) 115026
6. "Tuning the properties of sprayed CuZnS films for fabrication of solar cell", M.S. Sreejith, **D.R. Deepu**, C.S. Kartha, K. Rajeevkumar, K.P. Vijayakumar, Appl. Phys. Lett. 105 (2014) 202107
7. "Improvement of sprayed $CuZnS/In_2S_3$ solar cell efficiency by making multiple band gap nature more prominent", M.S. Sreejith, **D.R. Deepu**, C. SudhaKartha, K. Rajeevkumar, K.P. Vijayakumar, J. Renew. Sustain. Energy. 8 (2016) 023502

8. *"*Sprayed ZnO As Effective Window Layer For CIS/CdS Solar Cell*",* M.S. Sreejith, **D.R. Deepu**, C.S. Kartha, K.P. Vijayakumar, AIP Conf. Proc. 1576, (2014) 67
9. "Tuning of properties of sprayed CuZnS films", M.S. Sreejith, **D.R. Deepu**, C.S. Kartha, K.P. Vijayakumar, AIP Conf. Proc.1591 (2014) 1741–1743
10. "How spray rate influences the formation and properties of transparent conducting SnO_2 thin films", **D.R. Deepu**, C. Sudha Kartha, K.P. Vijayakumar, Journal of analytical and applied pyrolysis. (under review)
11. "All sprayed transparent homo junction employing Ag mono doped p-type ZnO", **D.R. Deepu**, J. Jubimol, C. Sudha Kartha, Godfrey Louis, and K. P. Vijayakumar (under review)
12. "Sprayed ZnO as an effective barrier layer for preventing metal ion diffusion from steel substrates*",* **D.R. Deepu**, C. Sudha Kartha, K.P. Vijayakumar (under review)

Abbreviations

AFM	-	Atomic force microscopy
APCVD	-	Atmospheric pressure chemical vapor deposition
CSP	-	Chemical spray pyrolysis
CBD	-	Chemical bath deposition
CVD	-	Chemical vapor deposition
FESEM	-	Field emission scanning electron microscope
FF	-	Fill factor
FTO	-	Fluorine doped tin oxide
ITO	-	Tin doped indium oxide
J_{sc}	-	Short circuit current density
LED	-	Light emitting diode
MOCVD	-	Metalorganic chemical vapor deposition
PV	-	Photovoltaics
RMS	-	Root mean square
TCO	-	Transparent conducting oxide
V_{oc}	-	Open circuit voltage
XPS	-	X-ray Photo electron spectroscopy
XRD	-	X-ray diffraction

Chapter

1

INTRODUCTION

Contents

1.1 Introduction

The urge towards the production and consumption of renewable energy has expanded in recent years and solar power is one of the world's fastest growing sources of electricity. Solar cells generate power from solar energy by converting sunlight to electricity. The photovoltaic (PV) technology has gained a potential growth through the production of PV cells. Photovoltaics are green, pollution free, reliable, quiet, have no moving parts, virtually maintenance free and durable at moderate cost. Another important aspect of photovoltaics is the wide range of power generation from a few watts to megawatts. So solar cell installation is ideal for both domestic and industrial needs.

Solar cells based on silicon (Si) account for 90% of photovoltaic device production because of its relatively good efficiency and well understood

technology[1]. Even though the cost to produce Si solar cells has dropped significantly and efficiencies have improved during recent years, it is still out of common man's reach and payback time is more than 20 years. The production of high efficiency solar cells at reduced cost is the most critical issue in the field of photovoltaics. One of the main reasons for the high cost of Si based solar cells is the complex production technique needed for high purity crystalline silicon substrates.

The next generation photovoltaic devices will be thin film based and they can significantly reduce the material cost by reducing the quantity of materials consumed. In a thin film solar cell, transparent conducting oxide (TCO) layer plays a significant role and the wide band gap indium tin oxide (ITO) is the most widely used one. ITO exhibits exceptionally good conductivity and transmittance in the visible region. The need for ITO in other applications such as light emitting diodes (LEDs), digital displays, and touch sensors etc.[2,3] increased the worldwide consumption of this material. This noticeable demand resulted in indium (In) scarcity and its cost hike. Even though the material consumption is less for thin film solar cells, the use of ITO or the use of indium containing absorber or buffer layers makes the device expensive[2,3]. Hence the cost of today's thin film solar cells is attributed to In based layers in solar cells. It highlights the necessity of an alternative TCO material for current day photovoltaic applications.

In addition to efficient production of green energy, the consumption also should be in a careful and conservative manner. It is said that "energy conserved is equal to energy produced" [4]. About 50% of energy produced worldwide is utilized for household or industrial heating and cooling processes, which usually consume and waste a huge amount of energy. Use of proper thermally insulated buildings, heat reflecting smart windows, high

efficiency solid state lighting and usage of solar light (with the help of optical fibers and properly designed glass windows) can significantly reduce the energy consumption.

Even though wide band gap materials are commonly used in transparent electronic and smart window applications, they have functional roles in solar cells as buffer layers, intrinsic layers and metal diffusion barrier layers etc.

1.2 Importance of wide band gap materials

The invention of Si based electronics paved the way for the modern electronics era. "Moore's law" predicts that the number of transistors in silicon microprocessors tends to double every 18 – 24 months, mainly through reduction in the size of the transistors[5]. Beyond a certain limit, continuous miniaturization of devices leads to collapse of Moore's law due to the heat dissipation and current leakage issues[6,7]. Development of efficient devices employing novel materials at reduced cost is a challenge for current day power electronic devices. The potential of wide band gap materials is utilized in rapidly developing solid state lighting industry as it provides green, durable, long life and energy saving alternative to incandescent and fluorescent lamps. Greater durability and reliability of wide band gap materials make them suitable for applications like LEDs. In high power electronics, wide band gap semiconductors like silicon carbide (SiC) and gallium nitride (GaN) have added advantages like better conductivity and better switching properties than Si. Replacing Si with wide band gap materials can increase DC to DC conversion efficiency from 85% to 95%, AC to DC conversion efficiency from 85% to 90% and DC to AC from 96 to 99%[8]. These materials also find applications in solar cells as they transmit visible light and their electrical and optical properties can be tuned easily according to the need. This thesis

explores the possibility of developing SnO_2 and ZnO thin films for different energy applications.

1.3 Wide band gap materials as transparent conducting oxides - review

Materials exhibiting good electrical conductivity and high optical transmittance in the visible region are called as transparent conducting oxides (TCO). Since electrical contacts in devices like solar cells, LEDs, flat panel displays, etc. should not obstruct light from entering or leaving the device[9], TCOs are necessary for these applications. The first TCO was reported more than 100 years back in cadmium oxide (CdO) thin films by Badeker in 1907[10]. Currently cadmium (Cd) based TCOs are not widely used in TCO applications because of its toxicity. Post oxidation of evaporated metal films to form metal oxide was the earlier method to fabricate TCOs. Fabrication of tin and indium oxides (TO and IO) are reported by T.G. Bauer in 1937 and G. Ruppercht in 1954 respectively[11]. The practical development of TCOs showed only a little progress until chemical routes for depositing TO and IO were developed in 1940s[12]. Early TCOs were developed for applications such as anti-static coatings, electrodes for electroluminescent panels and wind shield defrosters etc. In the 1950s and 60s, the most popular and widely explored TCO was tin doped indium oxide (ITO). Vacuum evaporation, DC and radio frequency (RF) sputtering followed by post oxidation treatments at temperatures 300^0C to 500^0C were the deposition methods used at that time. In 1970s, a more controllable TCO production process was introduced by using oxidized sputtering targets than metal/metal alloy targets in reactive sputtering. In 1972, D.B. Fraser and H.D. Cook reported the deposition of ITO films with 85%

transmittance and 3 $x10^{-4}\Omega$.cm resistivity[13]. These values for TCOs were considered as "Gold Standard" for a long time[11].

Ternary compounds like Cd_2SnO_4 (CTO) with good electro-optic properties were investigated in the late 1970s[14,15]. But its use was limited due to Cd toxicity and high temperature post deposition treatments (> 600^0C). Interest in ZnO as TCO begins in 1970s and 1980s[16–19], but the low thermal stability of ZnO hindered its further use. Ternary compounds like ZnSnO, GaInO, ZnInO etc. and multi component oxides of binary compounds (ZnO, SnO_2, In_2O_3, Ga_2O_3, MgO etc.) were studied in 1990s[20]. Development of $CuAlO_2$, a p-type TCO with conductivity 1S/cm, raised an interest in p-type TCOs and the first TCO based p-n junctions were made in the late 1990s[21–23].

In 2001, Y. Meng *et al.* discovered high mobility TCO (100 – 130cm^2/V.s) by doping IO with molybdenum (IMO). Resistivity of the film was 1.7 x $10^{-4}\Omega$.cm[24]. This result invoked interest in high mobility TCOs and a number of works were reported on IO doped with Zr and Ti, but none had reached high mobility reported by Y. Meng on IMO[25]. The current interest is in developing economical and affordable TCOs for flexible optoelectronics devices, solar cells, and other energy conservative applications.

1.4 General properties of TCOs

TCOs are wide band gap materials (Band gap > 3.1eV) having low resistivity. Wide band gap ensures that the visible light passes through the material without absorption and thereby not exciting the electrons in the valence band to conduction band. If the TCO has perfect stoichiometry, then the material will be a perfect insulator or ionic conductor[9,26–29]. But the formation of intrinsic defects like oxygen vacancies or the presence of extrinsic dopants gives rise to considerable charge carrier concentrations[11,30–40]. Electrical conductivity

(σ) of TCO thin films depends on the charge carrier density (n), effective mass (m^*) and the relaxation time (τ) as given by the equation 1.1.

$$\sigma = \frac{ne^2\tau}{m^*} \tag{1.1}$$

where e is the electronic charge. The charge mobility (μ) is expressed as

$$\mu = \frac{ne}{m^*} \tag{1.2}$$

Therefore the conductivity in terms of mobility and charge carrier density can be expressed as

$$\sigma = ne\mu \tag{1.3}$$

The electrical conductivity of TCO materials is limited due to the dependency between carrier concentration (n) and mobility (μ). If the carrier concentration is increased beyond certain limits, mobility will be adversely affected due to scattering. Other than that, an increase in carrier concentration affects the transmittance at the near infrared (NIR) edge. In TCOs, there is always a balance between electrical conductivity and optical transmittance, because for a solid material these two properties are opposing each other.

1.4.1 Correlation between conductivity and transparency

The solution of Maxwell's equation for electromagnetic waves passing through an uncharged semiconductor will give real and imaginary parts of the refractive index[41].

$$n^2 = \frac{\varepsilon}{2}\left[\left\{1 + \left(\frac{2\sigma}{\upsilon}\right)\right\}^{\frac{1}{2}} + 1\right] \tag{1.4}$$

and

$$k^2 = \frac{\varepsilon}{2}\left[\left\{1 + \left(\frac{2\sigma}{\upsilon}\right)\right\}^{\frac{1}{2}} - 1\right] \quad (1.5)$$

where *n* is the refractive index, *k* is extinction coefficient, ε is dielectric constant and σ is the conductivity of the medium. υ is the frequency of the incident radiation.

For an insulator, conductivity (σ) will be zero. Therefore refractive index, $n = \varepsilon^{1/2}$ and extinction coefficient $k = 0$. It means the insulating semiconductor medium will be transparent to electromagnetic waves. But for a perfect conductor, the incident wave will reflect back with 180^0 phase difference.

1.4.2 Correlation between electrical and optical properties

Effect of carrier concentration on the optical transmission on NIR edge can be explained on the basis of Drude's free electron theory[42,43]. Polarization is induced within the material due to the interaction of free electrons with electromagnetic radiation.

The equation of motion of free electron is given by

$$F = m\left[\frac{d}{dt} + \frac{1}{\tau}\right]\delta V(t) \quad (1.6)$$

Where, *m* is the mass of electron, *V(t)* is the velocity of electron at any instant of time t and τ is the relaxation time.

Force acting on an electron in an alternating electric field E(t)= E.$e^{-i\omega t}$ can be written as

$$F = -eE.e^{-i\omega t} \tag{1.7}$$

Assuming a solution, $\delta V(t) = \delta V.e^{-i\omega t}$,for equation (1.6), then

$$m\left[-i\omega + \frac{1}{\tau}\right]. = -eE \tag{1.8}$$

Or

$$\delta V = \frac{e\,\tau/m}{1 - i\omega\tau} \tag{1.9}$$

Current density in the material can be obtained as

$$j = ne\delta V = \frac{ne^2\tau}{m(1 - i\omega\tau)}E \tag{1.10}$$

According to Drude model, the ac electrical conductivity is given by

$$\sigma(\omega) = \frac{ne^2\tau}{m(1 - i\omega\tau)} = \sigma_0\left[\frac{1 + i\omega\tau}{1 + (\omega\tau)^2}\right] \tag{1.11}$$

where, σ_0 corresponds to dc electrical conductivity and is given by $\sigma_0 = ne^2\tau/m$

At higher frequencies, $\omega\tau >> 1$ and the ac conductivity can be modified as

$$\sigma(\omega) = \sigma_0\left[\frac{1}{(\omega\tau)^2} + \frac{i}{\omega\tau}\right] = \frac{ne^2}{m\omega^2\tau} + i\frac{ne^2}{m\omega} \tag{1.12}$$

Therefore, the imaginary term of ac conductivity is dominant and is independent of τ. The result can be expressed as a complex dielectric constant rather than considering it as complex electrical conductivity.

The dielectric constant, $\varepsilon = 1 + \left(4\pi P/_E\right)$ (1.13)

Where P is the polarization and is given by

$$P = -\frac{ne^2/m}{\omega^2 + i\omega/\tau}E \tag{1.14}$$

Hence the dielectric constant of free electron can be expressed in terms of n, τ and ω as

$$\varepsilon(\omega) = 1 - \frac{4\pi ne^2/m}{\omega^2 + i\omega/\tau} \tag{1.15}$$

When relaxation time tends to infinity, i.e. in the absences scattering, the dielectric constant will be positive only if $\omega^2 > 4\pi ne^2/m$

When the dielectric constant is negative, electromagnetic waves cannot propagate in to the medium because the wave decays exponentially. Hence in the medium with imaginary wave vectors, incident waves get reflected. The corresponding cut off frequency is known as plasma frequency (ω_p). The material is transparent to those waves with frequencies higher than ω_p. The relation connecting the plasma frequency of material to its carrier concentration is given by equation (1.16).

$$\omega_p = \left(4\pi ne^2/m\right)^{\frac{1}{2}} \tag{1.16}$$

Equation (1.16) tells that the plasma frequency of material can be tuned to higher frequencies by increasing its carrier concentration[44,45].

1.4.3 Electrical properties of TCO

Origin of electrical conductivity of TCO is from non-stoichiometry of the material. Charge carriers are supplied by the shallow donor sites created by

oxygen vacancies and metal interstitial defects[9]. Intentional doping and diffusion of alkali ions such as Na from the glass substrate can significantly affect the electrical properties of TCOs. A moderate doping can increase the carrier concentration and there by electrical conductivity of TCOs. But further increase in carrier concentration reduces the carrier mobility by scattering mechanisms and set a limit to the conductivity[28]. High doping concentration can also cause clustering of dopant ions which could significantly increase the scattering rate[36,46].

1.4.4 Optical properties of TCO

Besides good electrical conductivity, TCO films should have high transmittance in the visible region. Photons in the ultra violet (UV) region will be absorbed by the material if its energy is greater than the band gap of TCO and a transmission edge in the UV region can be observed. The material will exhibit second transmission edge in the NIR or IR region due to the reflection of photons whose frequencies are below the plasma frequency of the film. The transmission spectrum of a typical TCO film is shown in Figure 1.1.

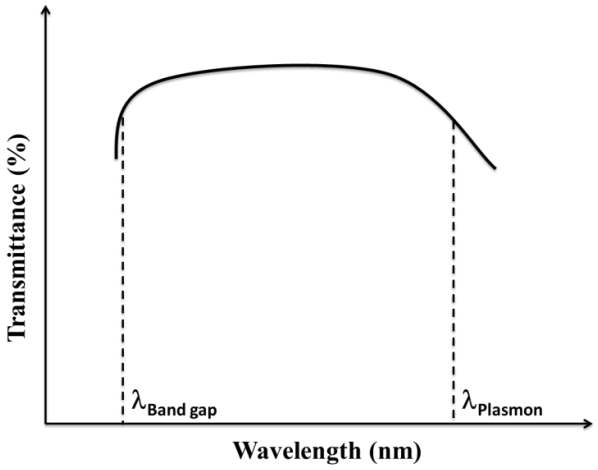

Figure 1.1. Transmission spectrum of TCO

Ideal TCO should transmit all the photons with energy less than its band gap, but there are no ideal TCO films. All real TCO films have

transmission window between UV and IR region. The width of the window is related to the carrier concentration in the material.

1.4.5 Thermal stability

Electrical conductivity of TCOs remains stable up to a threshold temperature which depends on the material characteristics and deposition techniques. TCO shows degradation in their properties after heated to threshold temperature for a long time. Threshold temperature of various TCO materials is given in the following order. ZnO (250^0C) < SnO_2 (500^0C) < and Cd_2SnO_4 (700^0C)[47]. Thermal stability of TCO is essential for photovoltaic applications as the fabrication process may involve high temperature deposition conditions and the finished device has to work in very harsh environmental conditions where temperature variations are natural.

1.4.6 Chemical stability

Chemical stability of TCO is the ability of the material to withstand corrosive environments without deteriorating its properties. Fabrication of amorphous Si based thin film solar cells involves hydrogenation process to passivate the Si surface so as to reduce the density of dangling bonds. But in 'hydrogen rich' environments, ITO undergoes heavy reduction[48]. ZnO and SnO_2 are more stable in the presence of reducing plasma and fluorine doped tin oxide (FTO) films are extensively used for the fabrication of amorphous Si solar cells[40,48].

1.4.7 Mechanical durability

Mechanical durability of TCO materials is related to the hardness of the corresponding crystals. Titanium nitride and tin oxide are harder than glass and they can be utilized in applications where these layers are exposed. The mechanical hardness of ZnO is low and is readily scratched and can be used only with protective coatings[41].

1.5 n-type TCO materials

Oxides of In, Sn and Zn are the three popular transparent conducting materials that evoked commercial interest, among which tin doped indium oxide (ITO), available with high transmittance and high electrical conductivity on various substrates holds the major share. Most of the ITO produced worldwide is utilized for display applications. The high cost of ITO and low stability of ZnO has spanned the interest on economical and stable SnO_2 for the fast emerging photovoltaic and low emissivity, smart window industries.

1.5.1 Tin oxide (SnO_2)

Tin oxide crystallizes in tetragonal rutile structure and belongs to $P4_2/mnm$ space group[9,49]. The unit cell consists of two tin cations and four oxygen anions. The Sn cations are situated at the corners of a regular octahedron and each oxygen anion is surrounded by three Sn cations at the corners of an equilateral triangle. The lattice parameters are a = b = 4.737Å, c = 3.186Å and c/a ratio is 0.672Å[9,50,51]. The ionic radii of Sn^{4+} and O^{2-} are 0.71Å and 1.4Å respectively[52,53].

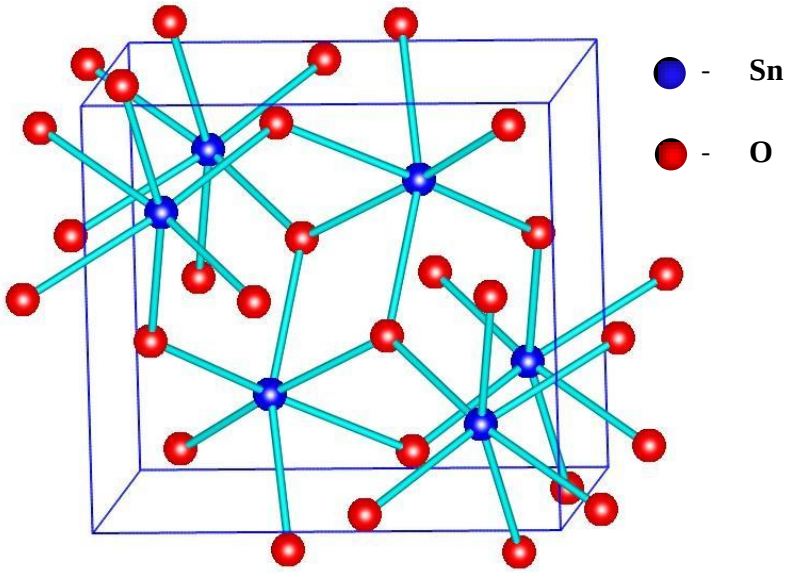

Figure 1.2. Rutile structure of SnO_2[54]

Similar to other wide band gap binary oxide TCOs, the conductivity of SnO_2 also arise due to the intrinsic non-stoichiometric defects like oxygen vacancies. C. Kilic and A. Zunger reported that the formation of Sn interstitials and oxygen vacancies are due to their very low formation energies. The high conductivity exhibited by this material, even without doping can be due to this non-stoichiometry[55]. There are three ways of generating charge carriers in the material by intrinsic or extrinsic doping[9].

1. Generation of free electrons to the conduction band without the expense of additional energy.
2. Creation of localized defect levels below the conduction band at the expense of external energy source (light or heat).
3. Donor band becomes the conduction band.

The defect level for Sn interstitial is found to be about 203meV above the conduction band minimum and it spontaneously donates the electrons to

the conduction band. But the defect level for oxygen vacancies is 114meV below the conduction band and they can be easily activated by thermal energy[55]. That means for the pure tin oxide films, generation of the conduction electrons can be attributed to the first two mechanisms mentioned above[9]. The electrical conductivity of tin oxide can be further improved by doping with a pentavalent dopant like Sb to substitute Sn cation or a halogen like F to substitute oxygen anion. In both the cases, dopants provide additional electrons to the lattice resulting in the increase in carrier concentration[9,56,57].

1.5.2 Review on SnO_2 based TCOs

Even though SnO_2 based TCO has been widely used for various applications such as thin film solar cells, low emissivity windows and window defrosters, commercially available tin oxide based TCO is not economical for practical applications. Sb doped SnO_2 thin films were prepared using electron beam evaporation by M.F. Arendt and John S. Swinnea. They investigated structural, optical and electrical properties of the films with respect to annealing time and temperature in oxygen atmosphere[58]. Abdul Faheem Khan *et al.* studied the effect of annealing temperature on the structural and electrical properties of tin oxide films prepared by electron beam evaporation and RF sputtering. It was reported that the films deposited through electron beam evaporation were amorphous in nature, but annealing up to 400^0C improves crystallinity and conductivity. But further increase in annealing temperature resulted in decrease in electrical conductivity[59]. Films prepared using RF sputtering at room temperature were crystalline in nature and the lowest resistivity of the films was about $1x10^{-3}\Omega$.cm.[60]

P.M. Gorley *et al.* studied effect of substrate temperature and annealing on tin oxide films prepared by reactive sputtering. Preheating the substrate and

annealing the deposited films resulted in enhancement in transmittance and conductivity. The lowest resistivity and highest transmittance for the films were reported to be about $6x10^{-4}\Omega$.cm and 95% respectively[61].

The effect of oxygen to argon ratio on the properties of tin oxide thin films deposited by reactive DC sputtering was studied by J. Montero *et al*. The lowest resistivity of the films was about $3x10^{-3}\Omega$.cm.[62] They have also studied effect of different discharge power densities without preheating the substrate. The lowest resistivity of the films was about $3.3x10^{-3}\Omega$.cm.[63]

Toshiro Maruyama and Kenji Tabata have prepared fluorine doped tin oxide thin films by low temperature atmospheric pressure chemical vapor deposition (APCVD) technique. The organometallic compound, Tin(II) trifiuoroacetate was used as the precursor for film deposition. The resistivity of the best deposited film with thickness 1.26μm was $5.9x10^{-4}\Omega$.cm.[64]

Ta doping in tin oxide by metalorganic chemical vapor deposition method is reported by Sang woo Lee *et al*. The films were prepared on corning 7059 glass substrates. The lowest resistivity of the films was about $2.01x10^{-4}$ Ω.cm. The report suggests that Ta is an excellent dopant for enhancing the electrical properties of tin oxide thin films[65].

The effect of substrate temperature, distance of the substrate from precursor inlet and precursor flow rate on the properties of tin oxide were reported by Geeta Sanon *et al*. Films were deposited on quartz substrate and the lowest sheet resistance obtained was 57Ω/sq.[66]

Understanding the detailed chemical reaction mechanisms for tin oxide thin film fabrication using chemical vapor deposition (CVD) could lead to the development of high quality TCOs cost effectively[67].

James Proscia and Roy G. Gordon reported the effect of various concentration ratios of precursors, tetramethyltin and bromotrifluoromethane (Freon) on the formation of fluorine doped tin oxide thin films by atmospheric pressure chemical vapor deposition technique. The films produced under optimized deposition conditions were reported to have conductivities near $3000\Omega^{-1}cm^{-1}$.[68]

Preparation of fluorine doped tin oxide thin films on silicon, glass and quartz substrates at various substrate temperatures using atmospheric pressure chemical vapor deposition from $(CH_3(CH_2)_3)2Sn(O_2CCF_3)_2$ and oxygen was reported. The films showed 75% transparency in the visible region and resistivity of $8.2x10^{-4}$ Ω.cm.[69]

Richard J. McCurdy explored possibilities for depositing TCO through chemical vapor deposition technique on glass manufacturing line. CVD deposition parameters like thickness insensitive film design, float line compatible CVD chemistry, and flexible deposition technology etc. are discussed in this report[70].

Fundamental framework for atmospheric pressure chemical vapor deposition of tin oxide coatings on glass using monobutyltintrichloride as the precursor was developed using computational fluid dynamics (CFD) in impinging flow geometry. Effects of reactor-substrate spacing and glass line speed on the simulated deposition profile and comparison of modeling results with experimental data were discussed. The study showed that the effect of reaction kinetics is less important and the deposition process is mainly diffusion controlled[71].

Development of atmospheric pressure CVD processes for high quality transparent conductive oxides was presented by Ariël de Graaf *et al*. It was

shown that high transmittance (80%) and low resistivity (4 x$10^{-4}\Omega$.cm) film can be obtained in combination with an intrinsic surface structure that enhances light trapping effect[72].

A comparative study of the growth of tin oxide thin films by atomic layer deposition (ALD) and CVD were reported by Jonas Sundqvist *et al*. It is identified that low growth rate of ALD promotes the formation of high quality epitaxial films. CVD grown films were reported to have high surface roughness and grain boundaries[73].

Ü. Dagkaldiran *et al.* reported preparation of fluorine doped tin oxide films by APCVD technique for the fabrication of amorphous Si solar cells. The cells fabricated on the deposited FTO films were reported to giving 9.3% efficiency with 73% fill factor[74].

Y. Wang *et al.* synthesized self-organized Sb, Nb, and Ta doped mesoporous SnO_2 thin films with adjustable doping levels on organic substrates using evaporation induced self-assembly[75]. In this work, precursor of Sn along with the dopant was mixed in an alcoholic solution and was coated on to the substrate by dip coating technique. Electrical conductivity of the films was in the order of $10^{-2}\Omega$.cm only.

Effect on annealing of pure and antimony doped tin oxide thin films in different atmospheres were reported by E. Shanthi *et al*. The method of preparation of the films was chemical spray pyrolysis. They identified that change in electrical properties was due to the adsorption or desorption of oxygen originating at grain boundaries[76]. They also investigated effects of different dopants like Sb,F and Sb & F at various concentrations and compared their properties. It was observed that F is the best dopant for improving the

optical as well as electrical properties of the films. lowest sheet resistance was observed to be less than 10Ω/sq.[77]

E. Elangovan *et al.* have investigated effect of different fluorine to tin ratios on FTO films by chemical spray pyrolysis (CSP); here $SnCl_2$ and NH_4F were the precursors for Sn and F. They reported that the increase in fluorine concentration helped to improve transmission in the visible region and reflectance in the IR region. The best films were of about 1.2μm thick and had 85% transmittance and 94 to 98% reflectance in the IR region (above 1500 nm), while sheet resistance was reported to be 1.75Ω/sq.[78] They also studied effect of antimony doping on tin oxide films. Here the dopant source was $SbCl_3$. On Sb doping, it was identified that carrier concentration increased and hall mobility decreased drastically. The lowest sheet resistance obtained with Sb doping was 2.17Ω/sq.[79]

Seung-Yup Lee reported preparation of Sb doped tin oxide thin films by using ultrasonic spray technique. Effect of antimony doping on structural, electrical and optical properties of tin oxide thin films were discussed. Change in preferential orientation from (211) plane to (200) plane with doping is observed. The lowest resistivity for the best films was about 8.4×10^{-4}Ω.cm.[80]

Low temperature growth of fluorine-doped tin oxide films by intermittent spray pyrolysis was reported by Tatsuo Fukano and Tomoyoshi Motohiro. They used 'perfume atomizer' for spraying the precursors at a temperature between 325^0C to 340^0C and the resulted films had 92% transparency. The lowest resistivity of 5.8×10^{-4}Ω.cm was obtained after annealing the samples at 450^0C for 60 minutes in air[81].

G.C. Morris and A.E. McElnea reported preparation of FTO films with tin fluoride in methanol solvent with and without addition of HCl. Dependence

of properties on deposition time, substrate temperature, and solution composition were studied and the best films had resistivity of 5.6 $x10^{-4}\Omega$.cm.[82]

Effect of F, Sb, and F & Sb doping on spray pyrolysed tin oxide thin films was studied by B. Thangaraju. All doped films were observed to have degenerate carrier concentrations in the range 10^{20} to 10^{21}. But better transmittance and lower sheet resistance were obtained on fluorine doping. the lowest sheet resistance obtained on fluorine doping was 5.65Ω/sq.[28]

K.S. Shamala *et al.* compared pure and Sb doped tin oxide thin films prepared by using electron beam evaporation and spray pyrolysis. The substrate temperature required for obtaining crystalline films by spray pyrolysis was found to be higher than that for electron beam evaporation. Resistivity of undoped films was observed to be lower for e-beam evaporated films, but on antimony doping resistivity of the films prepared through spray pyrolysis decreased drastically. The lowest resistivity obtained for Sb-dopped was 1 $x10^{-2}\Omega$.cm (e-beam evaporated films) and 7.74 $x10^{-4}\Omega$.cm (spray deposited films)[83].

Effect of solvents and fluorine dopant concentration on formation and properties of spray deposited nanocrystalline tin oxide thin films was studied by A.V. Maholkar *et al*. Precursor solutions were prepared by dissolving stannic chloride and ammonium fluoride in different solvents such as methanol, ethanol, isopropyl alcohol and distilled water. Film thickness was varying from 880nm to 2200nm for different solvents and the best electrical properties are exhibited by the films prepared with isopropyl alcohol as the solvent. Sheet resistance of the best undoped film was 3.71Ω/sq.[84] Best fluorine doped film showed resistivity of 3.8 $x10^{-4}\Omega$.cm and charge mobility 6.59cm^2/V.s.[85]

Chin-Ching Lin *et al.* analyzed temperature dependence of FTO films produced by ultrasonic spray pyrolysis on glass substrates. A change in preferential growth from (211) plane to (200) plane of rutile structure was observed with increase in temperature. Electrical properties of the prepared films were found to be largely influenced by the doping concentration and deposition temperature. Maximum transmittance and minimum resistivity shown by the best film were 77% and 6.2 $x10^{-4}\Omega$.cm respectively[86].

In the thickness dependence study on the properties of spray deposited films, it was reported that mobility and hall concentration increased linearly with thickness and resistivity could brought down to $3x10^{-4}\Omega$.cm.[87] Effect of thickness of FTO films prepared through spray pyrolysis was analyzed by A.A. Yadav *et al.* by varying the quantity of precursor solution. Films of thickness up to 1700nm were prepared at 3nm/s growth rate. The best films showed 77% transmittance. Low resistivity of $3.91x10^{-4}\Omega$.cm and mobility of $11cm^2/V.s$ were reported[88].

D.R. Acosta *et al.* prepared FTO films by varying the F concentration using CSP. The substrate temperature was 300^0C and the deposition time was 15 minutes. Resistivity was brought down from 33 $x10^{-4}\Omega$.cm to 6 $x10^{-4}\Omega$.cm with fluorine doping. Increase in surface roughness with increase in dopant concentration was also reported[89].

P. Veluchami *et al.* synthesized large area FTO thin films using ultrasonic CSP to use it as a substrate for CdS/CdTe solar cells. Organometallic compound of tin (dimethyltindichloride) with NH_4F and HF were the precursors used and the growth rate was greater than 15nm/s. Thickness of the films was reported to be around 500 nm with sheet resistance less than 10Ω/sq. Mobility of the films was $43.8cm^2/V.s$. Fabricated

CdS/CdTe thin film solar cell on the deposited FTO films exhibited maximum conversion efficiency of 14.95%[90].

Even though doped conducting oxides with lower resistivity as low as 2 x$10^{-4}\Omega$.cm with transmittance greater than 80% are reported, charge mobility for those films was lower. High conductivity with high mobility was achieved only when the precursors were made of organometallic compounds. But considering the cost and environment, better understanding on the spray deposition of FTO is needed.

1.6 p-type TCO materials

n-type TCO films are commercially available and are used in a wide variety of applications as transparent window electrodes. The absence of p-type TCO was hindering the development of active transparent electronic devices such as diodes, transistor, and UV LEDs. First p-type TCO was reported by H. Sato *et al.* on NiO films with transmittance around 40%. They also fabricated a thin film p-i-n diode using the p-type NiO. Transmittance of the device was reported to be about 20%. Ni vacancies and oxygen interstitial sites are the reason for the p-type conductivity of NiO films[91]. The real progress in p-type TCOs started with invention of p-type conductivity in $CuAlO_2$ thin films by Kawazoe *et al*.

There is an extensive review on p-type TCOs by A.N. Banerjee and K.K. Chattopadhyay[92]. GaN along with AlGaN and InGaN are presently dominating in the light emitter market due to their viable p-type conductivity. Now n-type ZnO is used in conjunction with GaN to make blue LEDs. Developing p-type ZnO has added advantages like possibility of low temperature growth of epitaxial films, radiation hardness and little lattice

mismatch with n-type ZnO. Therefor the development of p-type ZnO is also equally essential[93].

ZnO is a wide band gap, group II-VI compound semiconductor that crystallizes normally in hexagonal wurtzite structure and belongs to $p6_3mc$ space group[94]. In wurtzite structure, zinc and oxygen atoms are arranged alternatively to form a hexagonal close packed lattice of zinc as shown in Figure 1.3, whereas oxygen are positioned in the tetrahedral groups of four Zn atoms. All these tetrahedral groups are aligned along the hexagonal axis. The lattice parameters of ZnO are a = 3.24Å and c =5.2Å with c/a ratio 1.66.

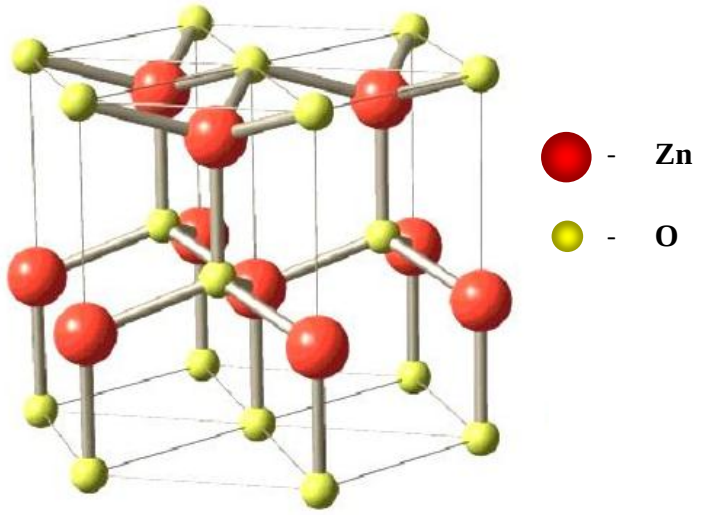

Figure 1.3. Wurtzite structure of ZnO [94]

Wide and direct band gap of ZnO (> 3.3eV) along with its high exciton binding energy (60meV) makes it a suitable candidate for optoelectronic devices such as LEDs and lasers. Strong luminescence exhibited by ZnO in the wide green - white region makes it suitable for phosphor applications[35,95]. ZnO can be easily etched at low temperatures using chemical routes and it makes ZnO suitable for electronic and optoelectronic application, design and

processing. ZnO exhibits exceptionally high radiation hardness and it makes this material suitable candidate for high altitude and space applications.

There are a number of reports regarding the experimental and theoretical aspects of p-type ZnO[96–105]. p-type ZnO can be achieved by substituting Zn with group-I elements (Li, Na and K) or oxygen by group V elements (N,P and As). Theoretically, group-I elements are better dopants than group V elements in terms of creating shallow acceptor levels. However, due to the small ionic radii of group-I elements, this will result in the occupation of interstitial sites rather than Zn sites and will act as donors[106]. Doping with group V elements will create deep acceptor levels, among which only nitrogen is likely to result in a shallow acceptor level[35]. Since the size mismatch between the group-I elements and Zn prevents the formation of p-type ZnO, group-I_b element Ag is suggested to be a better dopant[107]. H.S. Kang *et al.* have fabricated Ag doped p-type ZnO employing pulsed laser deposition method in 2006[108].

First principle calculations of doping effect of group-I_b elements were done by Y. Yan *et al.* and they calculated transition and formation energies for the dopants. They found that, at oxygen rich growth conditions, formation energy for Zn substitutional defects is low and favors p-type ZnO formation[107,109]. I.S. Kim *et al.* prepared p-type ZnO films with Ag doping by using e-beam evaporation and B.D. Ahn could get p-type ZnO films by pulsed laser deposition[110,111].

Reports on achieving p type Ag:ZnO by spray pyrolysis was reported in a few papers. W. Bin *et al.* and W. Jing-Wei *et al.* deposited p-type ZnO films by Ag-N co-doping using ultrasonic spray pyrolysis method[112,113]. However, achieving p-type ZnO using single dopant Ag by spray pyrolysis technique is

not reported earlier. In the present work, p-type nature of ZnO was achieved through CSP technique by doping it with Ag alone.

1.7 TCO as low emissivity windows

Solar radiation is absorbed by the earth and is re-radiated as black body radiation in the IR region (wavelength from 3μm to 50μm). Ability of TCO materials to reflect electromagnetic waves whose frequencies are less than that of their plasma frequencies (ω_p) is widely utilized to fabricate low emissivity windows. Low emissivity windows are TCO coated glass windows, which can transmit visible light but reflects the IR radiation from the earth. The usage of low emissivity windows can reduce energy losses by at least 15%.

1.8 Motivation of the present work

Growing interest in clean energy sources like photovoltaics and the increasing demand for low emissivity-smart windows, solid state lighting etc. for energy conservation resulted in the wide spread interest in non-conventional methods and materials. Among the various deposition techniques, chemical spray pyrolysis attains a prominent position because of its simplicity and cost effectiveness. The necessity to avoid expensive indium based TCOs and other compounds in solar cells are a major concern. The cost of indium has increased by several orders in the last three decades. It demands the significance of wide band gap materials like SnO_2 and ZnO. Among these, SnO_2 will be more suitable for photo voltaic applications due to its high mechanical, thermal and chemical stability and it is not easily affected by the harsh out door weather conditions. Perovskite solar cells are a recent breakthrough in the photovoltaic research with its efficiency exceeding 20%. And FTO substrates are the best established TCO material for perovskite solar cells.

Commercially available FTO substrates are mostly produced through expensive techniques like chemical vapor deposition, which hinder the cost to come down. Preparation of these materials through a scalable and automated technique like spray pyrolysis will be largely appreciated, if we can produce materials with required properties. The thesis explores the possibility of developing tin oxide based n-type TCO for solar cell and other energy applications like low power transparent heaters, low emissivity windows etc. In this work, the use of ZnO based p-type TCO for transparent electronic applications and the possibility of using ZnO layers as intrinsic layer, buffer layer and absorber layer in solar cells is also studied. Potential of ZnO as metal ion diffusion barrier layer over steel substrates for flexible solar cell application is also investigated.

References

1. www.nrel.gov/pv.
2. T. Minami, Thin Solid Films **516**, 5822 (2008).
3. A. Stadler, Materials **5**, 661 (2012).
4. R. Banerjee, Int. J. Innov. Res. Adv. Eng. **2**, 186 (2015).
5. R.R. Schaller, Spectrum, IEEE **34**, 52 (1997).
6. N.S. Kim, T. Austin, D. Blaauw, T. Mudge, K. Flautner, J.S. Hu, M. Jane Irwin, M. Kandemir, and V. Narayanan, Computer (Long. Beach. Calif). **36**, 68 (2003).
7. L.B. Kish, Phys. Lett. Sect. A Gen. At. Solid State Phys. **305**, 144 (2002).
8. www.mouser.in/applications.
9. M. Batzill and U. Diebold, Prog. Surf. Sci. **79**, 47 (2005).

[10] K. Badeker, Ann Phys. **22**, 749 (1907).

[11] C.I. Bright, 50 Years Vac. Coat. Technol. 38 (2007).

[12] J.M. MOCHEL, U.S. Patent 2,564,706 (1946).

[13] D.B. Fraser and H.D. Cook, J. Electrochem. Soc. **119**, 1368 (1972).

[14] G. Haacke, Appl. Phys. Lett. **28**, 622 (1976).

[15] N. Miyata, K. Miyake, and S. Nao, Thin Solid Films **58**, 385 (1979).

[16] J.M. Nobbs and F.C. Gillespie, J. Phys. Chem. Solids **31**, (1970).

[17] J. Aranovich, J. Vac. Sci. Technol. **16**, 994 (1979).

[18] J. Yen, J. Vac. Sci. Technol. **12**, 47 (1975).

[19] T. Minami, H. Nanto, and S. Takata, Jap. J. Appl. Phys. **23**, L280 (1984).

[20] T. Minami, MRS Bull. 38 (2000).

[21] H. Kawazoe, M. Yasukawa, H. Hyodo, M. Kurita, H. Yanagi, and H. Hosono, Nature **389**, 939 (1997).

[22] A. Kudo, H. Yanagi, K. Ueda, H. Hosono, H. Kawazoe, and Y. Yano, Appl. Phys. Lett. **75**, 2851 (1999).

[23] H. Ohta, K. Kawamura, M. Orita, M. Hirano, N. Sarukura, and H. Hosono, Appl. Phys. Lett. **77**, 475 (2000).

[24] Y. Meng, Thin Solid Films **394**, 218 (2001).

[25] M.F.A.M. Van Hest, M.S. Dabney, J.D. Perkins, D.S. Ginley, and M.P. Taylor, Appl. Phys. Lett. **87**, 2003 (2005).

[26] F. de Moure-Flores, J.G. Quiñones-Galván, A. Hernández-Hernández, A. Guillén-Cervantes, M. a. Santana-Aranda, M.D.L.L. Olvera, and M. Meléndez-Lira, Appl. Surf. Sci. **258**, 2459 (2012).

[27] A.V. Moholkar, S.M. Pawar, K.Y. Rajpure, P.S. Patil, and C.H. Bhosale, J. Phys. Chem. Solids **68**, 1981 (2007).

[28] B. Thangaraju, Thin Solid Films **402**, 71 (2002).

[29] S. Ebrahimiasl, W.M.Z.W. Yunus, A. Kassim, and Z. Zainal, Sensors **11**, 9207 (2011).

[30] T.V. Vimalkumar, N. Poornima, K.B. Jinesh, C.S. Kartha, and K.P. Vijayakumar, Appl. Surf. Sci. **257**, 8334 (2011).

[31] T.V. Vimalkumar, N. Poornima, C. Sudha Kartha, K.P. Vijayakumar, T. Abe, and Y. Kashiwaba, Phys. B Condens. Matter **405**, 4957 (2010).

[32] A.N. Gruzintsev, V.T. Volkov, and E.E. Yakimov, Semiconductors **37**, 259 (2003).

[33] J. Montero, C. Guillén, and J. Herrero, Sol. Energy Mater. Sol. Cells **95**, 2113 (2011).

[34] H. Hosono, Thin Solid Films **515**, 6000 (2007).

[35] A. Janotti and C.G. Van de Walle, Reports Prog. Phys. **72**, 126501 (2009).

[36] L. Castañeda, Mater. Sci. Appl. **2**, 1233 (2011).

[37] A. Klein, C. Körber, A. Wachau, F. Säuberlich, Y. Gassenbauer, S.P. Harvey, D.E. Proffit, and T.O. Mason, Materials (Basel). **3**, 4892 (2010).

[38] Ü. Özgür, Y.I. Alivov, C. Liu, A. Teke, M. A. Reshchikov, S. Doğan, V. Avrutin, S.J. Cho, and H. Morkǫ, J. Appl. Phys. **98**, 1 (2005).

[39] E. Fortunato, D. Ginley, H. Hosono, and D.C. Paine, MRS Bull. **32**, 242 (2007).

[40] T. Minami, Semicond. Sci. Technol. **20**, S35 (2005).

[41] R. Manoj, Characterisation of Transparent Conducting Thin Films Grown by Pulsed Laser Deposition and RF Magnetron Sputtering, Ph.D. thesis,Cochin University of Science And Technology, 2006.

[42] I. Hamberg and C.G. Granqvist, J. Appl. Phys. **59**, 2950 (1986).

[43] J. Hu and R.G. Gordon, J. Appl. Phys. **71**, 880 (1992).

[44] J. Shi, P. Li, B. Liu, and S. Shen, Appl. Phys. Lett. **102**, (2013).

[45] R.K. Vinnakota and D. A Genov, Sci. Rep. **4**, 4899 (2014).

[46] P. Ebert, T. Zhang, F. Kluge, M. Simon, Z. Zhang, and K. Urban, Phys. Rev. Lett. **83**, 757 (1999).

[47] R.G. Gordon, MRS Bull. **25**, 52 (2000).

[48] S. Major, S. Kumar, M. Bhatnagar, and K.L. Chopra, Appl. Phys. Lett. **49**, 394 (1986).

[49] O. Lupan, L. Chow, G. Chai, H. Heinrich, S. Park, and A. Schulte, J. Cryst. Growth **311**, 152 (2008).

[50] Lattice parameters and illustrations of the bulk crystal structures, Phys. Chem. Chem. Phys. 1 (2013).

[51] C.J. Howard, T.M. Sabine, and F. Dickson, Acta Crystallogr. Sect. B **47**, 462 (1991).

[52] M. Shokooh-saremi, J. Phys. D Appl. Phys. **37**, 1248 (2004).

[53] www.wiredchemist.com.

[54] Emuch.net.

[55] Cetin Kilic and Alex Zunger, Phys. Rev. Lett. **88**, 095501 (2002).

[56] A.V. Moholkar, S.M. Pawar, K.Y. Rajpure, C.H. Bhosale, and J.H. Kim, Appl. Surf. Sci. **255**, 9358 (2009).

[57] M.J. Atmane B, Achour rahal, Boubaker Benhaoua, Superlattices Microstruct. **70**, 61 (2014).

[58] M.F.A. and J.S. Swinnea, J.Mater.Res. **8**, 3131 (1993).

[59] A.F. Khan, M. Mehmood, M. Aslam, and M. Ashraf, Appl. Surf. Sci. **256**, 2252 (2010).

[60] A.F. Khan, M. Mehmood, A.M. Rana, and M.T. Bhatti, Appl. Surf. Sci. **255**, 8562 (2009).

[61] P.M. Gorley, V.V. Khomyak, S.V. Bilichuk, I.G. Orletsky, P.P. Horley, and V.O. Grechko, Mater. Sci. Eng. B **118**, 160 (2005).

[62] J. Montero, J. Herrero, and C. Guillén, Sol. Energy Mater. Sol. Cells **94**, 612 (2010).

[63] J. Montero, C. Guillén, and J. Herrero, Sol. Energy Mater. Sol. Cells **95**, 2113 (2011).

[64] T. Maruyama and K. Tabata, J. Appl. Phys. **68**, 4282 (1990).

[65] S.W. Lee, Y. W. Kim, and H. Chen, Appl. Phys. Lett. **78**, 350 (2001).

[66] G. Sanon, R. Rup, and A. Mansingh, Thin Solid Films **190**, 287 (1990).

[67] A.M.B. Van Mol, Y. Chae, A.H. McDaniel, and M.D. Allendorf, Thin Solid Films **502**, 72 (2006).

[68] J. Proscia and R.G. Gordon, Thin Solid Films **214**, 175 (1992).

[69] S. Suh, Z. Zhang, W. K. Chu, and D.M. Hoffman, Thin Solid Films **345**, 240 (1999).

[70] R.J. McCurdy, Thin Solid Films **351**, 66 (1999).

[71] M. Li, J.F. Sopko, and J.W. McCamy, Thin Solid Films **515**, 1400 (2006).

[72] A. De Graaf, J. Van Deelen, P. Poodt, T. Van Mol, K. Spee, F. Grob, and A. Kuypers, Energy Procedia **2**, 41 (2010).

[73] J. Sundqvist, J. Lu, M. Ottosson, and A. Hårsta, Thin Solid Films **514**, 63 (2006).

[74] Ü. Dagkaldiran, A. Gordijn, F. Finger, H.M. Yates, P. Evans, D.W. Sheel, Z. Remes, and M. Vanecek, Mater. Sci. Eng. B Solid-State Mater. Adv. Technol. **159-160**, 6 (2009).

[75] Y. Wang, T. Brezesinski, M. Antonietti, and B. Smarsly, ACS Nano **3**, 1373 (2009).

[76] E. Shanthi, A. Banerjee, V. Dutta, and K.L. Chopra, Thin Solid Films **71**, 237 (1980).

[77] E. Shanthi, A. Banerjee, and K.L. Chopra Thin Solid Films **88**, 93 (1982).

[78] E. Elangovan and K. Ramamurthi, J. Optoelectron. Adv. Mater. **5**, 45 (2003).

[79] E. Elangovan, S.A. Shivashankar, and K. Ramamurthi, J. Cryst. Growth **276**, 215 (2005).

[80] S.Y. Lee and B. O. Park, Thin Solid Films **510**, 154 (2006).

[81] T. Fukano and T. Motohiro, Sol. Energy Mater. Sol. Cells **82**, 567 (2004).

[82] G.C. Morris and A.E. McElnea, Appl. Surf. Sci. **92**, 167 (1996).

[83] K.S. Shamala, L.C.S. Murthy, and K. Narasimha Rao, Mater. Sci. Eng. B **106**, 269 (2004).

[84] A.V. Moholkar, S.M. Pawar, K.Y. Rajpure, S.N. Almari, P.S. Patil, and C.H. Bhosale, Sol. Energy Mater. Sol. Cells **92**, 1439 (2008).

[85] A.V. Moholkar, S.M. Pawar, K.Y. Rajpure, C.H. Bhosale, and J.H. Kim, Appl. Surf. Sci. **255**, 9358 (2009).

[86] C.C. Lin, M.C. Chiang, and Y.W. Chen, Thin Solid Films **518**, 1241 (2009).

[87] C. Agashe, J. Hüpkes, G. Schöpe, and M. Berginski, Sol. Energy Mater. Sol. Cells **93**, 1256 (2009).

[88] A.A. Yadav, E.U. Masumdar, A. V. Moholkar, K.Y. Rajpure, and C.H. Bhosale, Phys. B Condens. Matter **404**, 1874 (2009).

[89] D.R.Acosta, E.P.Zironi, E.Montoya, And, and W.Estrada, Thin Solid Films **288**, 1 (1996).

[90] P. Veluchamy, M. Tsuji, T. Nishio, T. Aramoto, H. Higuchi, S. Kumazawa, S. Shibutani, J. Nakajima, T. Arita, H. Ohyama, A. Hanafusa, T. Hibino, and K. Omura, Sol. Energy Mater. Sol. Cells **67**, 179 (2001).

[91] H. Sato, T. Minami, S. Takata, and T. Yamada, Thin Solid Films **236**, 27 (1993).

[92] A.N. Banerjee and K.K. Chattopadhyay, Prog. Cryst. Growth Charact. Mater. **50**, 52 (2005).

[93] D.C. Look, B. Claflin, Y.I. Alivov, and S.J. Park, Phys. Stat. Solidi A **2212**, 2203 (2004).

[94] S. Hagino, K. Yoshio, T. Yamazaki, H. Satoh, K. Matsuki, and A. Onodera, Adv. Ferroelectr. **264**, 235 (2001).

[95] S. Shionoya, W.M. Yen, and H. Yamamoto, *Phosphor Handbook* (CRC Press, 2006).

[96] K. Minegishi, Y. Koiwai, Y. Kikuchi, K. Yano, M. Kasuga, and A. Shimizu, Jpn. J. Appl. Phys. **36**, 1453 (1997).

[97] M. Joseph, H. Tabata, H. Saeki, K. Ueda, and T. Kawai, Phys. B Condens. Matter **302-303**, 140 (2001).

[98] T. Yamamoto, Thin Solid Films **420-421**, 100 (2002).

[99] Y. Ryu, S. Zhu, D. Look, J. Wrobel, H. Jeong, and H. White, J. Cryst. Growth **216**, 330 (2000).

[100] Y.R. Ryu, W.J. Kim, and H.W. White, J. Cryst. Growth **219**, 419 (2000).

[101] X. Li, Y. Yan, T. A. Gessert, C.L. Perkins, D. Young, C. DeHart, M. Young, and T.J. Coutts, J. Vac. Sci. Technol. A Vacuum, Surfaces, Film. **21**, 1342 (2003).

[102] A.B.M.A. Ashrafi, I. Suemune, H. Kumano, and S. Tanaka, Japanese J. Appl. Physics, Part 2 Lett. **41**, 2 (2002).

[103] S. Zhang, S. H. Wei, and A. Zunger, Phys. Rev. B **63**, 1 (2001).

[104] C.H. Park, S.B. Zhang, and S. H. Wei, Phys. Rev. B **66**, 073202 (2002).

[105] L.G. Wang and A. Zunger, Phys. Rev. Lett. **90**, 25 (2003).

[106] H.S. Kang, B. Du Ahn, J.H. Kim, G.H. Kim, S.H. Lim, H.W. Chang, and S.Y. Lee, Appl. Phys. Lett. **88**, 202108 (2006).

[107] Y. Yan, M.M. Al-Jassim, and S. H. Wei, Appl. Phys. Lett. **89**, 181912 (2006).

[108] H.S. Kang, B. Du Ahn, J.H. Kim, G.H. Kim, S.H. Lim, H.W. Chang, and S.Y. Lee, Appl. Phys. Lett. **88**, 86 (2006).

[109] O. Volnianska, P. Boguslawski, J. Kaczkowski, P. Jakubas, a. Jezierski, and E. Kaminska, Phys. Rev. B **80**, 245212 (2009).

[110] B. Du Ahn, H.S. Kang, J.H. Kim, G.H. Kim, H.W. Chang, and S.Y. Lee, J. Appl. Phys. **100**, (2006).

[111] I.S. Kim, E. K.K. Jeong, D.Y. Kim, M. Kumar, and S.-Y.Y. Choi, Appl. Surf. Sci. **255**, 4011 (2009).

[112] W. Bin, Z. Yue, M. Jiahua, and S. Wenbin, Appl. Phys. A **94**, 715 (2009).

[113] W. Jing-Wei, B. Ji-Ming, L. Hong-Wei, S. Jing-Chang, Z. Jian-Ze, H. Li-Zhong, L. Ying-Min, and D. Guo-Tong, Chinese Phys. Lett. **25**, 3400 (2008).

…….ଓଓ…….

Chapter

2

PREPARATION AND CHARACTERIZATION OF TRANSPARENT AND CONDUCTING TIN OXIDE THIN FILMS USING CHEMICAL SPRAY PYROLYSIS

Contents

2.1 Introduction

Intense research is going on all around the globe for developing an economically alternative material to substitute the use of tin doped indium oxide (ITO) in energy applications[1–3]. ITO coated substrates are the major component in thin film photovoltaics, digital displays, and touch screen sensors[1,4–8]. The ever increasing rate of use of modern touch sensitive digital displays keeps the demand for ITO high. The increased demand for ITO as well as scarcity of elemental indium (raw material to produce ITO) is the real reason for the increase in cost for such devices. To develop affordable solar cells, ITO substrates should be replaced with TCO having similar/better properties. Two prominent candidates falling under this category are ZnO and SnO_2[1,3,5]. But for photovoltaic applications, other than high transmittance and

conductivity, the TCO material should possess high thermal, chemical and mechanical stability[3,9], because, the deposition of thin film solar cells usually involves high-temperature processing steps and the resulting device has to be used in outdoor weather conditions.

Aim of the present work is to develop an n-type TCO material, which can probably replace the costly ITO for solar cells and other energy applications. Among ZnO and SnO_2, the latter possess high thermal, chemical and mechanical stability[10–12]. Hence for the development of n-type TCO, the material selected is SnO_2. The material deposition technique should be economical and scalable too. Therefore automated chemical spray pyrolysis (CSP) technique is employed as deposition technique for the present study as it is simple, economical and scalable process suitable for the roll to roll production process.

2.2 Deposition technique

Well-developed deposition techniques are available for the fabrication of thin films and devices. The deposition techniques are broadly classified as 'physical' and 'chemical' processes. Among these, chemical routes are relatively simple and economical; out of chemical processes, CSP is selected here for the deposition of SnO_2 thin films. As stated earlier, the technique is a simple, economical and scalable process, as it does not require vacuum[13]. This process can be utilized for the deposition of a number of organic and inorganic materials onto a variety of substrates such as soda-lime glass, quartz, silicon wafer, metals and alloys, ceramics etc. An important criteria for a material to be selected as a substrate in spray pyrolysis is its temperature tolerance.

In spray pyrolysis, films are deposited by spraying a solution of the constituents onto a preheated substrate, where the constituents react themselves or with the surrounding atmosphere to yield the specific thin film. Composition of the films can be easily controlled by changing the concentration of precursors in the solution. Doping is also an easy procedure as soluble salt of dopants can be added to the precursor solution[14,15].

2.3 Effect of various deposition parameters

In CSP, properties of the deposited films is controlled by various factors; of which major parameters are substrate temperature, selection of precursors and solvents, precursor concentration, spray rate etc. This chapter describes the optimization of each of these parameters for obtaining transparent and conducting SnO_2 thin films. Several groups have reported the deposition of SnO_2 thin films by CSP using different precursors such as chlorides or organometallic compounds of Sn[16–24]. Use of water, alcohols, and a mixture of these two as the solvents has been suggested by various reports[25,26]. Our aim is the economical production of high-quality TCO thin films using environment-friendly materials. Hence use of organometallic compounds is ruled out and stannic chloride ($SnCl_4.5H_2O$) is selected as the precursor for Sn. A low molecular weight alcohol is used as the solvent. (**Patent protected data**.)

2.4 Deposition of SnO_2 thin films by optimizing the substrate temperature

For the deposition of thin film of a compound through CSP, there exists a window of substrate temperature at which films with desirable properties are formed. In order to identify the optimum substrate temperature, SnO_2 films

were deposited by varying substrate temperature from 375^0C to 500^0C in steps of 25^0C. The samples were named as T-375, T-400, T-425, T-450, T-475 and T-500. Normal soda lime glass (SLG) of thickness 1 - 1.2mm was used as the substrate. The substrates were ultrasonically cleaned using acetone followed by rinsing with demineralized water and dried in a hot air current. After cleaning, these substrates were heated to a required temperature by keeping over a hot plate. Temperature was controlled and maintained at appropriate value by a proportional–integral–derivative (PID) temperature controller with k-type thermocouple inserted beneath the heater surface. After the substrates were heated to the desirable temperature, 100ml of the precursor solution was sprayed onto the hot substrate at the dispensing rate of 7ml/min. The distance between the spray nozzle and substrate was maintained at 20cm. Scanning area of the spray head was fixed at 18cm x18cm.

The structural characterization of the deposited films was carried out by X-ray diffraction (XRD) technique. In XRD, when the X-rays incident on the samples satisfy the Braggs diffraction condition, ($n\lambda = 2d\sin\theta$, where n is the order of the diffraction, λ is the wavelength of X-ray, θ is the Bragg angle and d is the interplanar spacing), it gets diffracted and a detector records the pattern. X-ray diffractograms [obtained by employing Rigaku (Model No: D. Max.C) X-ray diffractometer, using Cu-Kα line with Ni filter (30kV and 20mA),(λ=1.54Å)] of the SnO_2 thin films, deposited at different substrate temperatures are shown in Figure 2.1.

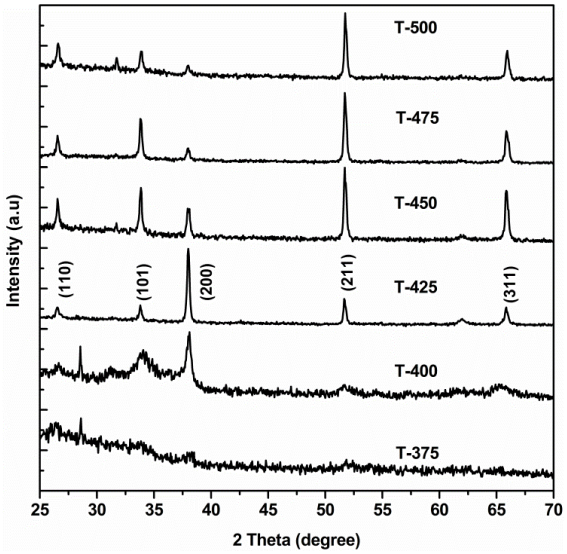

Figure 2.1. XRD pattern of SnO_2 thin films prepared at different substrate temperatures

From the Figure 2.1, it is observed that all the films are polycrystalline in nature and all the peaks matched with the characteristic peaks of tetragonal structure of rutile tin oxide (ICDD card number 041- 1445). Crystallinity of the films prepared at 375^0C is very low and films with better crystallinities are obtained for higher substrate temperatures. The SnO_2 films deposited at 400^0C and 425^0C is preferentially orientated along (200) plane and the preferential orientation is shifted to (211) plane for the films prepared at a substrate temperature of 450^0C onwards. It is reported that (200) plane is a low density plane that is linked to oxygen vacancies in the film[27]. For a particular precursor concentration, films with oxygen vacancies grow only up to a particular substrate temperature and at higher temperatures, Sn salt in the precursor will undergo more oxidation with less number of oxygen vacancies. Better electrical conductivity can be expected from films with more number of oxygen vacancies. Grain size of the films is calculated using Scherer formula and its variation for different deposition temperatures is depicted in Figure 2.2. Grain size of the films prepared at 400^0C is about 17nm and increases to 30nm for the films deposited at a substrate temperature of 425^0C onwards.

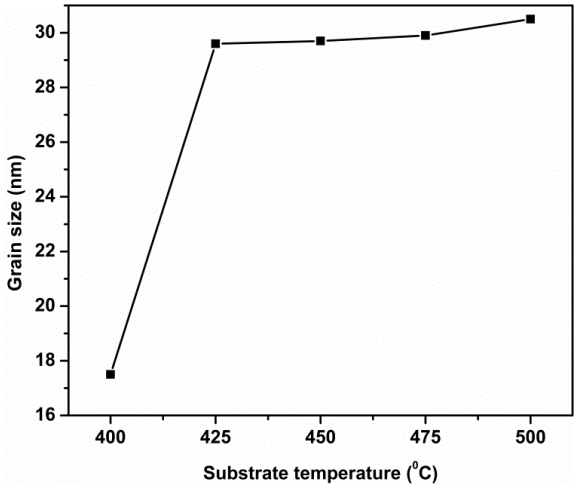

Figure 2.2. Grain size of SnO_2 films prepared at different substrate temperatures

Important parameters for a TCO material are its sheet resistance and transmittance in the visible region. Sheet resistance and transmission spectra of the SnO_2 thin films deposited at different temperatures were measured [Figure 2.3.(a) and Figure 2.3.(b)] using National Instruments PXI-4130 SMU and UV–Vis–NIR spectrophotometer (Model No: Jasco-V-570). It is evident that substrate temperature has a large impact on the sheet resistance of the deposited films.

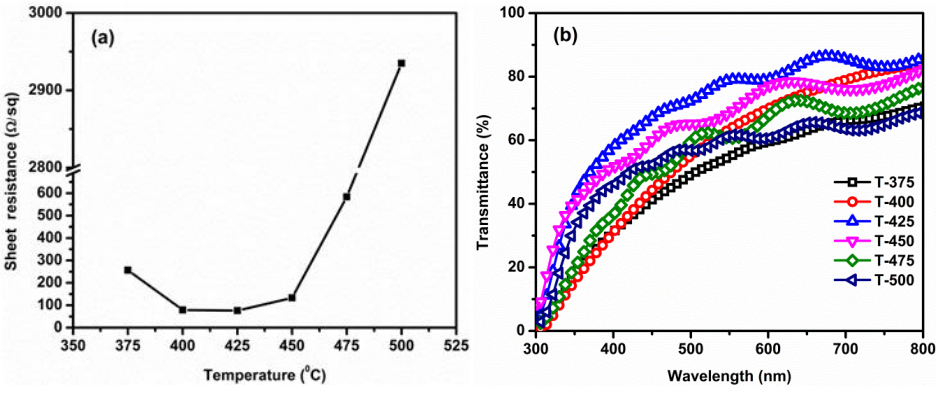

Figure 2.3. Variation of (a) sheet resistance and (b) transmittance of SnO_2 thin films with substrate temperature

Table 2.1. Grain size, sheet resistance and transmittance of SnO_2 thin films prepared at different substrate temperatures

Substrate Temperature (^{0}C)	Avg. Grain size (nm)	Sheet resistance (Ω/sq)	Transmittance in 400 nm – 800 nm (%)
375	--	257	31 – 71
400	17.5	79	31 – 84
425	29.6	76	58 – 86
450	29.7	133	51 – 82
475	29.9	584	37 – 77
500	30.5	2935	46 – 69

Sheet resistance is least (76Ω/sq) for films deposited at 425^{0}C, while optical transmittance of the deposited films progressively increases with increase in substrate temperature from 375^{0}C to 425^{0}C and decreases thereafter. Films deposited at a substrate temperature of 425^{0}C exhibit maximum transmittance. At lower temperatures, thickness of the films will be higher and this may be the possible reason for the reduction in transmittance of the films prepared at temperatures below 425^{0}C. The increase in temperature favors the formation of films with lower thickness, which should eventually lead to films with higher transmittance. But on contrary to this assumption, films prepared at temperatures higher than 425^{0}C shows a decrease in transmittance. At optimum substrate temperature, pyrolysis of the precursor occurs at the substrate surface and results in the formation of uniform thin films. But at temperatures higher than the optimum temperature, pyrolysis of the droplets may occur before reaching the substrate surface and will result in deposition of piles of materials. Therefore non-uniform films with increased surface roughness and reduced transmittance is formed over the substrates. Increase in sheet resistance is also attributed to the non-uniform formation of the films at higher temperatures. The variation of grain size, sheet resistance and transmittance in the range 400nm to

800nm with substrate temperature are given in Table 2.1. In this study, the optimum substrate temperature for depositing SnO_2 films with low sheet resistance and good transmittance is observed as 425^0C and is used for further optimization of SnO_2 thin film deposition.

2.5 Deposition of SnO_2 thin films by optimizing concentration of the precursor solution

In order to optimize concentration of precursor solution, which plays a vital role in the properties of the thin films, SnO_2 thin films were deposited by varying molar concentration of the precursor from 0.1M to 0.3M in steps of 0.05M. 100ml of the precursor solution was sprayed onto the substrate kept at the optimized substrate temperature of 425^0C at a spray rate of 7ml/min. The samples were named as C-1, C-1.5, C-2, C-2.5 and C-3.

Figure 2.4 shows the XRD pattern of tin oxide films prepared by varying the precursor solution concentration. The preferential orientation of the films prepared using 0.1M solution is along (101) plane of rutile SnO_2 and it changes to (200) plane for films prepared using higher precursor concentrations. It is observed that for films prepared using precursor concentration 0.25M or higher, intensity of the peak corresponding to (200) plane decreases and an unknown broad peak appears. However, the grain size is found to be decreasing in a step-like manner with increase in molarity (Figure 2.5). The decrease in grain size and crystallinity is evident from the XRD pattern for concentrations above 0.2M. The possible reason for the decrease in crystallinity with increase in precursor concentration is this: at higher precursor concentrations, the substrate temperature may not be adequate to oxidize enough salt molecules in precursor and that can result in the formation of films with reduced crystallinity.

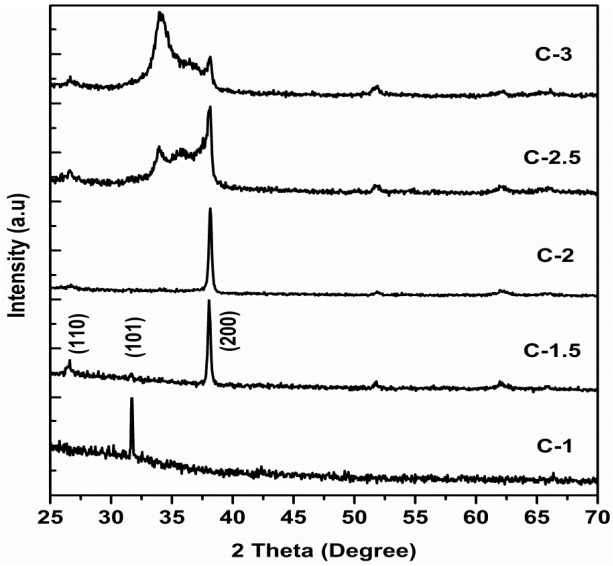

Figure 2.4. XRD pattern of SnO_2 thin films prepared using different precursor concentrations

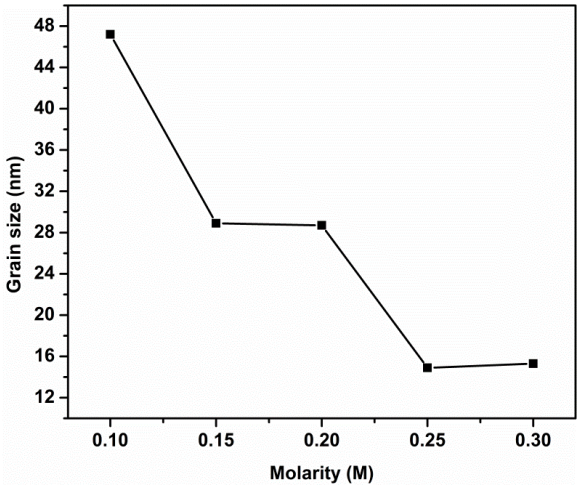

Figure 2.5. Grain size of SnO_2 thin films prepared using different precursor concentrations

The sheet resistance of the films showed a decreasing tendency with increase in precursor concentration [Figure 2.6.(a)]. Transmittance is lower for films prepared using high precursor solution concentrations and is higher for the films prepared using lower precursor concentration [Figure 2.6.(b)]. But

the transmittance of the films remained almost similar for the films prepared at moderate concentrations. The decrease in sheet resistance and transmittance can be attributed to the possible increase in thickness of the films with increase in precursor concentration. The variation of grain size, transmittance in the range 400nm to 800nm and sheet resistance with precursor concentration is given in Table 2.2.

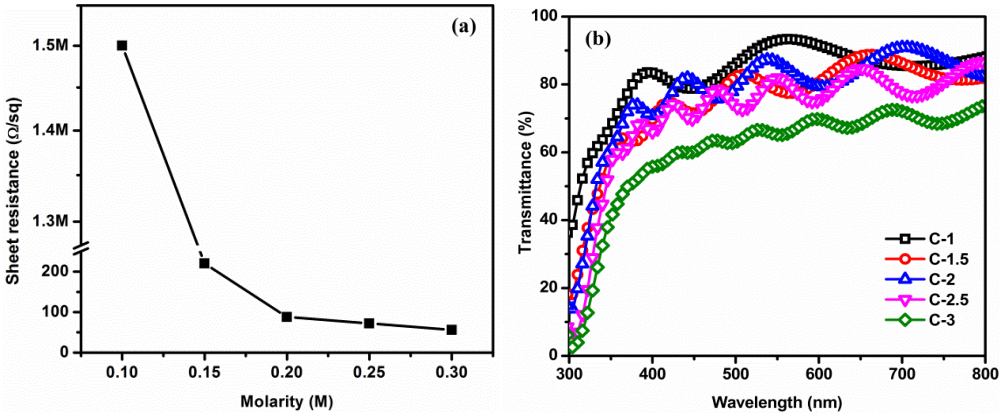

Figure 2.6. Variation of (a) sheet resistance and (b) transmittance of SnO_2 thin films with different precursor concentrations

Table 2.2. Average grain size, sheet resistance, and transmittance of SnO_2 thin films prepared using different precursor concentrations

Molarity of $SnCl_4$ (M)	Avg. Grain Size (nm)	Sheet resistance (Ω/sq)	Transmittance in 400nm – 800nm (%)
0.10	47.2	1.5×10^{6}	78 – 93
0.15	28.9	2.2×10^{2}	70 – 88
0.20	28.7	8.8×10^{1}	70 – 90
0.25	14.9	7.2×10^{1}	66 – 87
0.30	15.3	5.6×10^{1}	56 – 74

Here the optimum precursor concentration was fixed by considering both transmittance and sheet resistance of the deposited films. Films deposited with 0.2M precursor concentration show an average transmittance of 80% and sheet resistance of 88Ω/sq. Hence for further optimization of SnO_2 thin film deposition, precursor concentration of 0.2M was selected.

2.6 Deposition of SnO_2 thin films by optimizing spray rate

Another critical parameter in CSP for the formation of thin films is "spray rate". It is the rate at which the precursor solution is dispensed to the spray head to mix with the air to form fine droplets. Films were deposited by fixing the molarity of the precursor at 0.2M and the substrate temperature at 425^0C from the previous studies. Here 100ml of the precursor solution was sprayed onto the substrate at different spray rates, from 3ml/min to 9ml/min in steps of 2ml/min. The samples were named as S-3, S-5, S-7 and S-9.

Figure 2.7 shows the X-ray diffraction patterns of SnO_2 thin films prepared at different spray rates. All the films are polycrystalline in nature and there is no change in preferential growth from (200) plane of rutile SnO_2 with spray rate. It is already confirmed that for films prepared with 0.2M concentration at 425^0C, growth is along (200) plane. The intensity of the (200) peak is low for the films prepared at 9ml/min. Grain size is calculated using Scherer formula and it is observed that crystallinity and grain size are better for films prepared at lower spray rates. Grain size and thickness of the films with spray rate is shown in Table 2.3.

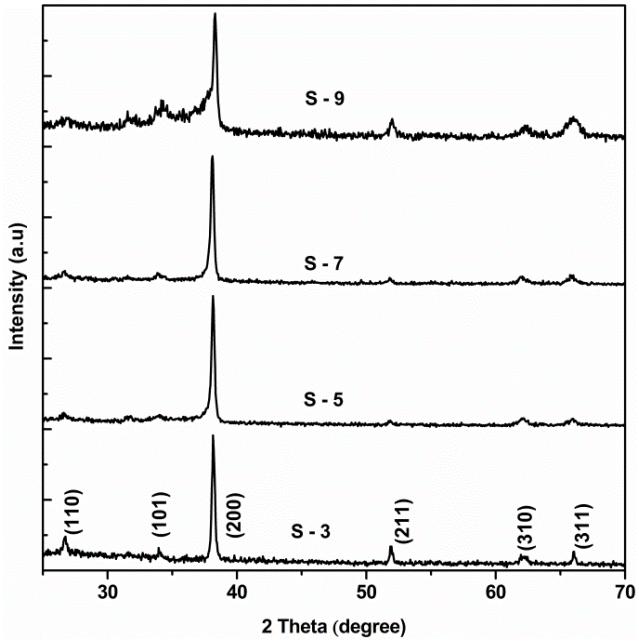

Figure 2.7. XRD pattern of SnO_2 thin films prepared by varying spray rate

Table 2.3. Grain size and thickness of SnO_2 thin films prepared by varying spray rate

Sample	Spray rate (ml/min)	Avg. Grain Size (nm)	Thickness (nm)
S – 3	3	28.9	450
S – 5	5	28.8	510
S – 7	7	27.6	540
S – 9	9	24.3	590

Thickness of the films was measured using stylus profiler (Dektak 6M), in which a sharp diamond tipped stylus was moved over the film edge. The stylus is mechanically coupled to the core of a linear variable differential transformer (LVDT) and any change in stylus position will change the core position of the LVDT and will produce corresponding electrical signal. These electrical signals are converted into digital format and the thickness values are measured from it. It is observed that the average thickness of the films increased from 450 ± 20nm to 590 ± 40nm with increase in spray rate and is shown in Table 2.3.

Electrical properties of the films were measured using Ecopia HMS 5300 Hall measurement system. Hall Effect measurement of semiconductors can give important information about its electrical properties like carrier concentration, conductivity type, resistivity and mobility of carriers. When a strong uniform magnetic field is applied perpendicular to the current flow direction, a voltage is developed in the sample perpendicular to both the applied current and magnetic field and this phenomenon is known as Hall Effect. The voltage developed is known as the Hall voltage (V_H) and is proportional to the carrier mobility and its sign depends on the type of majority carriers. Carrier concentration can be determined from the Hall voltage and along with the conductivity measurement, mobility can be determined. Here the measurement was done using the four probe

Van der Pauw configuration with a 0.57T magnetic field produced by permanent magnets. The instrument is capable of sourcing current in 1nA to 20mA. Samples were prepared by cutting them in square shape and applying small electrodes at the four vertices. Gold plated electrodes were used to take electrical contacts from the samples.

From Table 2.4, it is clear that the increase in spray rate has direct impact on electrical properties of the films. Carrier concentration and mobility are found to be linearly increasing with increase in spray rate. It is noted that resistivity and sheet resistance of the films decreased by two orders at high spray rates. The variation in sheet resistance of the films with spray rate is shown in the Figure 2.8.(a). All the films are found to be n-type in nature.

The decrease in resistivity and sheet resistance at higher spray rates can be explained as follows: the precursor content in air-solution mixture is higher at high spray rate and as a result, the quantity of precursor falling on substrate per unit area per unit time is more than that at lower spray rates. Increased quantity of precursor can lead to the formation of films with higher metal concentrations. The resulting films will have non-stoichiometric defects due to excess metal which ultimately lead to lower resistive films with higher carrier concentrations with a compromise in crystallinity. This is clearly evident from Hall measurement and XRD analysis.

Table 2.4. Electrical and optical properties of SnO_2 thin films prepared by varying spray rate

Sample	Resistivity (Ω.cm)	Mobility ($cm^2/V.s$)	Carrier concentration (cm^{-3})	Conductivity type	Transmittance in 400nm – 800nm (%)
S – 3	1.03×10^{-1}	7.2	8.4×10^{18}	n	65 – 91
S – 5	1.43×10^{-2}	10.5	4.7×10^{19}	n	65 – 90
S – 7	4.94×10^{-3}	15.2	8.3×10^{19}	n	66 – 86
S – 9	3.39×10^{-3}	16.8	1.1×10^{20}	n	66 – 88

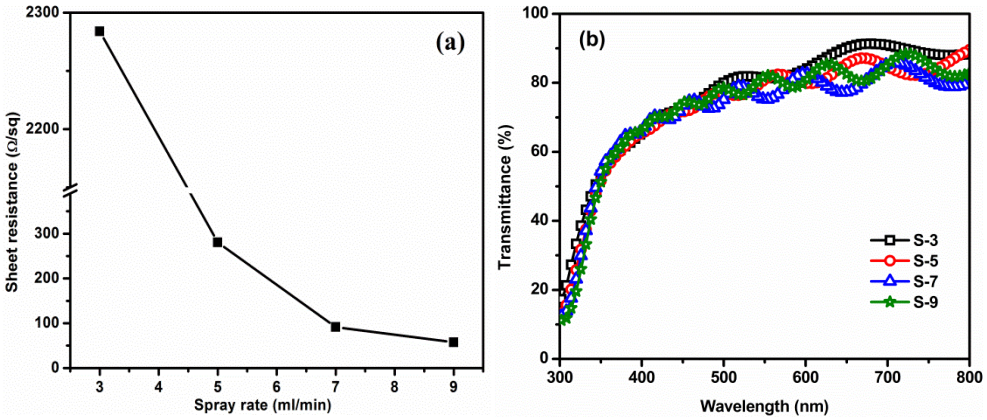

Figure 2.8. Variation of (a) sheet resistance and (b) transmittance of SnO_2 thin films with spray rate

Transmission spectra of the films are shown in Figure 2.8.(b). Average transmittance in the visible spectrum is greater than 75%. Transmittance is slightly better for the films prepared at lower spray rates, because of the low thickness of the films. The air pressure used to atomize the precursor solution in the spray head is constant for all spray rates. Therefore at lower spray rates, mixing of the solution with air will be more and it can result in the formation of smaller droplets. Also the substrate temperature used here is enough for the re-evaporation of some of these small droplets reaching the substrate and thus film with lower thickness is formed. But at higher spray rates, the larger size of the droplets will compensate re-evaporation of the material and result in the formation of films with higher thickness.

It is observed that with increase in spray rate, transmittance in the IR region decreases and is shown in Figure 2.9. The decrease in transmittance in IR region is due to the shift in plasma frequency to the higher energy regions. The plasma frequency is given by the equation 2.1.

$$\omega_p = \sqrt{\frac{4\pi n e^2}{m}} \qquad 2.1$$

Where ω_p is the plasma frequency, n is the number density of electrons, e is the charge of an electron and m is the effective mass.

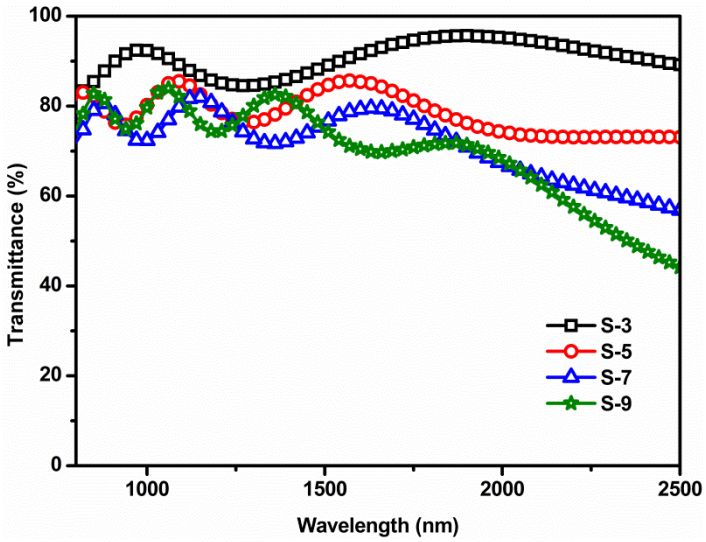

Figure 2.9. Transmission spectra in IR-NIR region of SnO_2 thin films prepared by varying spray rate

From equation 2.1, it is clear that plasma frequency is directly related to the free carrier density and shifts to high energy regions with increase in carrier concentration. Frequencies below the plasma frequency are reflected back by the material due to free carrier absorption[26,28] and is the reason for the decrease in transmittance in IR region with increase in spray rate. Increase in carrier concentration with spray rate is observed from Hall measurement also.

Surface morphology of the films deposited at different spray rates was analyzed using atomic force microscopy (AFM). In AFM, a cantilever beam fixed with a sharp tip of diameter less than 10nm scans the selected portion of the sample surface. AFM can work either in contact mode or in non-contact mode. For the present analysis, 'Nanosurf easyScan 2' table top AFM was used, which operates in contact mode only. When the cantilever beam moves over the sample surface, it deflects due to the surface - tip interaction and this deflection

is measured by the reflection of a laser beam from the back of the cantilever. The digitalized data is utilized to create topography of the sample surface.

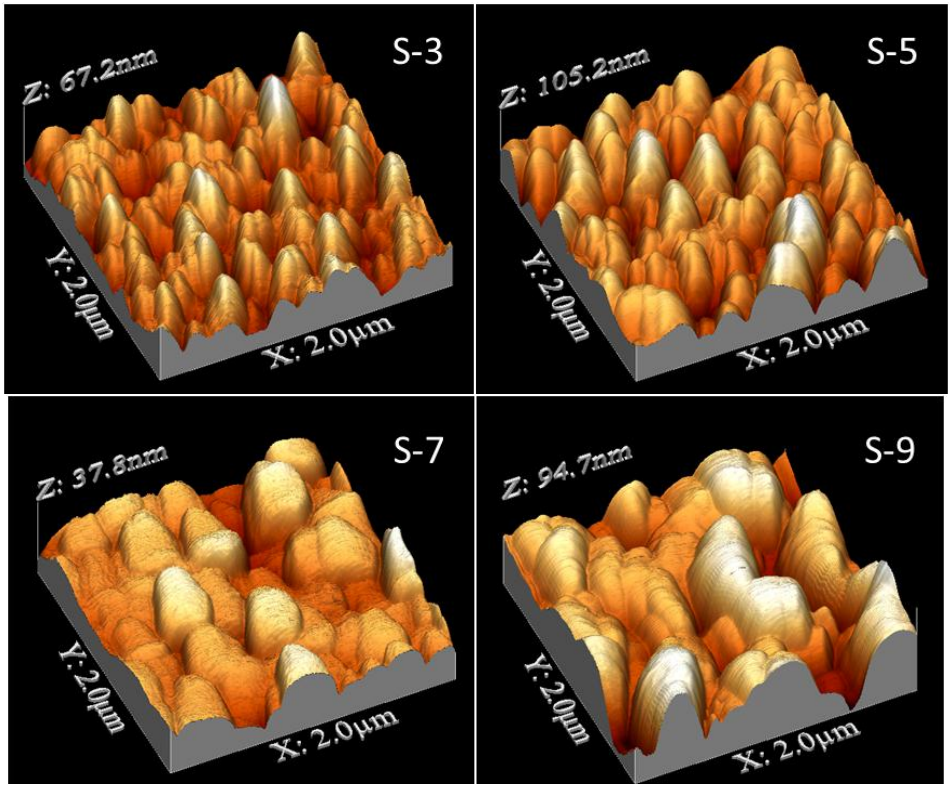

Figure 2.10. AFM images of SnO_2 thin films prepared by varying spray rate

Figure 2.10. shows three-dimensional AFM images of SnO_2 films deposited by varying spray rate. It is clear that the root mean square (RMS) value of surface roughness of the films increases linearly with increase in spray rate. RMS surface roughness of the samples deposited at 3ml/min is observed to be 14nm and it increases to 21nm, 26nm and finally to 33nm when the spray rate is increased to 5ml/min, 7ml/min and 9ml/min respectively. Considerable variations in surface morphology are observed for the films deposited by varying spray rate. With increase in spray rate, surface morphology of the deposited films changes from small sharp structures to

large blunt structures. This can be attributed to the positive correlation between droplet size and spray rate. At lower spray rates, the formation of small droplets of precursor solution promotes the growth of films with small sharp structured morphology and lower surface roughness. But with increase in spray rate, droplet size increases, and the resulted films are with large blunt morphology and with high surface roughness.

SnO_2 films deposited by varying spray rate showed clear improvement in electrical properties and shift in plasma frequency to higher energy regions. This is attributed to the increase in carrier concentration with increase in spray rate due to the increase in metal excess non-stoichiometric defects. X-ray photoelectron spectroscopy (XPS) was employed to analyze the composition and stoichiometry of the films deposited with various spray rates. XPS is a surface sensitive quantitative analysis technique and the basic principle behind XPS is photoelectric effect. XPS spectra of samples are obtained by irradiating the sample surface with a beam of X-rays and by measuring the number and kinetic energy of the photoelectrons produced simultaneously. The binding energy of each of the emitted electrons can be calculated using the following equation.

$$E_{binding} = E_{photon} - (E_{kinetic} + \phi) \qquad 2.2$$

where $E_{binding}$ is the binding energy (BE) of the electron, E_{photon} is the energy of X-ray used, $E_{kinetic}$ is the kinetic energy (KE) of electrons and ϕ is the work function. The work function depends on both the sample and spectrometer.

Kratos Analytical AMICUS spectrometer was employed for the present study. The XPS is equipped with a nonmonochromatic Mg Kα/Al Kα dual anode X-ray source and for the present study Mg Kα (1253.6eV) anode is used at 120W (12KV & 10mA). Unlike the common hemispherical electron analyzer,

this system is equipped with a DuPont type energy analyzer, which can be operated at three different pass energies (25eV, 75eV & 150eV) using electron transfer lens. The main chamber is maintained at high vacuum of pressure less than $2x10^{-6}$Pa. The system is equipped with a high-speed Ar ion sputtering gun (2KV, 100mA, 10^{-3}Pa) and is used for the surface cleaning of the samples from atmospheric contaminants and for etching the samples for depth profile studies. The spectrometer is calibrated by measuring Ag $3d_{5/2}$ (368.2eV) line.

The samples were mounted on stainless steel holders using conducting carbon tape. Prior to the measurement, the samples were subjected to Ar ion sputtering in order to remove any surface contamination. The resolution of the analyzer is set at 25meV. Binding energy values of the elements present in the samples were calibrated and calculated on the basis of C 1s peak at 284.6eV of adventitious Carbon. Main core level photoemission spectra (with 25meV energy increment) of C, Sn and O were recorded and relative atomic concentrations of the elements were determined from appropriate core level integrated peak areas and sensitivity factors provided by the Kratos analysis Vision 2.2. Shirley background subtraction was used for the calculation of relative atomic concentrations. Results of composition analysis of the films using XPS are given in Table 2.5.

Table 2.5. Composition of SnO_2 thin films prepared by varying spray rate

Sample	Atomic % of Sn	Atomic % of O	Sn/O ratio
S-3	32.37	67.63	0.478
S-5	33.95	66.05	0.514
S-7	34.27	65.73	0.521
S-9	36.58	63.42	0.577

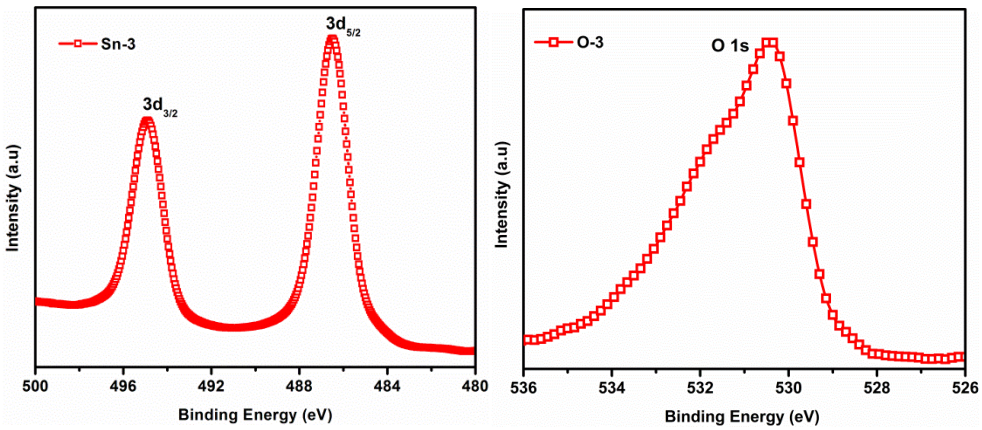

Figure 2.11. Core level peaks of Sn 3d and O 1s of SnO_2 thin films prepared at 3ml/min

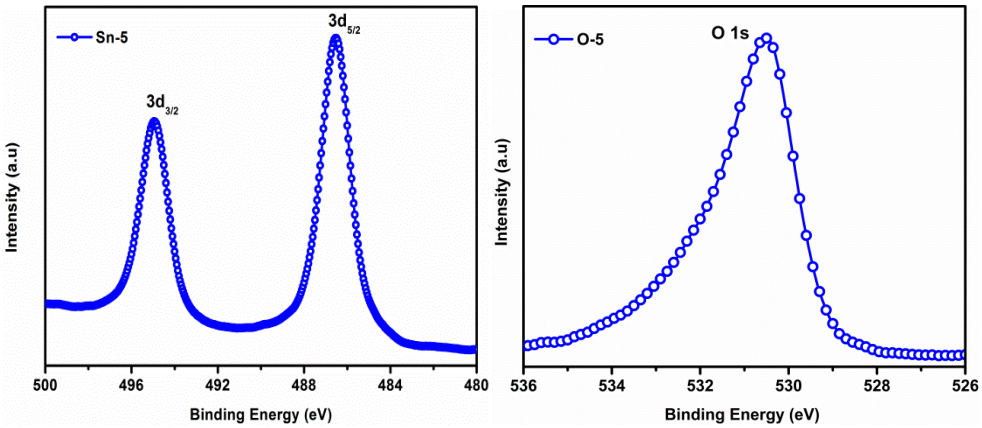

Figure 2.12. Core level peaks of Sn 3d and O 1s of SnO_2 thin films prepared at 5ml/min

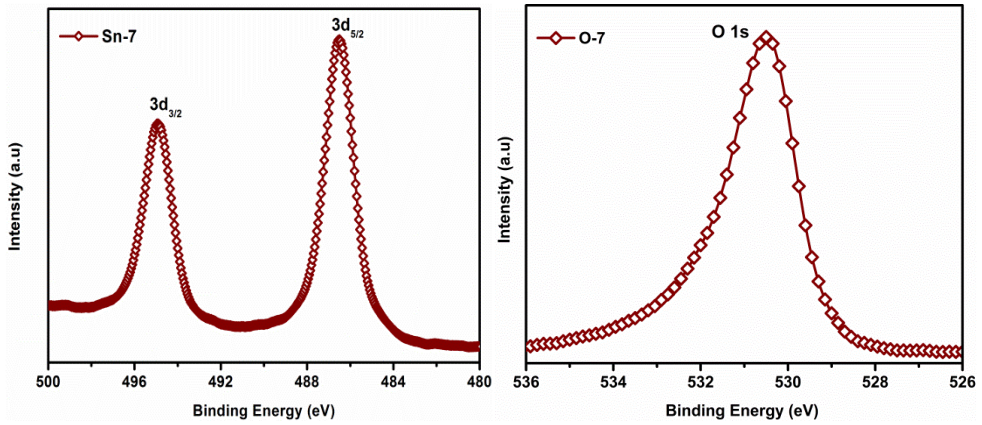

Figure 2.13. Core level peaks of Sn 3d and O 1s of SnO_2 thin films prepared at 7ml/min

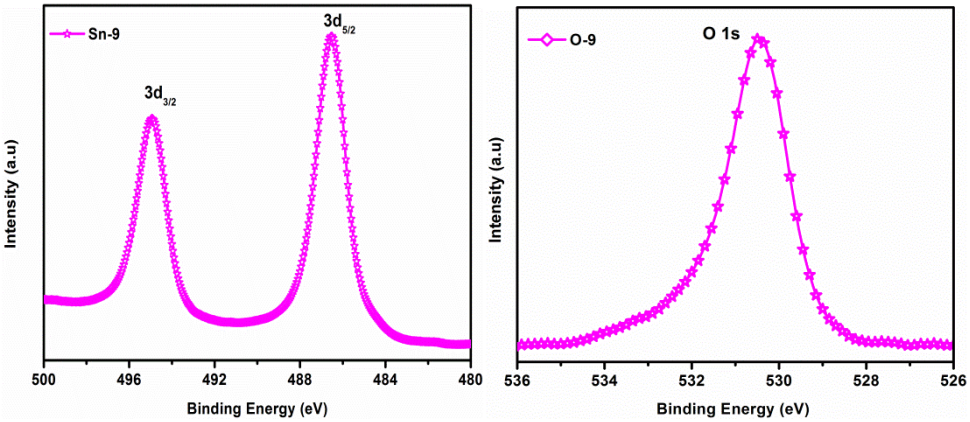

Figure 2.14. Core level peaks of Sn 3d and O 1s of SnO_2 thin films prepared at 9ml/min

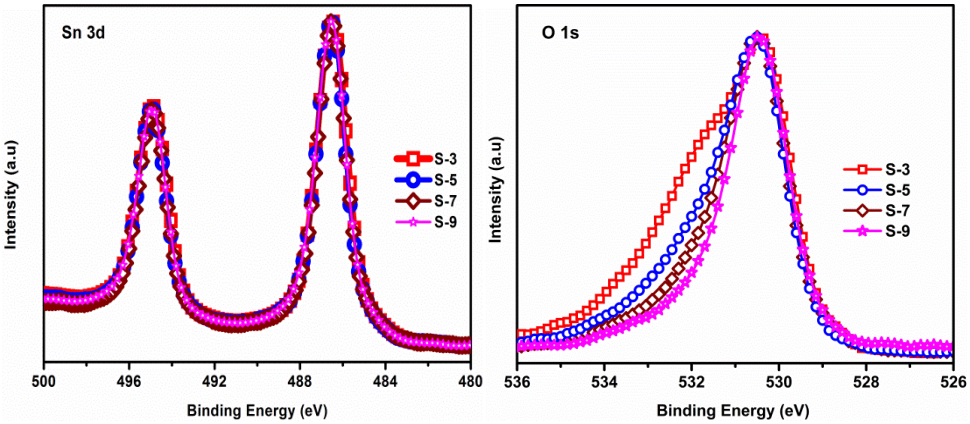

Figure 2.15. Comparison of core level peaks of Sn 3d and O 1s of SnO_2 thin films prepared by varying spray rate

Chemical states of Sn and O in the films were analyzed and it is observed that there is no change in the shape or position for Sn 3d core level peaks. Sn 3d core level peaks are at 486.4 ±0.2eV and 494.8 ±0.2eV, separated by 8.4eV, which is corresponding to the chemical state of Sn in SnO_2[20]. The chemical states of Sn in all the films remain the same irrespective of the spray rate. XPS core level peaks corresponding to Sn and O for the films prepared at 3ml/min, 5ml/min, 7ml/min and 9ml/min are shown in Figures 2.11.to 2.14. Figure 2.15 shows the comparison of core level peaks of Sn 3d and O 1s of SnO_2 films prepared at different spray rates.

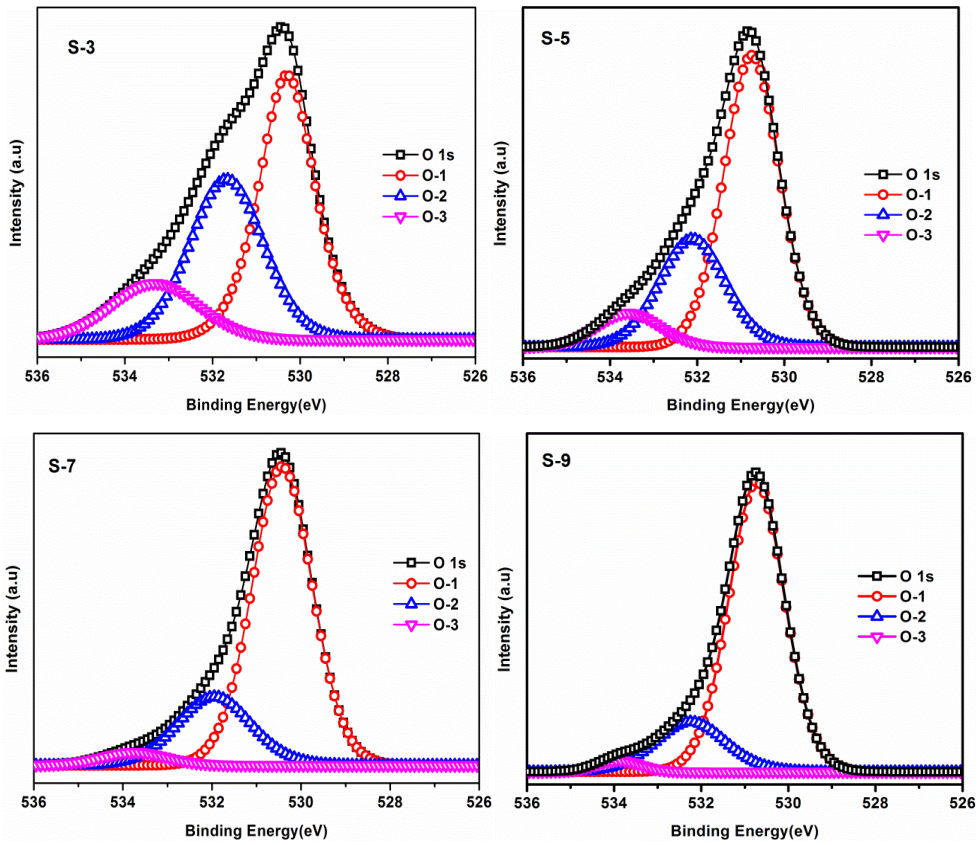

Figure 2.16. Deconvoluted components of O 1s peaks of SnO_2 thin films prepared at 3ml/min, 5ml/min, 7ml/min and 9ml/min

From the XPS analysis, it is observed that the O 1s core level peak in the films become narrower with increase in spray rate and the deconvoluted spectrum shows three component peaks. The deconvoluted components of O 1s peak of SnO_2 thin films prepared at different spray rates are shown in Figure 2.16. The three components of O 1s level are at 530.3eV, 531.8eV, and 533.5eV and are represented as O-1, O-2 and O-3 respectively. The peak O-1corresponds to O^{2-} state of oxygen in SnO_2 lattice. Peaks O-2 and O-3 correspond to the O in non-stoichiometric oxides and hydroxyl groups or weakly adsorbed oxygen respectively[29,30]. The relative concentration of each oxygen component is given in Table 2.6. It is clear that the amount of unwanted O species is reduced in the films prepared at 9ml/min.

Table 2.6. Relative concentration of oxygen components in SnO_2 thin films

Oxygen components	Binding energy (±0.2eV)	Relative concentration (%)			
		Sample S-3	Sample S-5	Sample S-7	Sample S-9
O-1	530.3	48	63.7	75.4	80.2
O-2	531.8	36.7	27.8	21.1	17.3
O-3	533.5	15.3	8.5	3.6	2.5

Hence metal-excess films with reduced quantity of detrimental oxygen components (such as interstitial and chemisorbed oxygen species) were obtained at higher spray rate. This result supports the observed changes in electrical and optical properties of SnO_2 thin film with spray rate.

Conclusion

In this chapter, the effects of some important spray parameters, such as substrate temperature, precursor concentration and spray rate on the formation and properties of tin oxide thin films were studied in detail. From the temperature variation studies, it is established that 425^0C is the optimum temperature for the films with good crystallinity, lower sheet resistance, and higher optical transmittance. Similarly, precursor concentration and spray rate were optimized as 0.2M and 9ml/min respectively. The best SnO_2 thin films deposited at optimized spray parameters showed a sheet resistance of 50Ω/sq (resistivity 3.39×10^{-3}Ω.cm) and average transmittance greater than 75% in the visible region.

References

[1] T. Minami, MRS Bull. 38 (2000).

[2] M. Chen, X. Wang, Y. Yu, Z. Pei, X. Bai, C. Sun, R. Huang, and L. Wen, Appl. Surf. Sci. **158**, 134 (2000).

[3] E. Fortunato, D. Ginley, H. Hosono, and D.C. Paine, MRS Bull. **32**, 242 (2007).

[4] A.M.B. Van Mol, Y. Chae, A.H. McDaniel, and M.D. Allendorf, Thin Solid Films **502**, 72 (2006).

[5] C.I. Bright, 50 Years Vac. Coat. Technol. 38 (2007).

[6] A. Klein, C. Körber, A. Wachau, F. Säuberlich, Y. Gassenbauer, S.P. Harvey, D.E. Proffit, and T.O. Mason, Materials. **3**, 4892 (2010).

[7] G.J. Exarhos and X. D. Zhou, Thin Solid Films **515**, 7025 (2007).

[8] H. Hosono, Thin Solid Films **515**, 6000 (2007).

[9] R.G. Gordon, MRS Bull. **25**, 52 (2000).

[10] T. Fukano and T. Motohiro, Sol. Energy Mater. Sol. Cells **82**, 567 (2004).

[11] P. Veluchamy, M. Tsuji, T. Nishio, T. Aramoto, H. Higuchi, S. Kumazawa, S. Shibutani, J. Nakajima, T. Arita, H. Ohyama, A. Hanafusa, T. Hibino, and K. Omura, Sol. Energy Mater. Sol. Cells **67**, 179 (2001).

[12] G. Sanon, R. Rup, and A. Mansingh, Thin Solid Films **190**, 287 (1990).

[13] N. Naghavi, D. Abou Ras, N. Allsop, N. Barreau, S. Bücheler, A. Ennaoui, C.H. Fischer, C. Guillen, D. Hariskos, J. Herrero, R. Klenk, K. Kushiya, D. Lincot, R. Menner, T. Nakada, C. Platzer-Björkman, S. Spiering, A.N. Tiwari, and T. Törndahl, Prog. Photovoltaics Res. Appl. **18**, 411 (2010).

[14] T.V. Vimalkumar, Highly Conductive and Transparent ZnO Thin Film Using Chemical Spray Pyrolysis Technique : Effect of Doping and Deposition Parameters, Ph.D. thesis, Cochin University of Science and Technology, 2011.

[15] T.V. Vimalkumar, N. Poornima, K.B. Jinesh, C.S. Kartha, and K.P. Vijayakumar, Appl. Surf. Sci. **257**, 8334 (2011).

[16] B. Thangaraju, Thin Solid Films **402**, 71 (2002).

[17] S.Y. Lee and B. O. Park, Thin Solid Films **510**, 154 (2006).

[18] E. Elangovan, S.A. Shivashankar, and K. Ramamurthi, J. Cryst. Growth **276**, 215 (2005).

[19] A.V. Moholkar, S.M. Pawar, K.Y. Rajpure, C.H. Bhosale, and J.H. Kim, Appl. Surf. Sci. **255**, 9358 (2009).

[20] C. Quijada, J.L. Va, F. Vicent, E. Morallo, D.D.I. Textil, E.P.S. De Alcoy, and U.P. De Valencia, J. Appl. Electrochem. **28**, 607 (1998).

[21] A.V. Moholkar, S.M. Pawar, K.Y. Rajpure, C.H. Bhosale, and J.H. Kim, Appl. Surf. Sci. **255**, 9358 (2009).

[22] Y. Wang, T. Brezesinski, M. Antonietti, and B. Smarsly, ACS Nano **3**, 1373 (2009).

[23] A.B. and K.L.C. E. Shanthi, Thin Solid Films **88**, 93 (1982).

[24] A. Smith, J.M. Laurent, D.S. Smith, and J.P. Bonnet, Thin Solid Films **315**, 17 (1998).

[25] A.V. Moholkar, S.M. Pawar, K.Y. Rajpure, S.N. Almari, P.S. Patil, and C.H. Bhosale, Sol. Energy Mater. Sol. Cells **92**, 1439 (2008).

[26] M.J. Atmane B, Achour rahal, Boubaker Benhaoua, Superlattices Microstruct. **70**, 61 (2014).

[27] N. Noor and I.P. Parkin, Jounal Mater. Chem. C **1**, 984 (2013).

[28] Z. Remes, M. Vanecek, H.M. Yates, P. Evans, and D.W. Sheel, Thin Solid Films **517**, 6287 (2009).

[29] H. Xue, Y. Chen, X.L. Xu, G.H. Zhang, H. Zhang, and S.Y. Ma, Phys. E Low-Dimensional Syst. Nanostructures **41**, 788 (2009).

[30] F.M. Amanullah, K.J. Pratap, and V. Hari Babu, Mater. Sci. Eng. B **52**, 93 (1998).

…….ଓଡ଼……

Chapter

3

DEPOSITION OF FLUORINE DOPED TIN OXIDE THIN FILMS AND ITS APPLICATIONS

Contents

3.1. Introduction

The previous chapter of this thesis discusses effect of different spray parameters on the formation and properties of undoped tin oxide thin films. Tin oxide thin films prepared under optimized deposition conditions were showing sheet resistance of 50Ω/sq and average transmittance greater than 75% in the visible region. Even though the sheet resistance is low, for the fabrication of efficient photo voltaic devices, this has to be further reduced to make it comparable with the costly ITO (sheet resistance ~10-15Ω/sq) to find a space in TCO business. It can then possibly substitute ITO, at least in energy sector, for applications such as photovoltaics, low emissivity, heat reflecting/ retaining smart windows etc.

Doping with suitable dopant is one of the possibilities to further reduce the sheet resistance of tin oxide thin films. There are many reports suggesting the effective role of different dopants, among which the role players are fluorine (F)[1–12] and antimony (Sb)[4,13–17]. In CSP technique, doping is easy compared to the other vacuum based deposition techniques. In CSP, doping can be achieved by just adding the corresponding salt containing dopant atom (dopant source) into the precursor solution. Doping concentration can be easily varied by varying the concentration of dopant source[7]. Dopant sources also can be varied in CSP. Only limitation in doping in CSP is the solubility of the dopant source in the precursor solution without precipitation. This can easily achieved by varying the dopant source, solvent for precursors or by adjusting the pH of the solution etc. Among fluorine and antimony, both are well studied dopants for the fabrication of doped tin oxide. Fluorine is selected as the dopant for the present study, because on comparing the cost of pure dopant sources, the compounds of fluorine are cheaper than that of antimony.

3.2. Selection of dopant source

This chapter discusses the effect of different dopant sources as well as doping concentrations on the properties of SnO_2 thin films. Ammonium fluoride (NH_4F) and hydrogen fluoride (HF) were selected as dopant sources and dissolved in suitable solvents. For doping SnO_2 thin films by CSP, different quantities of dopant sources were added to the precursor solution and ultrasonically agitated for 10 minutes to get uniform distribution of the dopants in the precursor. In order to deposit fluorine doped tin oxide (FTO) thin films, concentration of NH_4F or HF was varied in increasing order. The samples were named as pristine a, b, c etc. with increase in fluorine

concentration (**patent protected data)**. In order to fix best dopant source for the deposition of device quality FTO films, the deposited films were characterized as follows.

3.2.1 Structural characterization

XRD spectra of fluorine doped tin oxide thin films using NH_4F and HF as the dopant sources is shown in the Figure 3.1.(a) and Figure 3.1.(b). Pristine and fluorine doped tin oxide samples shows a preferential orientation along (200) plane of rutile SnO_2 structure. However, there is a shift in diffraction peak corresponding to (200) plane with doping which is due to the variation in the ionic radii of oxygen and fluorine. Well defined peaks corresponding to (110), (101), (211), (310) and (301) planes are also observed. It is observed that the intensity of the diffraction peak corresponding to (200) plane decreases with increase in HF concentration and the intensity of peaks corresponding to (110), (101) and (211) planes increases. On NH_4F doping, the grain size of the films is found to be better than the pristine films. But with doping with HF as the dopant source, grain size is observed to be reduced (Figure 3.2). Choices of the dopant sources have definite effects in crystallinity of the deposited films. Crystallinity is improved with fluorine doping with NH_4F as dopant source as compared to that of undoped films and is shown in Figure 3.1.(a). On the other hand, with HF as the dopant source, crystallinity of the films is decreased.

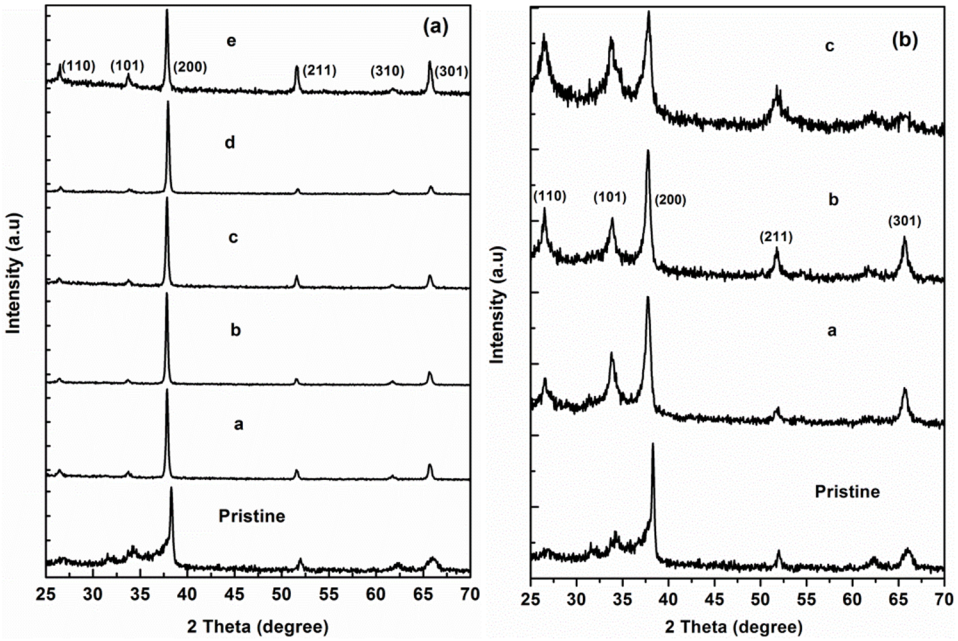

Figure 3.1. XRD pattern of SnO_2 thin films with different concentrations of (a) NH_4F and (b) HF

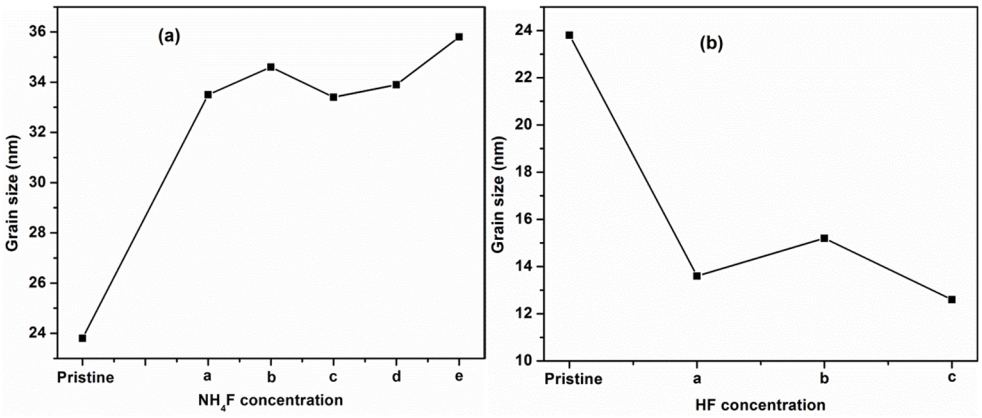

Figure 3.2. Grain size of SnO_2 thin films with different concentrations of (a) NH_4F and (b) HF

3.2.2 Electrical characterization

Sheet resistances of the films with different dopant concentration of NH_4F and HF are shown in Figure 3.3.(a) and Figure 3.3.(b) respectively. In both cases, it is found that up to a particular concentration, sheet resistance of the films got

reduced and after that, the sheet resistance of the film showed an increase in value. The lowest sheet resistance is obtained for films doped with NH_4F and is 6Ω/sq. Role of fluorine is to provide free electrons to the lattice through the substitution of double valent oxygen[7,9]. This results in decrease of sheet resistance with increase in doping concentration up to an optimum level of doping. But after a certain doping level, the excess F can create scattering centers and also can occupy the interstitial sites to act as "charge killers" which result in charge compensation as well as decrease in carrier mobility[4,7,18,19]. Thus the sheet resistance increases after an optimum level of doping concentration.

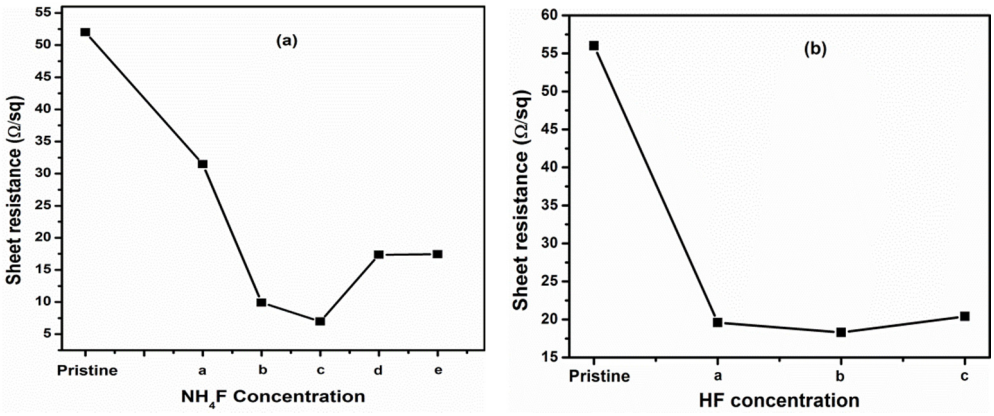

Figure 3.3. Sheet resistance variation of SnO_2 thin films with different concentrations of (a) NH_4F and (b) HF

3.2.3 Optical characterization

Figure 3.4 shows the transmission spectra of films with different dopant sources and dopant concentrations. For the films doped with NH_4F as the dopant source, transmittance is found to be better than that of pristine films (Figure 3.4.(a)). Transmittance and film quality are found to be deteriorating with concentration of HF and it is evident from Figure 3.4.(b).

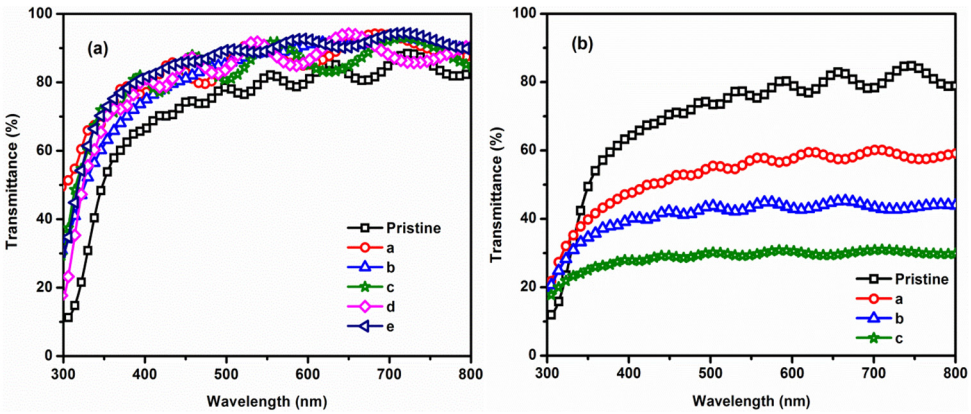

Figure 3.4. Transmission spectra of SnO_2 thin films with different concentrations of (a) NH_4F and (b) HF

Table 3.1. Grain size, sheet resistance and transmittance of SnO_2 thin films prepared with different concentrations of NH_4F

NH4F	Avg. Grain Size (nm)	Sheet resistance (Ω/sq)	Transmittance in 400nm – 800nm (%)
Pristine	23.8	56	65 – 86
a	33.5	31.5	76 – 94
b	34.6	9.9	73 – 97
c	33.4	6.9	77 – 95
d	33.9	17.4	76 – 92
e	35.8	17.8	81 – 94

Table 3.2. Grain size, sheet resistance and transmittance of SnO_2 thin films prepared with different concentrations of HF

HF	Avg. Grain Size (nm)	Sheet resistance (Ω/sq)	Transmittance in 400 nm – 800 nm (%)
Pristine	23.8	56	65 – 86
a	13.6	19.6	47 – 60
b	15.2	18.3	40 – 45
c	12.6	20.4	28 – 31

From the structural, electrical and optical analysis of F doped SnO_2 thin films (Table 3.1 and 3.2), it is clear that best quality films are obtained by incorporating NH_4F in the precursor solution as the dopant source.

3.2.4 Morphological characterization

Surface morphology of the best film was analyzed using AFM and found that the films are uniform in nature and the surface roughness is observed to be 17nm, which is nearly half of as that of undoped films. Field emission scanning electron microscope (FE SEM) image of the surface also proves the uniformity of the films. Cross sectional SEM image of the samples were utilized to find the exact thickness of the films and is found to be 540nm (Figure 3.5).

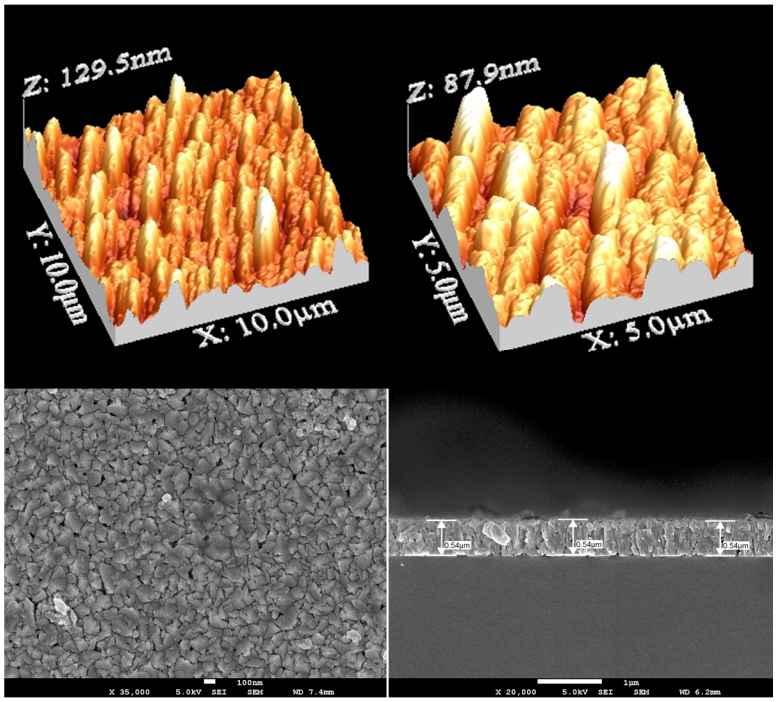

Figure 3.5. Surface morphology and cross section-view of fluorine doped SnO_2 thin film

Table 3.3 shows the comparison of electrical and optical properties of the undoped and fluorine doped tin oxide (FTO) thin films. It is clear that at an optimum level of fluorine doping using NH_4F, electrical and optical properties of tin oxide thin films can be improved significantly.

Table 3.3. Comparison of electrical and optical properties of the undoped and fluorine doped tin oxide thin films.

Sample	Resistivity (Ω.cm)	Mobility (cm^2/V.s)	Carrier concentration (cm^{-3})	Conductivity type	Transmittance in 400nm – 800nm (%)
Pristine	3.39×10^{-3}	16.8	1.1×10^{20}	n	66 – 88
$C_{(NH4F)}$	2.48×10^{-4}	28.7	8.77×10^{20}	n	77 – 95

3.2.5 Compositional characterization

In order to identify the composition of the deposited FTO thin films, XPS depth profile analysis was carried out. From the XPS analysis, it is observed that the elements are uniformly distributed throughout the film. The binding energy peaks of the elements present in the film are shown in Figure 3.6 and the concentration of elements in the film is calculated as Sn-34.8%, O-64.3% and F- 0.9%.

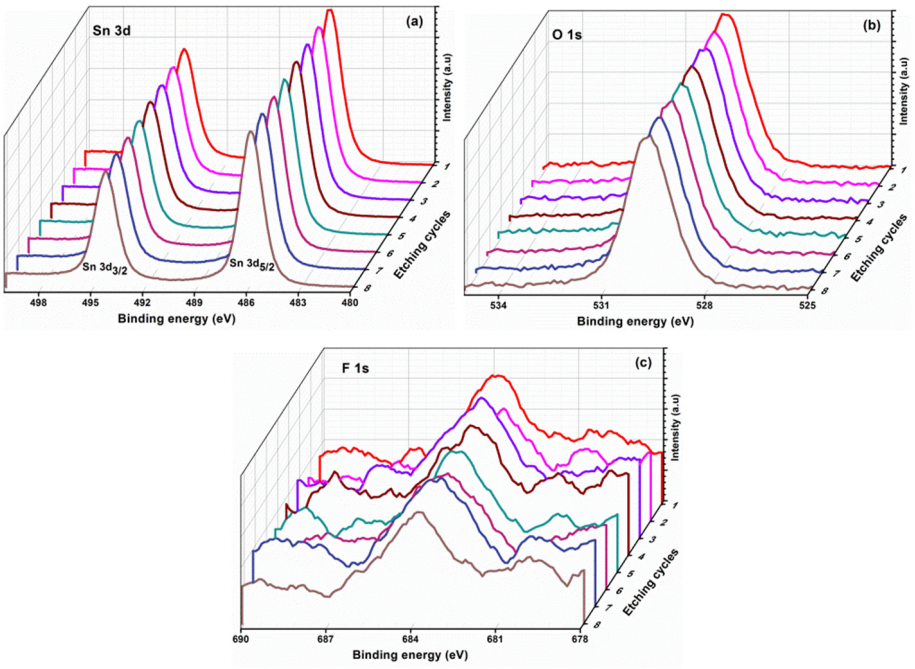

Figure 3.6. Binding energy peaks corresponding to (a) Sn, (b) O and (c) F in FTO thin film

3.3 Quality analysis of the deposited FTO substrates

Major aim of the present work is to develop a TCO as a substitute for ITO to be employed in spray deposited thin film solar cells. For that purpose, in addition to high transmittance and low resistivity, the deposited TCO films should essentially have good thermal stability and uniform spatial distribution of sheet resistance over the film. In solar cell fabrication through CSP, different solar cell layers are deposited over TCO coated glass substrate at elevated temperatures (300^0C to 375^0C) in open atmospheric conditions[20,21,22]. The variation in resistivity/sheet resistance with heating cycles should also be minimal. The prepared FTO films should possess good thermal stability in order to substitute ITO electrodes in the solar cells.

3.3.1 Thermal stability and electrical uniformity

Thermal stability of the prepared FTO films were analyzed by measuring the sheet resistance after heating the films at 400^0C for 20 minutes and subsequently cooling in open atmosphere. The process was repeated a number of times. For comparison, thermal stability of commercially available sputter deposited ITO films was also measured by following the same procedure. The variation in sheet resistance of FTO and ITO films with heating and cooling cycles is shown in Table 3.4.

Table 3.4. Sheet resistance variation of ITO and FTO substrates with heating and cooling cycles at 400^0C

Heating and cooling cycles at 400^0C	Sheet resistance of ITO Ω/sq	Sheet resistance of FTO Ω/sq
0	13	10.8
1	17	14.6
2	30.6	22.9
3	36.9	29
4	42.9	33
5	43.4	33.3
6	43.7	33.7

From Table 3.4, it is clear that sheet resistance increases on repeated heating and cooling cycles and reaches a constant value after a few cycles. Both the films follow the same trend and it is observed that the spray deposited FTO films perform better than ITO films (Figure 3.7). The distribution of sheet resistance of the deposited FTO film is depicted in the Figure 3.8 as sheet resistant mapping and it is clear that the film show uniform sheet resistance over the substrate.

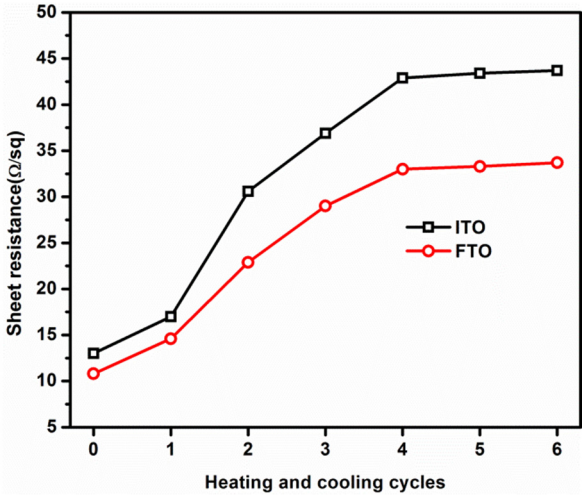

Figure 3.7. Variation of sheet resistance with heating and cooling cycles at 400^0C

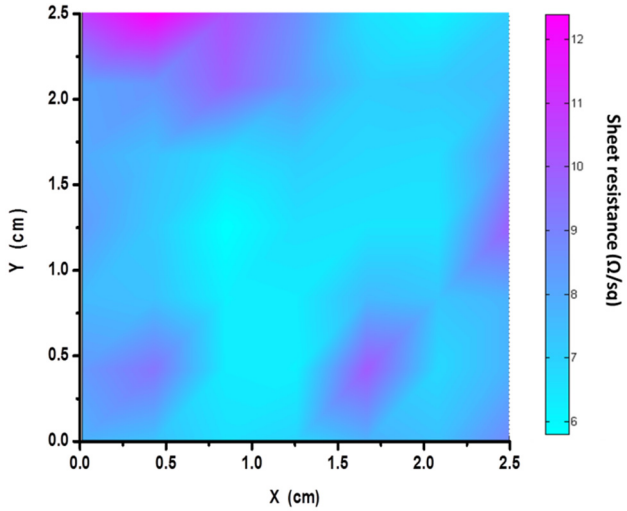

Figure 3.8. Sheet resistance mapping of FTO thin films

3.3.2 Selection of suitable electrode

For the fabrication of any device on the deposited FTO coated glass substrate, electrodes are required and it is important to choose the material which possesses lowest contact resistance. To identify the material, which make the least ohmic contact with FTO films, different electrode materials with same dimension were deposited over FTO substrate and the corresponding sheet resistance was measured. It is observed that the least resistive contacts are obtained for gold electrodes (Figure 3.9).

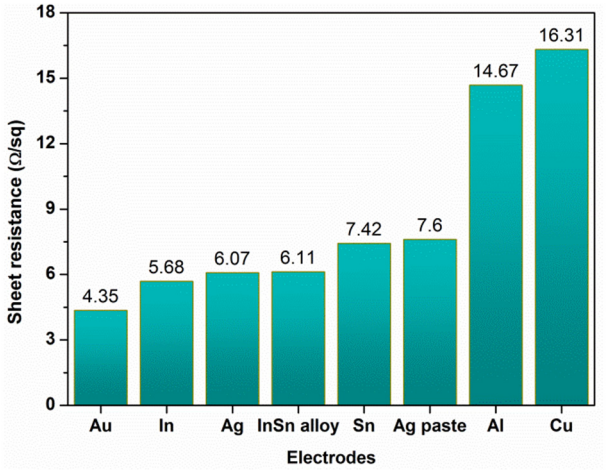

Figure 3.9. Sheet resistance with different electrodes over FTO thin film

3.4 Fabrication of "all layer sprayed solar cells" using FTO as TCO

Deposition conditions for obtaining uniform FTO films with conductivity 2.48 $x10^{-4}\Omega$.cm and transparency greater than 80% were identified and good quality films were prepared using chemical spray pyrolysis. To prove its applicability in energy sector, especially in photovoltaics, different solar cells were fabricated over the deposited FTO substrates using different absorber layers. CIS ($CuInS_2$), CZTS (Cu_2ZnSnS_4), and CZS (CuZnS) were the absorber materials and InS (In_2S_3) was the buffer

layer material selected for cell fabrication. Here all the solar cell layers were deposited by chemical spray pyrolysis and hence the name "**all layer sprayed solar cells**". All the solar cells were deposited in superstrate configuration, in which the TCO coated glass substrate functions as both as a supporting structure and as a window for light to enter the junction. The deposited solar cells were characterized by using NI-PXI-4130 SMU (National Instruments) and a class AAA solar simulator (Photo Emission Tech.).

3.4.1 FTO/TiO_2/InS/CIS solar cell

In order to demonstrate the applicability of as deposited FTO thin film as TCO layer in solar cells, solar cells with device structure FTO/TiO_2/InS/CIS was fabricated and compared with ITO/TiO_2/InS/CIS solar cell in which commercially available sputter deposited ITO is used as TCO layer. The ITO/TiO_2/InS/CIS cell fabrication procedure is as follows. Microporous TiO_2 films was deposited over ITO substrates by spraying a solution of commercially available TiO_2 powder (Degussa P25, Evonik industries, Japan) dissolved in hydrogen peroxide and ammonium hydroxide in the ratio 8:2. Spray rate and substrate temperature were maintained at 6 ml/min and 350^0C respectively. Copper chloride, indium chloride and thiourea were the precursors for CIS. Cu:In:S ratio in solution was maintained at 1.4:1:5 for depositing CIS and for InS, the In:S ratio is 1.2:12. InS and CIS films were deposited subsequently on TiO_2 deposited ITO substrates at 350^0C at a spray rate of 4 ml/min. More details about deposition condition for InS and CIS layers is available elsewhere[20]. The photovoltaic response of the fabricated device was carried out under an illumination of 100mW/cm^2. The device shows an open circuit voltage of 428mV, short circuit current of 7.97mA/cm^2. The fill factor is calculated to be 34%and the efficiency is 1.17%.

Solar cells were fabricated by replacing ITO with FTO and the performance of the cells is compared. Here the optimized deposition conditions of TiO_2, CIS and InS layers were the same as that used for depositing over ITO. CIS/InS/TiO_2 heterojunction over FTO shows open circuit voltage of 409mV, short circuit current of 3.9mA/cm^2. The fill factor and efficiency of the device is found to be 38% and 0.61% respectively. Device structure and J-V characteristics of the FTO based device are shown in Figure 3.10. The efficiency of the device is lower than the device fabricated on ITO due to low voltage and current values. Nevertheless better fill factor could be obtained for FTO based solar cell than ITO based cell.

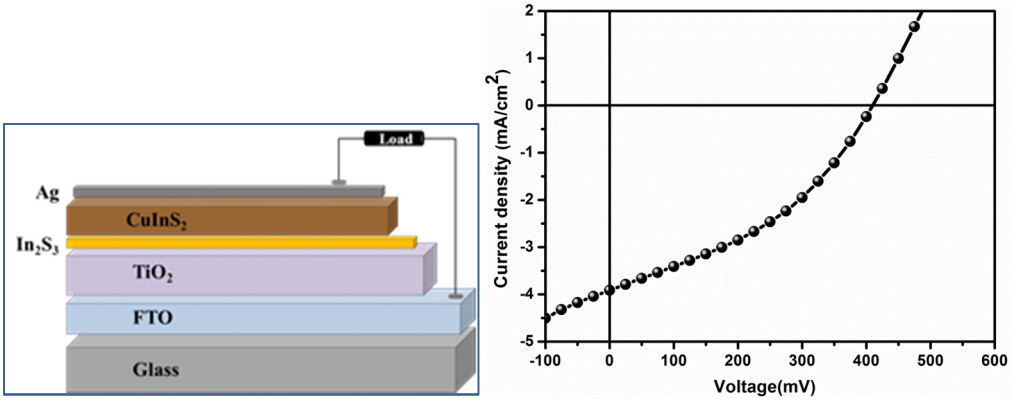

Figure 3.10. Device structure and J-V characteristics of FTO/TiO_2/ InS/CIS solar cell

3.4.2 FTO/CIS/InS Solar cell

Solar cells with device structure FTO/CIS/InS was also fabricated without microporous TiO_2 and compared with ITO/CIS/InS solar cell in which commercially available sputter deposited ITO was used as TCO layer. CIS and InS layers were deposited over ITO substrate by following the same deposition conditions used for fabricating the previous device. More details about deposition is reported by Santhosh *et al.*[21] Under an illumination of 100mW/cm^2, the device

shows open circuit voltage of 478mV, short circuit current of 12.13mA/cm^2 with a fill factor of 45%. The efficiency of the device is found to be 2.59%.

Solar cells with the same structure were fabricated by replacing ITO with FTO and the performance of the cells was compared. Device structure and J-V characteristics of FTO/CIS/InS device are shown in Figure 3.11. CIS/InS junction over FTO substrate shows an open circuit voltage of 457mV, short circuit current of 5.45mA/cm^2 and fill factor of 38%. The efficiency of the device is 0.94%. In this case also, the efficiency is lower than the device fabricated on ITO. Reduction in efficiency of CIS/InS based "all layer sprayed" solar cells is mainly due to reduction in short circuit current. Short circuit current in these devices are almost half of that of the cells fabricated over ITO.

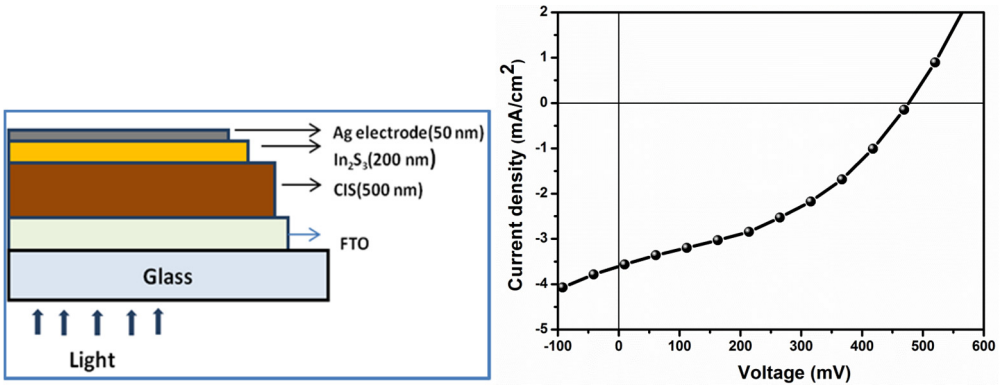

Figure 3.11. Device structure and J-V characteristics of FTO/CIS/InS solar cell

CIS is used as absorber material in both FTO/CIS/InS and FTO/TiO_2/CIS/InS solar cells. Avoiding In from the solar cell layers is the ultimate aim of researchers working for economical devices as In is a rare metal and it is very expensive. Replacing In based compounds from solar cell layers should be done step by step. Developing FTO coated substrates is the first step to achieve this goal. Next, the absorber material CIS is also replaced by CZTS and CZS, whose constituents are relatively abundant than In.

3.4.3 FTO/CZTS/InS solar cell

Solar cells with device structure CZTS/InS was fabricated over commercially available sputter deposited ITO and also on FTO coated glass substrate using CSP for comparison. The precursor solution for CZTS films was prepared by dissolving cupric chloride, zinc acetate, stannic chloride and thiourea. Cu:Zn:Sn:S atomic ratio in the precursor solution was adjusted to be 2.5:1:0.7:12 as optimized by Rajeshmon *et al.*[23] The solution was sprayed on to the substrates maintained at temperature of 300^0C and during the course of spray, temperature was increased to 350^0C. Approximately 550nm thick CZTS layer was deposited in single spray followed by InS layer. Indium chloride and thiourea were the precursors used. Deposition conditions of InS layer was retained as such from the previous devices.

Under an illumination of 100mW/cm^2, the device fabricated on sputtered ITO substrates shows an open circuit voltage of 430mV, a short circuit current of 8.3mA/cm^2 with a fill factor of 52%. The efficiency of the device is 1.85%. The output characteristics and device structure of the cell fabricated on FTO substrate is shown in Figure 3.12. The device had open circuit voltage of 406mV, short circuit current of 6mA/cm^2 and fill factor of 51%, with efficiency 1.25%.

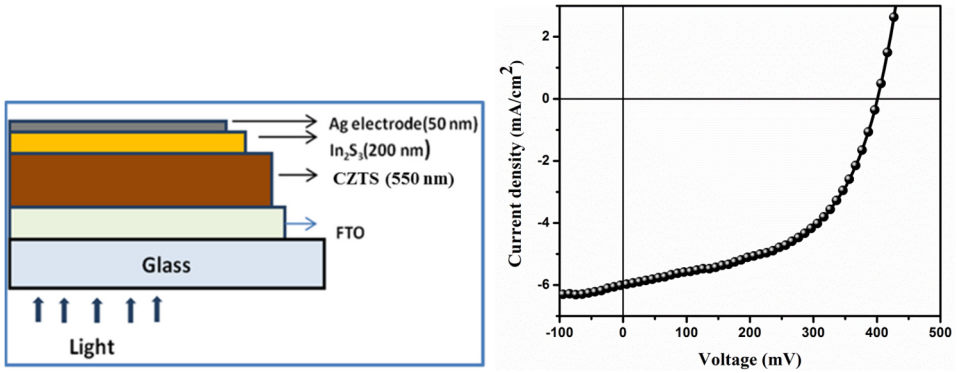

Figure 3.12. Device structure and J-V characteristics of FTO/CZTS/InS solar cell

3.4.4 FTO/CZS/InS solar cell

CZS is a relatively new absorber layer material which has been recently explored to replace CIS and even CZTS (with less number of elements). Solar cells with device structure FTO/CZS/InS was fabricated and compared with ITO/CZS/InS solar cell in which commercially available sputter deposited ITO is used as TCO layer. The precursor solution for CZS films was prepared by dissolving cupric chloride, zinc chloride and thiourea. Cu:Zn:S atomic ratio in the precursor solution is fixed at 0.4:1:6 as reported by Sreejith *et al.*[22] The prepared solution was sprayed on to ITO coated glass substrate maintained at temperature of 350^0 C, at spray rate of 4ml/min. Approximately 400nm thick CZS layer was deposited followed by depositing InS layer of thickness 200nm. Deposition conditions of InS layer was retained as such.

With the same device structure, solar cells were fabricated by replacing ITO with FTO and the performance of the cells is compared. Under illumination of 100mW/cm^2, CZS/InS junction on ITO substrate exhibited open circuit voltage 451mV, short circuit current of 5.5mA/cm^2 with a fill factor of 42%. The efficiency of the device is 1.04%. Solar cell characteristics and device structure of "all sprayed solar cell" fabricated by replacing ITO by sprayed FTO substrate is shown in Figure 3.13. The device shows open circuit voltage of 380mV, short circuit current of 5.6mA/cm^2 and fill factor of 41%. Cell efficiency is 0.9%. The efficiency and short circuit current for the "all sprayed" devices fabricated using indium free absorber layers are comparable to that of the devices fabricated on ITO. In both cases, the fill factor attained was almost same.

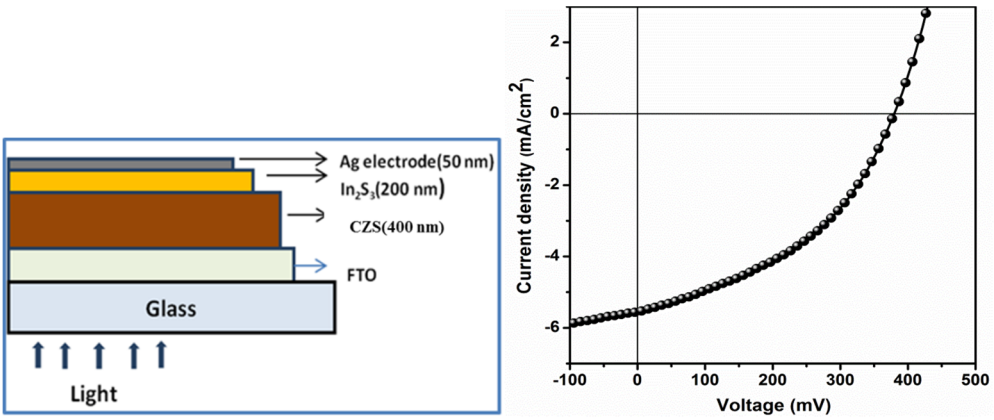

Figure 3.13. Device structure and J-V characteristics of FTO/ CZS/InS solar cell

The attempt to fabricate "all sprayed solar cell" using different absorber layers over the developed FTO substrate is a success. But the performance is low compared to the devices fabricated on commercially available sputtered ITO substrates. Still, the result is promising in the view point of reducing the usage of In in fabricating cost-effective solar cells. The performance of the devices can be improved further by optimizing the deposition conditions of individual solar cell layers separately for FTO substrates.

3.5 FTO as transparent thin film heater

Other than transparent electrode applications, TCO materials can be used as transparent, thin film electro-thermal heaters. Transparent thin film heaters have applications ranging from window defrosters[24–27],smart windows[28], device for thermal treatments in the conservation of paintings[29], heating elements for activating metal oxide gas sensors[30] to integrated transparent heater in micro channel chip for continuous flow-polymerase chain reaction[31]. Basic principle behind operation of thin film heater is "Joule heating". Hence materials which are efficient in converting electrical energy into heat and at the same time transparent in visible range are highly desirable for making transparent thin film heaters. Though conducting polymers[32],

carbon nanotubes[33,34], graphene[35,36], metal grids and metallic nanowires[26,37] have been suggested as transparent thin film heaters, transparent conducting oxide are widely used for these applications.

A transparent thin film heater was fabricated using the spray deposited FTO film in a 'two terminal' side contact configuration. DC voltages are applied using SMU (PXI-4130, National Instruments) to the device through silver contacts at the film edges. Temperature over the film surface was measured in real-time using k-type thermocouple connected to digital multimeter (PXI-4072, National Instruments).

Figure 3.14. shows the time-dependent temperature profiles of FTO based transparent thin film heater. Figure 3.14. also compares the temperature profiles of the transparent thin film heater which is plotted with respect to the input voltages (modulated from 6V to 20V).When the input voltage increases from 6V to 20V, the heater reaches steady temperature of 340^0C from 83^0C, which confirms its capacity to work with different low input voltages. A high steady temperature, at a low input voltage implies the efficient transduction of electrical energy into Joule heating. It can be observed that response time, i.e. the time required to reach the highest temperature, ranges from 2 - 4 minutes which is a key factor for evaluating the performance of film heaters. This lower value of response time demonstrates the fast response of the device. The maximum temperature attained by the device and the power consumption at different input voltages are shown in the Table 3.5.

Table 3.5. Maximum temperature attained by the device and the power consumption at different input voltages

Voltage (V)	Temperature (^{0}C)	Power (W)
6	88	7
9	170	15
12	258	26
15	284	41
20	340	72

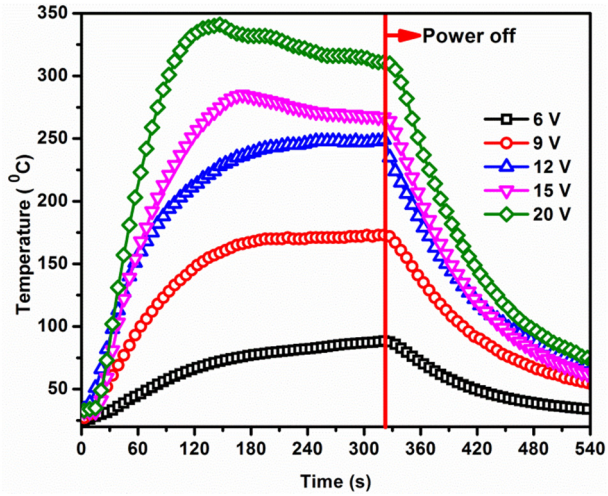

Figure 3.14. Temperature - time profile of the transparent thin film heater at different input voltages

3.6 Possible application of FTO coated glass as heat reflecting and retaining low emissivity smart window

Energy audit reveals that in air-conditioned buildings; at least 10 to 25% of the energy loss is through its windows as IR radiation[38–40]. In winter, a part of the energy utilized to warm the building will escape through the normal glass windows as IR radiation, and similarly in summer, the external heat will enter the building through the windows. This type of energy loss can be reduced significantly by using IR reflecting materials as windows. Certainly metals are good IR reflectors and windows with metal coatings can reduce the heat loss in

the buildings with a compromise in light transmission. But metal coatings can be affected by weather conditions and protective coatings are required to maintain it, more over it will result in considerable increase in cost. If TCO coated glass can reflect IR wavelengths greater than 3μm, then it can be used as heat reflecting/retaining windows. But unlike metal coated windows, TCO coated windows has an added advantage of higher transmittance in the visible region. Again, materials like FTO are not prone to damages like wear under environmental conditions due to its high mechanical, thermal and chemical stability.

Figure 3.15 shows the comparison of transmission spectra of undoped and fluorine doped tin oxide thin films deposited over soda-lime glass substrates by chemical spray pyrolysis. It is clear that the FTO films exhibits high reflectance in IR region. For wavelengths higher than 2 micrometers, the film reflects more than 95% of the IR radiation. And this property of the deposited FTO coated glass can be utilized to make IR reflecting, heat reflecting/retaining low emissivity smart windows.

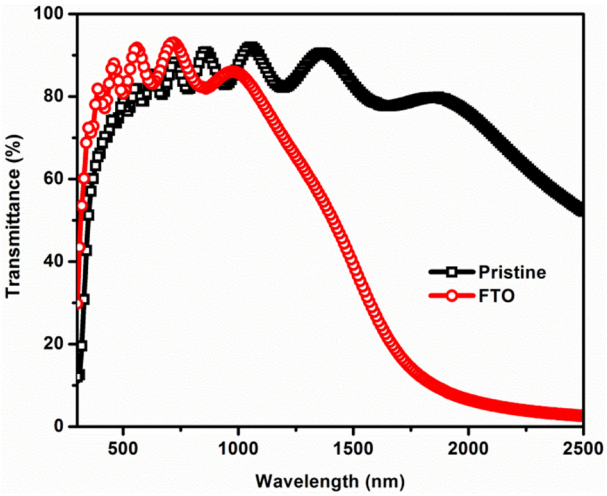

Figure 3.15. Comparison of transmission spectra of undoped and fluorine doped tin oxide thin films

Conclusion

This chapter discusses the effect of dopant sources and dopant concentration on the properties of fluorine doped tin oxide thin films. Among fluorine sources, NH_4F is found to be the best dopant source. For an optimized concentration of F, resistivity is decreased to 2.48 $x10^{-4}\Omega$.cm and transmittance is greater than 80% in the visible spectra. XPS depth profile of the films proved the uniform distribution of elements in the films. It is seen that the FTO thin films are thermally stable.

"All sprayed solar cells" using different absorber materials were successfully fabricated over FTO substrates. Initial trials of the devices exhibit promising solar cell performance. A transparent thin film heater was also fabricated using FTO thin films and is able to reach a temperature of 340^0C under an input voltage of 20V with a lower power consumption of 72W. High reflectance in the IR region is exhibited by the deposited FTO films and this property could be utilized to make IR reflecting, heat reflecting/retaining low emissivity smart windows.

References

1. A.V. Moholkar, S.M. Pawar, K.Y. Rajpure, P.S. Patil, and C.H. Bhosale, J. Phys. Chem. Solids **68**, 1981 (2007).
2. E.V.A. Premalal, N. Dematage, S. Kaneko, and A. Konno, Thin Solid Films **520**, 6813 (2012).
3. A.V. Moholkar, S.M. Pawar, K.Y. Rajpure, and C.H. Bhosale, Mater. Lett. **61**, 3030 (2007).
4. B. Thangaraju, Thin Solid Films **402**, 71 (2002).
5. A.V. Moholkar, S.M. Pawar, K.Y. Rajpure, C.H. Bhosale, and J.H. Kim, Appl. Surf. Sci. **255**, 9358 (2009).

[6] A. Purwanto, H. Widiyandari, and A. Jumari, Thin Solid Films **520**, 2092 (2012).

[7] A.I. Martinez and D.R. Acosta, Thin Solid Films **483**, 107 (2005).

[8] G.C. Morris and A.E. Mcelnea, Appied Surf. Sci. **92**, 167 (1996).

[9] M.J. Atmane B, Achour rahal, Boubaker Benhaoua, Superlattices Microstruct. **70**, 61 (2014).

[10] F.M. Amanullah, K.J. Pratap, and V. Hari Babu, Mater. Sci. Eng. B **52**, 93 (1998).

[11] K.K. Purushothaman, M. Dhanashankar, and G. Muralidharan, Curr. Appl. Phys. **9**, 67 (2009).

[12] N. Noor and I.P. Parkin, Jounal Mater. Chem. C **1**, 984 (2013).

[13] B. Benhaoua, S. Abbas, and A. Rahal, Superlattices Microstruct. **76**, 105 (2014).

[14] D. Zhang, L. Tao, Z. Deng, J. Zhang, and L. Chen, Mater. Chem. Phys. **100**, 275 (2006).

[15] J. Montero, C. Guillén, and J. Herrero, Sol. Energy Mater. Sol. Cells **95**, 2113 (2011).

[16] S.U. Lee, W.S. Choi, and B. Hong, Phys. Scr. **T129**, 312 (2007).

[17] A.B. and K.L.C. E. Shanthi, Thin Solid Films **88**, 93 (1982).

[18] C. Agashe and S.S. Major, J. Mater. Sci. **31**, 2965 (1996).

[19] A.N. Banerjee, S. Kundoo, P. Saha, and K.K. Chattopadhyay, J. Sol-Gel Sci. Technol. **28**, 105 (2003).

[20] M.V. Santhosh, D.R. Deepu, R. Geethu, K. Rajeev Kumar, C. Sudha Kartha, and K.P. Vijayakumar, Semicond. Sci. Technol. **29**, 115026 (2014).

[21] M.V. Santhosh, D.R. Deepu, C. Sudha Kartha, K. Rajeev Kumar, and K.P. Vijayakumar, Sol. Energy **108**, 508 (2014).

[22] M.S. Sreejith, D.R. Deepu, C.S. Kartha, K. Rajeevkumar, and K.P. Vijayakumar, Appl. Phys. Lett. **105**, 202107 (2014).

[23] V.G. Rajeshmon, M.R.R. Menon, C.S. Kartha, and K.P. Vijayakumar, J. Anal. Appl. Pyrolysis **110**, 448 (2014).

[24] L. Castañeda, Mater. Sci. Appl. **2**, 1233 (2011).

[25] S. Wang, X. Zhang, and W. Zhao, J. Nanomater. **2013**, 1 (2013).

[26] C. Celle, C. Mayousse, E. Moreau, H. Basti, A. Carella, and J.-P.P. Simonato, Nano Res. **5**, 427 (2012).

[27] B. Du Ahn, S.H. Oh, D.U. Hong, D.H. Shin, A. Moujoud, and H.J. Kim, J. Cryst. Growth **310**, 3303 (2008).

[28] C.G. Granqvist, Thin Solid Films **564**, 1 (2014).

[29] T. Markevicus, N. Olsson, M. Carfagni, R. Furferi, L. Governi, and L. Puggelli, in *EuroMed 2012* (2012), pp. 784–792.

[30] H.G. Moon, Y. S. Shim, D.H. Kim, H.Y. Jeong, M. Jeong, J.Y. Jung, S.M. Han, J.K. Kim, J. S. Kim, H. H. Park, J. H. Lee, H.L. Tuller, S. J. Yoon, and H.W. Jang, Sci. Rep. **2**, 588 (2012).

[31] K. Sun, A. Yamaguchi, Y. Ishida, S. Matsuo, and H. Misawa, Sensors Actuators B **84**, 283 (2002).

[32] D.S. Ghosh, T.L. Chen, V. Mkhitaryan, and V. Pruneri, ACS Appl. Mater. Interfaces **6**, 20943 (2014).

[33] J.S. Woo, J.T. Han, S. Jung, J.I. Jang, H.Y. Kim, H.J. Jeong, S.Y. Jeong, K. J. Baeg, and G. W. Lee, Sci. Rep. **4**, 4804 (2014).

[34] Y.H. Yoon, J.W. Song, D. Kim, J. Kim, J.K. Park, S.K. Oh, and C.S. Han, Adv. Mater. **19**, 4284 (2007).

[35] B.J. Lee and G.H. Jeong, Curr. Appl. Phys. **12**, 113 (2012).

[36] D. Sui, Y. Huang, L. Huang, J. Liang, Y. Ma, and Y. Chen, Small **7**, 3186 (2011).

[37] K.D.M. Rao and G.U. Kulkarni, Nanoscale **6**, 5645 (2014).

[38] www.glassdesignandbuild.co.uk/window-styles.

[39] www.energy-film.com/performance-data.

[40] Energy.gov/energysaver/tips-windows.

Chapter

4

EFFECT OF IN-SITU Ag DOPING ON SPRAY PYROLYSED ZnO THIN FILMS

Contents

4.1 Introduction

Zinc oxide always remained in the limelight, as it is an 'all-round performer' in optoelectronics, photovoltaic, piezoelectric, spintronic and sensor applications[1–3]. But the potential of this material is largely stuck by the difficulty in achieving stable p-type conductivity. By birth, ZnO films are n-type due to non-stoichiometric defects like metal interstitials or oxygen vacancies[4,5]. It is reported that the p-type ZnO can be obtained either by substituting Zn by group I elements or by substituting O by group V elements[6,7]. The small ionic radii of group I elements will result in the occupation of interstitial sites rather than Zn sites and will act as donors[8]. On the other hand, p-type conversion by substitution of O using group V elements is also limited due to the creation of deep acceptor levels and self-compensating effects[9]. There are reports on doping with group I_b element (Ag)

which says that in O-rich conditions, Zn sites are substituted by Ag, which creates shallow acceptor level above valence band by 0.23eV to 0.3eV.[8,10–13] N and Ag co-doping are also suggested for achieving p-type ZnO[14,15]. However, achieving p-type ZnO using single dopant Ag by spray pyrolysis technique is not reported earlier.

The aim of the present work is to identify the difficulties in developing p-type ZnO thin films by Ag mono doping and the methods to overcome those obstacles. The main difficulty in achieving p-type conductivity in Ag doped ZnO is reported to be the low solubility of the Ag ions in ZnO matrix[11,14,16,17]. Also the incorporated Ag should occupy Zn site to create acceptor levels to get p-type conductivity. Otherwise, it will act as 'donor impurity'. This condition can be achieved only by depositing the films in 'oxygen rich' atmosphere, which favors the substitution of Zn by Ag[11]. In the present work, low solubility issue of the dopant is overcome by increasing dopant concentration in the precursor solution. The reported 'oxygen rich' deposition condition was achieved by depositing the films at lower spray rates; because, from the previous spray rate variation studies of SnO_2 films,(chapter 2 of this thesis), it is identified that, oxygen rich oxide films can be fabricated by depositing at low spray rates.

4.2 Selection of solvent

In this chapter, the effect of dopant sources of Ag and its concentration in precursor solution in order to develop p-type ZnO films is discussed. Several groups have reported the fabrication of p-type ZnO thin films through CSP technique[7,9,15,18]. In this work, the optimized conditions reported by Vimalkumar *et al.* was followed to prepare the precursor solution[19], in which

zinc acetate dihydrate was used as the precursor for zinc. A mixture of demineralized water and isopropyl alcohol in 1:1 ratio was used as the solvent. 1.25% of acetic acid was added to the translucent precursor solution to obtain clear solution. Above 2at.% Ag doping was difficult because of the sudden precipitation of the precursor solution. Hence to avoid the precipitation of the precursor solution, the solvent was changed from water and propanol mixture to propanol only. But the precipitation of the precursor occurred for propanol also. Hence it was concluded that the presence of propanol in precursor solution causes the precipitation. In order to avoid the precipitation, presence of any alcohol in the precursor should be avoided and only demineralized water was used as solvent. Normal soda lime glass of thickness 1 – 1.2mm was used as substrate. The substrates were ultrasonically cleaned using isopropyl alcohol followed by rinsing with demineralized water and dried in a hot air current. Films were prepared by spraying 50ml of the precursor solution of molarity 0.3M, onto preheated substrates kept at 450^0C. Reports suggest that chances for the formation of p-type ZnO are in 'oxygen rich' deposition conditions. In order to achieve that, low spray rate of 5ml/min was selected for the deposition. In low spray rates, it was observed that thorough mixing and fine atomization of the precursor solution ultimately lead to O-rich deposition atmospheres. Substrate to nozzle distance was fixed at 20cm. Compressed dry air was used as the carrier gas and the spray head covered an area of 200mm x 200mm by raster scan. The variation in substrate temperature was maintained within $\pm 10^0$C.

4.3 Selection of dopant source

Silver nitrate [$AgNO_3$] and silver acetate [CH_3CO_2Ag] were selected as the sources for Ag and were dissolved in demineralized water. To overcome the lower solubility of silver acetate in water, a few microliters of concentrated HNO_3 was added. Different quantities of these two dopant sources were added to the Zn precursor solution to get desirable dopant concentrations. Samples were deposited by varying the concentration of the dopants in the precursor solution from 1at.% to 9at.%. Precursors (after adding the dopant sources) were ultrasonically agitated for 10 minutes for obtaining a solution with uniform distribution of dopants. All other deposition conditions were the same. Samples prepared using silver acetate [Ag(AC)] as dopant source are named as A-1, A-3, A-5, A-7 and A-9 and samples prepared with silver nitrate [$AgNO_3$] as dopant source are named as N-1, N-3, N-5, N-7, and N-9. Undoped samples are named as P. In order to know the best dopant source and doping concentration that yields p-type ZnO film with good crystallinity and transparency, deposited films were characterized and analyzed as follows.

4.3.1 Structural characterization

Figure 4.1.(a) and 4.1.(b) shows the XRD pattern of ZnO films prepared by varying the Ag doping concentrations using silver acetate and silver nitrate respectively. It is observed that choice of the dopant source has little impact on XRD pattern of the films. Films prepared with both dopants are poly crystalline in nature and having preferential growth along (002) plane of wurtzite ZnO (ICDD card number 79-0208). XRD does not reveal any phases pertaining to Ag or its oxides. But it is observed that grain size of Ag doped films is better than pristine films (Figure 4.2).

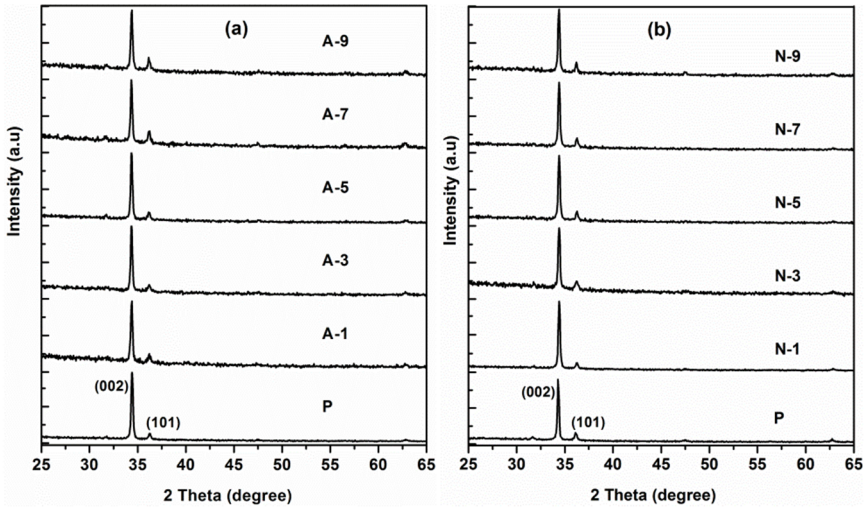

Figure 4.1. XRD pattern of ZnO thin films doped with Ag using (a) Ag(AC) and (b) $AgNO_3$

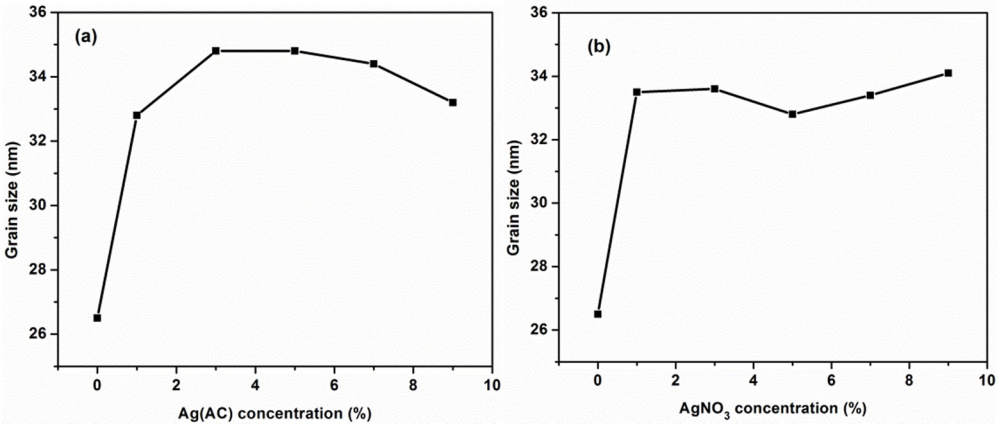

Figure 4.2. Variation in grain size of ZnO thin films doped with Ag using (a) Ag(AC) and (b) $AgNO_3$

4.3.2 Optical characterization

Figure 4.3.(a) and 4.3.(b) give the transmission spectra of films with varying dopant concentration of the two dopant sources. It is observed that for low doping percentages of Ag (1at.% and 3at.%), the transmittance is better than that of the pristine films. But at higher doping concentrations using Ag(AC), the transmittance of the films remain almost same as that of pristine

films. For higher doping concentrations of $AgNO_3$, transmittance decreases slightly compared to that of the pristine films.

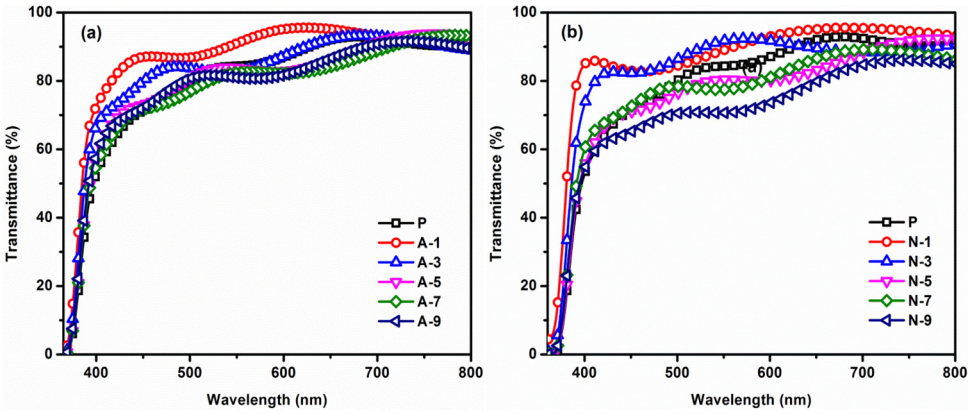

Figure 4.3. Transmission spectra of ZnO thin films with different concentrations of (a) $AgNO_3$ and (b) Ag(AC)

Average thickness of the films is found to be 420 ±40nm and it is observed that thickness of the films is nearly constant irrespective of whether the films are pristine or Ag doped.

4.3.3 Electrical characterization

Incorporation of Ag has a direct impact on electrical properties of the films. A reduction in conductivity, mobility and carrier concentration is clearly visible irrespective of the dopant sources. Results of electrical analysis of the films using Hall measurement system are depicted in Table 4.1 and Table 4.2. Change in electrical properties are not well correlated with change in doping concentration for Ag(AC) doped films. Resistivity is increased by two orders, from 10^{-1} to 10^{1} and carrier concentration is decreased by one order using silver acetate as dopant source and remained in the same order for doping concentration from 1at.% to 5at.%. But on further increase in doping concentration, a sudden surge in resistivity and decrease in carrier concentration is observed. Samples that are prepared with 9 at.% silver acetate

in the precursor are highly resistive and hence its electrical property studies are not possible using Hall measurement. All the films are identified to be n-type in nature.

Table 4.1. Electrical properties of pristine and Ag(AC) doped ZnO thin films

Sample	Resistivity (Ω.cm)	Mobility ($cm^2/V.s$)	Carrier concentration (cm^{-3})	Conductivity Type	Avg. grain size (nm)	Transmittance in 400nm – 800nm (%)
Pristine	3.82×10^{-1}	8.3	1.9×10^{18}	n	26.5	53 – 92
A-1	4.1×10^{1}	2.3×10^{-1}	6.7×10^{17}	n	32.8	72 – 91
A-3	0.85×10^{1}	1.6	4.6×10^{17}	n	34.8	67 – 89
A-5	1.8×10^{1}	1.4	2.4×10^{17}	n	34.8	57 – 92
A-7	6×10^{3}	1.8	5.5×10^{14}	n	34.4	55 – 93
A-9	2.1×10^{4}	--	--	--	33.2	58 – 90

Table 4.2. Electrical properties of pristine and $AgNO_3$ doped ZnO thin films

Sample	Resistivity (Ω.cm)	Mobility ($cm^2/V.s$)	Carrier concentration (cm^{-3})	Conductivity Type	Avg. grain size (nm)	Transmittance in 400nm – 800nm (%)
Pristine	3.82×10^{-1}	8.3	1.9×10^{18}	n	26.5	53 – 92
N-1	1.02×10^{1}	7.3×10^{-1}	8.4×10^{17}	n	33.5	82 – 95
N-3	2.77×10^{2}	1.1×10^{-1}	2.1×10^{17}	n	33.6	73 – 92
N-5	8.57×10^{3}	3.7×10^{-1}	1.9×10^{15}	p/n	32.8	55 – 92
N-7	5.7×10^{1}	3.8×10^{-1}	2.9×10^{17}	p	33.4	60 – 89
N-9	3.54×10^{3}	1.3×10^{-1}	1.3×10^{16}	n	34.1	55 – 86

For the films doped with Ag using $AgNO_3$, variation in resistivity with dopant concentration has a positive correlation whereas carrier concentration exhibit a negative correlation with Ag concentration up to an optimum percentage of doping and is tabulated in Table 4.2. Sample N-5 is highly resistive and hence Hall measurements are repeated. The sample N-5 exhibited a fluctuating nature of conductivity. i.e. both n and p nature. It is assumed that the 5at.% doped films are intrinsic in nature. Interestingly sample N-7 showed stable p-type conductivity and sample N-9 is again n-type in nature.

Further doping with 6at.%, 7at.% and 8at.% $AgNO_3$ were performed to identify the doping concentration at which the resistivity of the p-type ZnO thin film is a minimum. The samples are named as N-6c, N-7c, and N-8c. Electrical properties of these films are measured using Hall measurement and are shown in Table 4.3. Even though the films N-6c, N-7c, and N-8c are p-type in nature, the lowest resistivity is obtained for N-7c sample, i.e. for 7at.% doping concentration.

Table 4.3. Electrical properties p-type ZnO thin films with different Ag doping

Sample	Resistivity (Ω.cm)	Mobility (cm^2.V.s)	Carrier concentration (cm^{-3})	Conductivity type
N-6c	4.36×10^{2}	6×10^{-1}	2.4×10^{16}	p
N-7c	8.8×10^{1}	3.7×10^{-1}	1.8×10^{17}	p
N-8c	1.7×10^{2}	3.7×10^{-1}	9.6×10^{16}	p

Change in conductivity type of the films can be attributed to the formation of shallow acceptor level by substitution of Ag in Zn sites[5,11]. In ZnO lattice, Ag can either substitute Zn or it can occupy in the interstitial site. Substitutional Ag will create shallow acceptor levels and it can act as 'charge compensator' in ZnO. This may be the reason for the initial increase in resistivity and decrease in carrier concentration as well as the switching of the conductivity type of the films from n to p. On the other hand, Ag in the interstitial site is responsible for the creation of donor levels. This can be the reason for the n-type conductivity of ZnO thin films with 9at.% Ag doping. Even though n-type, these films are highly resistive due to the co-existence of substitutional and interstitial Ag, resulting in acceptor as well as donor levels respectively.

4.3.4 Morphological characterization

Surface morphology of the 7at.% Ag doped ZnO thin film with p-type conductivity was analyzed using SEM micrograph and is shown in Figure 4.4. It is observed that Ag doped ZnO films are grown to form petals and rods like nanostructures and are uniformly covered over the substrate. The size of nanorods is calculated to be less than 50nm.

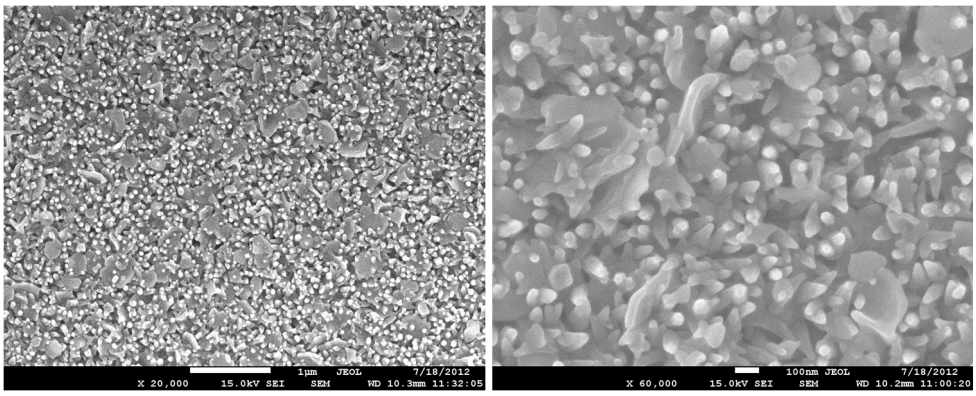

Figure 4.4. SEM micrograph of sample N-7 at 20K and 60K magnifications

4.3.5 Compositional characterization

Compositional analysis of 7at.% $AgNO_3$ doped p-type ZnO films was carried out using XPS measurement. The C 1s line (284.6eV) of the adventitious hydrocarbon is present in the film and any shift in XPS spectra (due to charging effect) could be corrected. XPS core level spectra of ZnO film prepared with 7at.% Ag in precursor solution shows Zn $2p_{1/2}$ peak at 1045.4 ±0.2eV and Zn $2p_{3/2}$ peak at 1022.3 ±0.2eV separated by 23.1eV. This suggests that Zn is in 2+ oxidation state in the film[20]. The core level peak of O 1s can be deconvoluted in to two component peaks at 530.4 ±0.2eV and 531.9 ±0.2eV. The first peak represents the O^{2-} oxidation state of oxygen in oxides and the peak at higher BE represents oxygen in interstitial sites[21]. Binding energy peaks for Ag $3d_{3/2}$ and Ag $3d_{5/2}$ are observed at 374.2±0.2eV and

368.3±0.2eV separated by 5.9eV and is corresponding to Ag^{+} state[22]. Atomic percentage of the constituents in the films is calculated from the binding energy peaks and atomic sensitivity factor. It is found that the atomic concentration of Zn and O are 50.5% and 49.2% respectively in the films which means that the ZnO film is nearly stoichiometric. Such stoichiometric oxide films are formed because of the deposition at a low spray rate of 5ml/min, where as in other cases the films are found to be oxygen deficient.

To know whether the reduction in spray rate has really helped to achieve 'oxygen rich' deposition conditions, ZnO samples were prepared at a higher spray rate of 8ml/min and these films were analyzed using XPS. Chemical states and atomic concentrations of Zn and O in both the samples were compared. Unlike the near stoichiometric ZnO film prepared at 5ml/min, the films prepared at 8 ml/minute are found to be Zn rich. Atomic concentration of Zn and O for this film is 59.8% and 40.2% respectively.

XPS core level peaks of Zn and O of Ag doped ZnO film prepared at 5ml/min and ZnO film prepared at 8ml/min are shown in Figure 4.5 and Figure 4.6 respectively. Figure 4.7 gives the comparison of core level peaks of Zn and O in both the samples. It is observed that there is no change in shape or position for Zn 2p core level peaks with spray rate variation. Chemical state of Zn remains the same in the films irrespective of spray rate. It is observed that the O 1s core level peak is narrower for the film prepared at a spray rate of 8ml/min the deconvoluted components of O 1s peak of ZnO prepared at 5ml/min and 8ml/min are shown in Figure 4.8. The two components of O 1s levels are at 530.4eV and 531.9eV and are represented as O-1 and O-2 respectively. The peak O-1 corresponds to O^{2-} state of oxygen in metal oxides and the O-2 correspond to the O in interstitial sites[23,24]. From Figure 4.7 and Figure 4.8, it is clear that in the case of ZnO films prepared at low spray rate,

the increase in the concentration of O is due to the increase in oxygen present in interstitial sites. Oxygen in interstitial sites can act as acceptor impurities[25]. Presence of high concentration of interstitial oxygen may promote the formation of p-type ZnO films on Ag doping. Table 4.4 shows the relative concentrations of oxygen components in ZnO films.

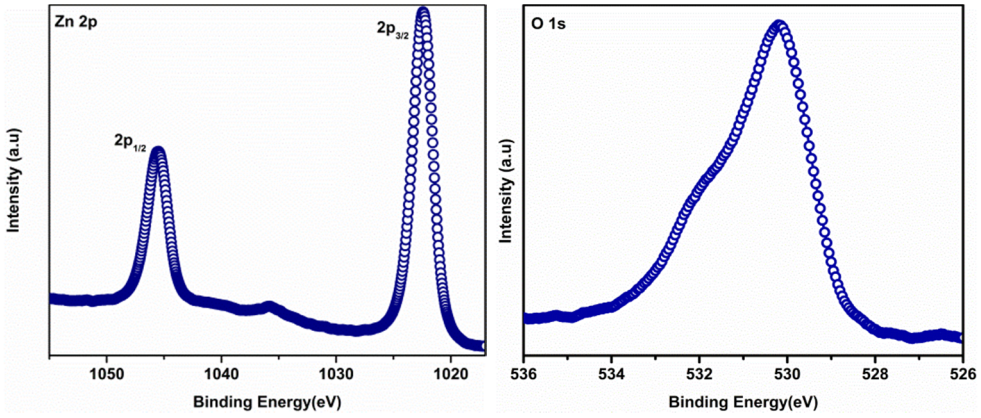

Figure 4.5. XPS core level spectra of Zn and O of Ag doped ZnO thin film prepared at 5ml/min

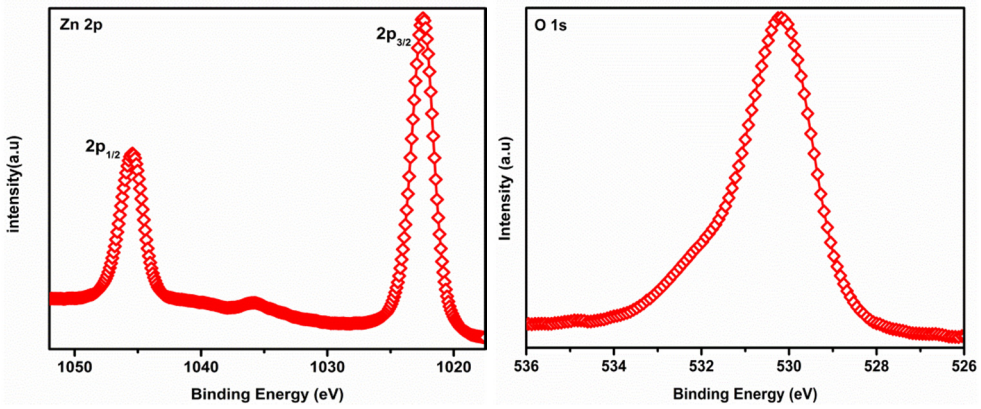

Figure 4.6. XPS core level spectra of Zn and O of ZnO thin film prepared at 8ml/min

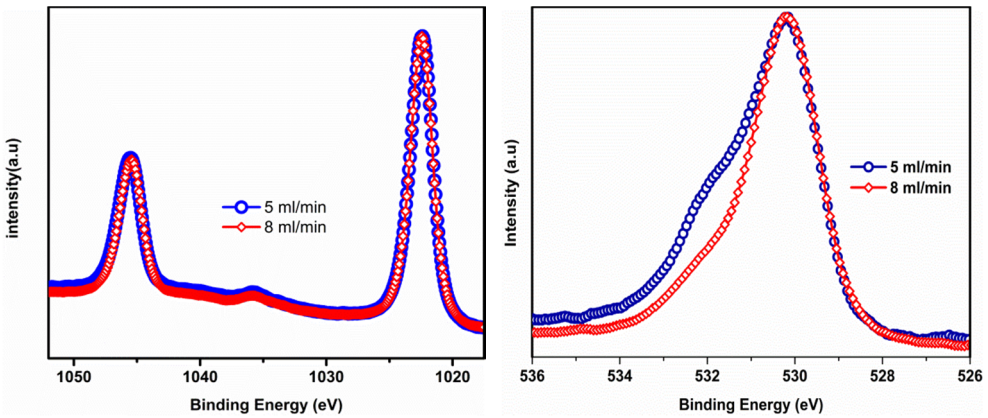

Figure 4.7. Comparison of XPS core level spectra of Zn in Ag doped ZnO thin film prepared at 5ml/min and ZnO film prepared at 8ml/min

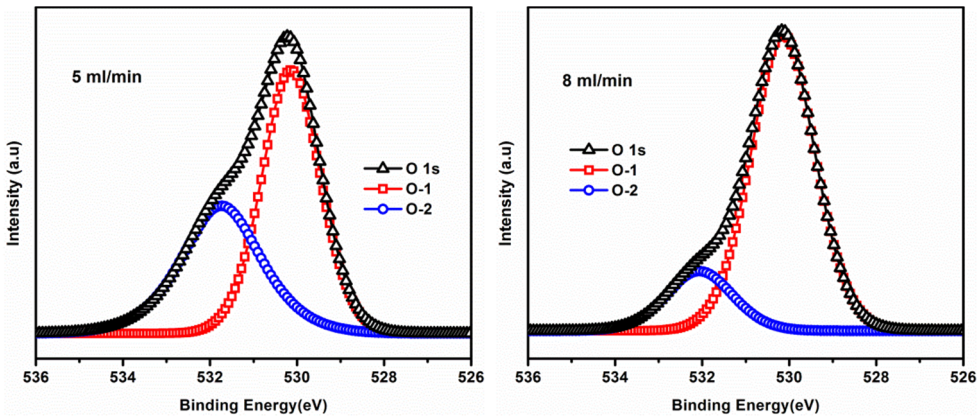

Figure 4.8. Deconvoluted components of O 1s peaks of ZnO thin films prepared at 5ml/min and 8ml/min

Table 4.4. Relative concentration of oxygen components in ZnO thin films

Oxygen components	Binding energy (±0.2eV)	Relative concentration (%)	
		5ml/min	8ml/min
O-1	530.4	59.4	82.7
O-2	531.9	40.6	17.3

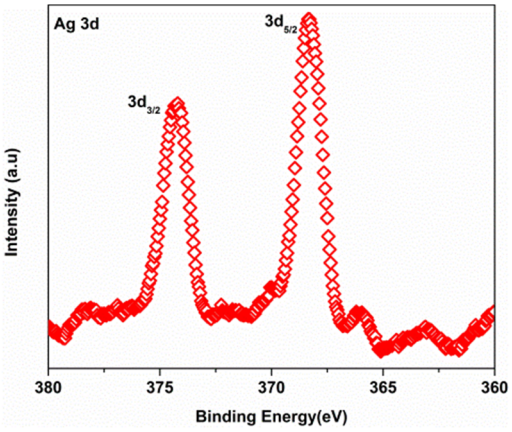

Figure 4.9. XPS core level spectra of Ag in 7at.% Ag doped p-type ZnO thin film

Figure 4.9 depicts the XPS core level spectra of Ag in Ag doped ZnO film. Even though the dopant concentration in the precursor solution is 7at.%, ZnO films contain only 0.3at.% Ag. This may be due to the less solubility of Ag ions in ZnO lattice[5]. Even if the dopant used and the carrier gas contains a considerable quantity of Nitrogen, there is no trace of N in the films as per XPS analysis. Hence, it is evident that only Ag is present as the dopant and the claim of Ag mono dopant is confirmed.

4.4 Fabrication of "All sprayed" ZnO based transparent thin film homojunction

To further verify p-type nature of the deposited Ag doped ZnO films, homojunctions are fabricated in the device structure TCO/ZnO:Al/ZnO/ ZnO:Ag/Ag (Figure 4.10). ZnO:Al layer was deposited over TCO coated glass substrate using the deposition conditions reported elsewhere[26]. The thickness of Ag and Al doped ZnO films were fixed around 400nm and that of pristine ZnO interlayer was varied by increasing the number of spray cycles. The number of cycles was varied from 1 to 3 and devices are named C-1, C-2, and

C-3. Exact measurements of the thickness of the intrinsic interlayers in samples C-1 and C-2 are difficult using stylus profiler due to their low thickness. But for the sample C-3, thickness was around 80nm. I-V characteristics of the junctions were measured using PXI-4130 SMU (National Instruments). From Figure 4.11, it is clear that good junction is obtained for the device with pristine ZnO layer thickness corresponding to three deposition cycles. The rectifying quality of a diode can be determined by calculating the ratio of forward to reverse current at a voltage above "knee voltage". The knee voltage and forward to reverse current ratio for the devices at 2V is shown in Table 4.5. The highest ratio is observed for the device with pristine ZnO layer thickness corresponding to three spray cycles.

Table 4.5. Knee voltage and forward to reverse current ratio for the devices at 2V

Device	Knee voltage (V)	Forward to reverse current ratio at 2V
C-1	0.64	1.83
C-2	1.1	2.32
C-3	1.1	400

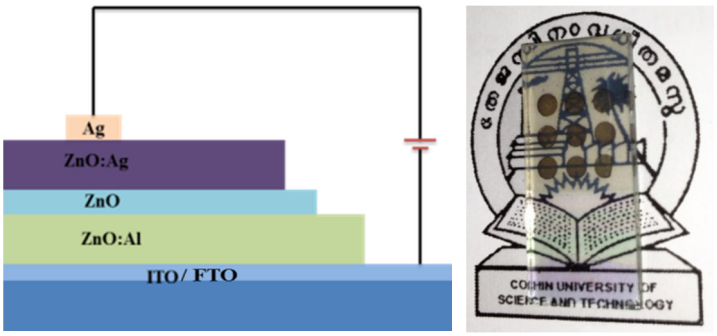

Figure 4.10. Device structure and photographic image of ZnO p-i-n homojunction

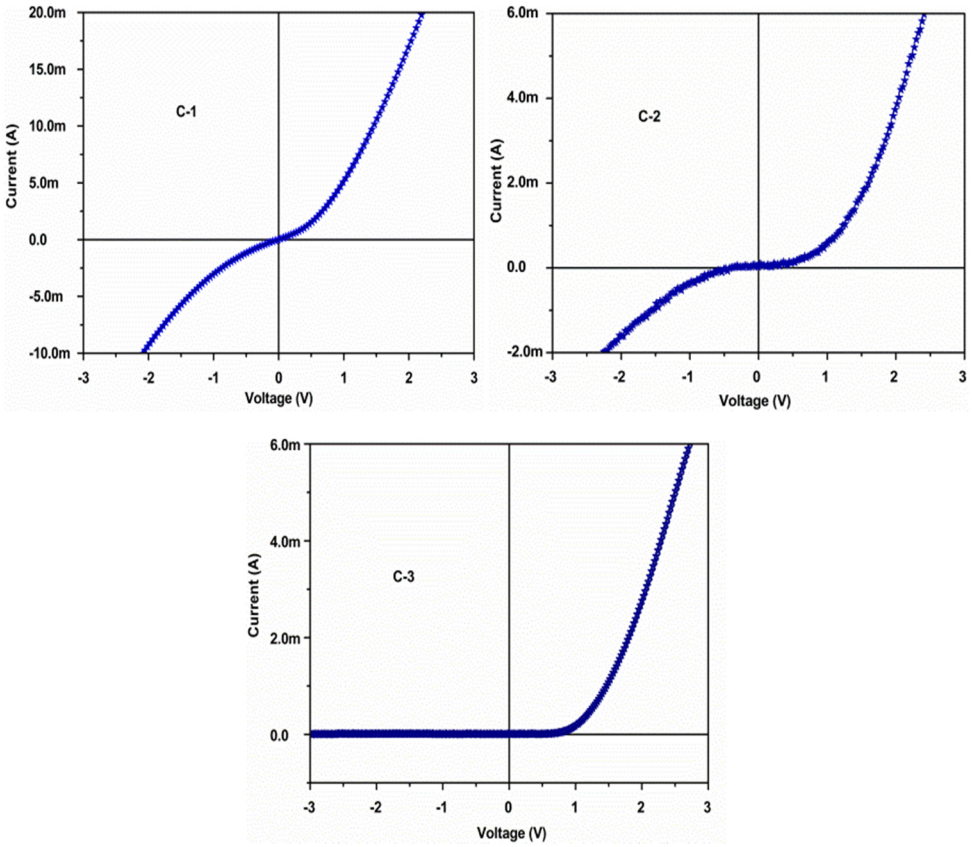

Figure 4.11. I-V characteristics of ZnO homojunctions with various ZnO interlayer thickness

4.5 Fabrication of CIS/CdS solar cells using ZnO:Ag window layer

In thin film solar cells, using an intrinsic ZnO (i-ZnO) window layer can reduce the leakage current by reducing the shunting paths[27–29]. Resistive intrinsic ZnO layer is widely utilized in thin film solar cells to improve the performance parameters. It is noticed that ZnO films deposited for a doping concentration of 5at.% using $AgNO_3$ are intrinsic in nature. The developed intrinsic ZnO thin film is tried as a window layer in CIS/CdS solar cell.

Intrinsic ZnO thin films of thickness ~ 80nm were deposited by spraying the precursor solution doped with 5at.% of $AgNO_3$ at a spray rate of 5ml/min over ITO coated glass substrates kept at 450^0C. Later a thin layer of CdS layer was deposited over this i-ZnO layer using chemical bath deposition. Cadmium sulphate (0.0125M), ammonia solution (35%), sodium hydroxide (0.025M) and thiourea (0.1M) were used as precursors for the deposition of CdS layer. The bath temperature was kept at 80^0C. CIS absorber layer was deposited over CdS layer using CSP and electrodes of diameter 2mm were deposited by vacuum evaporation of Ag. More details about the cell fabrication are described elsewhere[30]. Figure 4.12 shows the structure and J-V characteristics of the devices. For comparison, a CIS/CdS solar cell without intrinsic ZnO layer was also fabricated by using the same deposition conditions. Cell parameters are shown in Table 4.6. The positive effect of the i-ZnO layer is well proved from the cell measurements. All the cell parameters showed clear improvement with the addition of i-ZnO window layer. The open circuit voltage has shown an improvement of 5.65%, short circuit current density - 166%, fill factor - 65% and efficiency (η) showed an improvement of 27.1% with i-ZnO window layer.

Table 4.6. Solar cell performance parameters for CIS/CdS solar cells with and without i-ZnO window layer

CdS/CIS solar cell	V_{oc} (mV)	J_{sc} (mA/cm^2)	FF (%)	η (%)
Without i-ZnO	387	1.23	26.7	0.14
With i-ZnO	409	2.89	44.3	0.52

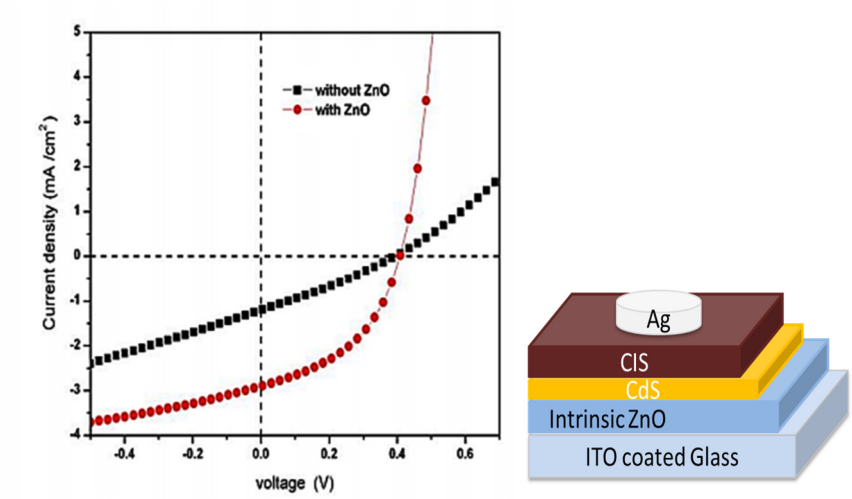

Figure 4.12. J-V characteristics of CIS/CdS solar cell with and without i-ZnO window layer and device structure

Conclusion

Transparent Ag doped ZnO thin films with p-type conductivity were prepared on soda lime glass substrates using chemical spray pyrolysis method. Structural, optical and electrical properties were analyzed as a function of Ag concentration in the precursor solution. Improvement in crystallinity of the films on Ag doping is observed in XRD analysis. Hall measurement revealed that ZnO thin film with good p-type conductivity is achieved for 7at.% Ag using $AgNO_3$ as the dopant source. Compositional analysis of the p-type film using XPS revealed that the film is nearly stoichiometric with traceable percentage of Ag. The p-type behavior of the film is further confirmed by the rectifying nature of the fabricated homojunction. I-V characteristics of the homo p-i-n junction clearly indicate that higher intrinsic layer thickness results in the formation of a good junction with significantly lower reverse leakage current. By using the 5at.% Ag doped intrinsic ZnO film as window layer in CdS/CIS solar cell, definite enhancements in cell parameters are observed.

References

[1] V. Avrutin, D.J. Silversmith, and H. Morkoç, Proc. IEEE **98**, 1269 (2010).

[2] Ü. Özgür, Y.I. Alivov, C. Liu, a. Teke, M. a. Reshchikov, S. Doğan, V. Avrutin, S.J. Cho, and H. Morkç, J. Appl. Phys. **98**, 1 (2005).

[3] U. Özgür, D. Hofstetter, and H. Morkoç, Proc. IEEE **98**, 1255 (2010).

[4] C.H. Park, S.B. Zhang, and S. H. Wei, Phys. Rev. B **66**, 073202 (2002).

[5] Q. Wan, Z. Xiong, J. Dai, J. Rao, and F. Jiang, Opt. Mater. (Amst). **30**, 817 (2008).

[6] S. Yu, L. Ding, H. Zheng, C. Xue, L. Chen, and W. Zhang, Thin Solid Films **540**, 146 (2013).

[7] J.M. Bian, X.M. Li, C.Y. Zhang, W.D. Yu, and X.D. Gao, Appl. Phys. Lett. **85**, 4070 (2004).

[8] H.S. Kang, B. Du Ahn, J.H. Kim, G.H. Kim, S.H. Lim, H.W. Chang, and S.Y. Lee, Appl. Phys. Lett. **88**, 202108 (2006).

[9] M.B. Islam, M.M. Rahman, M.K.R. Khan, M.A. Halim, M.A. Sattar, D.K. Saha, and M.A. Hakim, Thin Solid Films **534**, 137 (2013).

[10] Y. Yan, M.M. Al-Jassim, and S.H. Wei, Appl. Phys. Lett. **89**, 181912 (2006).

[11] O. Volnianska, P. Boguslawski, J. Kaczkowski, P. Jakubas, A. Jezierski, and E. Kaminska, Phys. Rev. B **80**, 245212 (2009).

[12] M.A. Myers, L. Joon Hwan, B. Zhenxing, and M. Haiyan, J. Phys. Condens. Matter **24**, 229501 (2012).

[13] I.S. Kim, E.K.K. Jeong, D.Y. Kim, M. Kumar, and S. Y.Y. Choi, Appl. Surf. Sci. **255**, 4011 (2009).

[14] L. Cao, L. Zhu, and Z. Ye, J. Phys. Chem. Solids **74**, 668 (2013).

[15] W. Bin, Z. Yue, M. Jiahua, and S. Wenbin, Appl. Phys. A **94**, 715 (2009).

[16] Y. Zhang, Z. Zhang, B. Lin, Z. Fu, and J. Xu, J. Phys. Chem. B **109**, 19200 (2005).

[17] J.M. Bian, X.M. Li, C.Y. Zhang, L.D. Chen, and Q. Yao, Appl. Phys. Lett. **84**, 3783 (2004).

[18] J.M. Bian, X.M. Li, X.D. Gao, W.D. Yu, and L.D. Chen, Appl. Phys. Lett. **84**, 541 (2004).

[19] T.V. Vimalkumar, N. Poornima, C.S. Kartha, and K.P. Vijayakumar, Mater. Sci. Eng. B Solid-State Mater. Adv. Technol. **175**, 29 (2010).

[20] L.S. Dake, D.R. Baer, and J.M. Zachara, Surf. Interface Anal. **14**, 71 (1989).

[21] M.S. Raven, Surf. Interface Anal. **1**, 20 (1979).

[22] K. Liu, B.F. Yang, H. Yan, Z. Fu, M. Wen, Y. Chen, and J. Zuo, Appl. Surf. Sci. **255**, 2052 (2008).

[23] P.T. Hsieh, Y.C. Chen, K.S. Kao, and C.M. Wang, Appl. Phys. A Mater. Sci. Process. **90**, 317 (2008).

[24] M. Chen, X. Wang, Y. Yu, Z. Pei, X. Bai, C. Sun, R. Huang, and L. Wen, Appl. Surf. Sci. **158**, 134 (2000).

[25] U. Ilyas, R.S. Rawat, Y. Wang, T.L. Tan, P. Lee, R. Chen, H.D. Sun, F. Li, and S. Zhang, Appl. Surf. Sci. **258**, 6373 (2012).

[26] T.V. Vimalkumar, Highly Conductive and Transparent ZnO Thin Film Using Chemical Spray Pyrolysis Technique : Effect of Doping and Deposition Parameters,Ph.D. thesis, Cochin University of Science and Technology, 2011.

[27] Y.J. Lee, E. S. Cho, and S.J. Kwon, Vacuum **126**, 91 (2016).

[28] S. Ishizuka, K. Sakurai, A. Yamada, K. Matsubara, P. Fons, K. Iwata, S. Nakamura, Y. Kimura, T. Baba, H. Nakanishi, T. Kojima, and S. Niki, Sol. Energy Mater. Sol. Cells **87**, 541 (2005).

[29] U. Rau and M. Schmidt, Thin Solid Films **387**, 141 (2001).

[30] M.S. Sreejith, D. R. Deepu, C. S. Kartha, and K.P. Vijayakumar, AIP Conf. Proc. **67**, 11 (2014).

Chapter

5

CREATING SUB BAND LEVELS IN SPRAY PYROLYSED ZnO THIN FILMS THROUGH EX-SITU METAL DOPING

Contents

5.1 Introduction

Previous chapter of this thesis discussed the deposition of p-type and intrinsic ZnO thin films by CSP. ZnO based homojunction was successfully fabricated and the related studies were also performed. In previous studies, all the doping was achieved by "in-situ doping procedure" i.e., the dopant is included in the precursor solution itself. In this chapter, effects of "ex-situ doping" on spray pyrolysed ZnO thin films are discussed. In "ex-situ doping", the dopant is introduced in to the material (i.e., into the film) by external means such as evaporation and subsequent thermal assisted diffusion[1].

ZnO is a wide band gap material having band gap ~ 3.3eV. Optical and electrical properties of this material can be modified either by changing the deposition conditions or by doping with suitable dopants[1–4]. Doped ZnO films with high electrical conductivity are extensively used in thin film solar cells as TCO layer[5–12]. Intrinsic ZnO films of thickness <100nm are also used in solar

cells as window layers[13–16]. Nano structured ZnO layers are used as electron selective layer/buffer layer in organic solar cells and dye sensitized solar cells[17–24]. But in thin film chalcogenide solar cells, common buffer layers are based on CdS or InS while common absorber materials are Cu based sulfides and/or selenides. Use of different materials as buffer and absorber layers in thin film solar cells will adversely affect the performance of the device mainly due to lattice mismatch and/or inter diffusion between the layers. If the band gap of ZnO is engineered properly, then it possibly could result in the development of an "all ZnO layer" solar cell. The major aim of this work is to fabricate ZnO films which absorb photons in the visible region. It is quite known that wide band gap of normal ZnO prevents absorption of photons in the visible region. Idea behind this work is to incorporate metals to reduce the band gap of ZnO and to create sub band defect levels by incorporating their low band gap oxides resulting in absorption in the visible region.

5.2 Film preparation and characterization

Pristine ZnO films were deposited on soda lime glass substrates using CSP technique. The substrates were cleaned in isopropyl alcohol in an ultrasonic bath followed by rinsing in demineralized water and dried in a hot air current. Precursor solution was prepared by dissolving zinc acetate dihydrate ($Zn(AC)_2.2H_2O$) in a mixture of demineralized water and isopropyl alcohol in 1:1 ratio with 1.25% of acetic acid to the total volume[3]. 50ml of the precursor solution (0.3M) was sprayed on to the preheated substrate kept at 450^0C at spray rate of 5ml/min. Compressed dry air was used as the carrier gas. After deposition, the films were immediately removed from the substrate surface and film surface was kept isolated from atmosphere by placing them inverted on a flat new wood surface. This procedure helps to prevent further

adsorption of any oxygen species to the film surface. Additional information on this regard is reported elsewhere[4].

Silver (Ag) and tin (Sn) were selected as the dopants for ex-situ doping studies. Different thicknesses of these two metals were vacuum evaporated over the pristine ZnO thin films and this resulted in the formation of thin layer of corresponding metal over ZnO films. The deposited metals were diffused in to the ZnO films by vacuum annealing at 450^0C for two hours. Chamber pressure was maintained around 1.5 $x10^{-5}$mbar. The metal film thickness was varied from 8nm to 20nm. Samples were named as Ag-8, Ag-12, Ag-16 and Ag-20 for silver doped ZnO and Sn-8, Sn -12, Sn -16 and Sn-20 for tin doped samples. Undoped samples were denoted as P.

5.2.1 Structural characterization

Figure 5.1.(a) and 5.1.(b) show XRD patterns of ZnO thin films with different doping concentrations of Ag and Sn respectively. Well defined peaks corresponding to (002) and (101) planes of wurtzite ZnO are observed (ICDD card number 79-0208). And all the films are preferentially oriented along (002) plane of wurtzite ZnO. No peaks other than that of ZnO are observed in XRD spectra which indicate the absence of any impurity phase formation in the films. Grain size of the films is calculated from Scherrer formula and is given in Table 5.1. It is observed that the crystallinity of the films is improved with ex-situ doping irrespective of the dopant. The reason for improvement in crystallinity could not be attributed to metal incorporation, because the vacuum annealing process done can also improve the crystallinity. To know the real reason behind the improvement in crystallinity (whether it is due to ex-situ metal doping or due to the vacuum annealing process) pristine ZnO samples were vacuum annealed at the same conditions used for Ag/Sn

diffusion. From Table 5.1, it is clear that vacuum annealing process is the major reason for enhancement in crystallinity of the films. Thus it is evident that incorporation of Ag/Sn into the film through ex-situ doping does not produce any improvement in the crystallinity of the films.

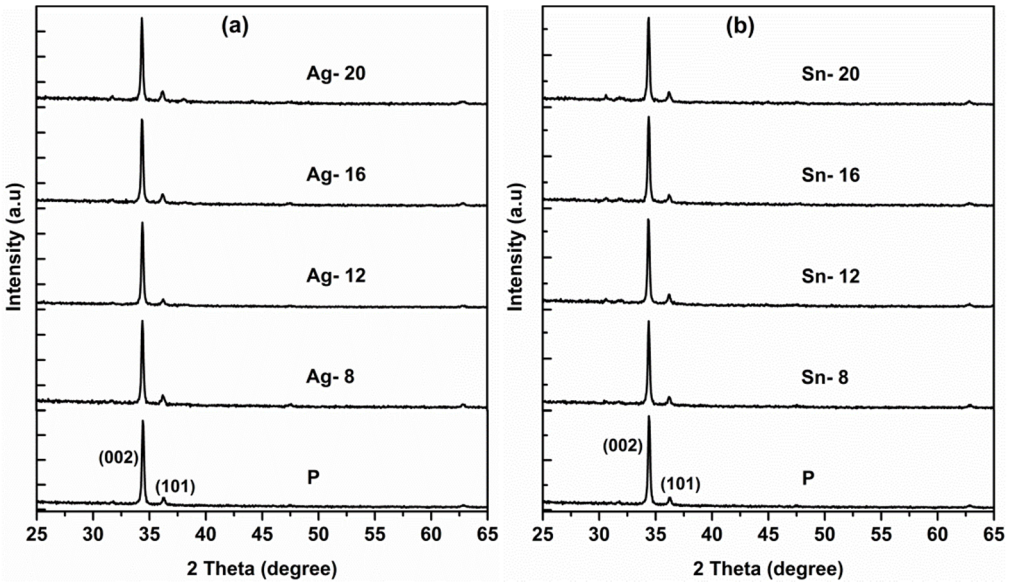

Figure 5.1. XRD pattern of ZnO thin films with (a) Ag and (b) Sn doping

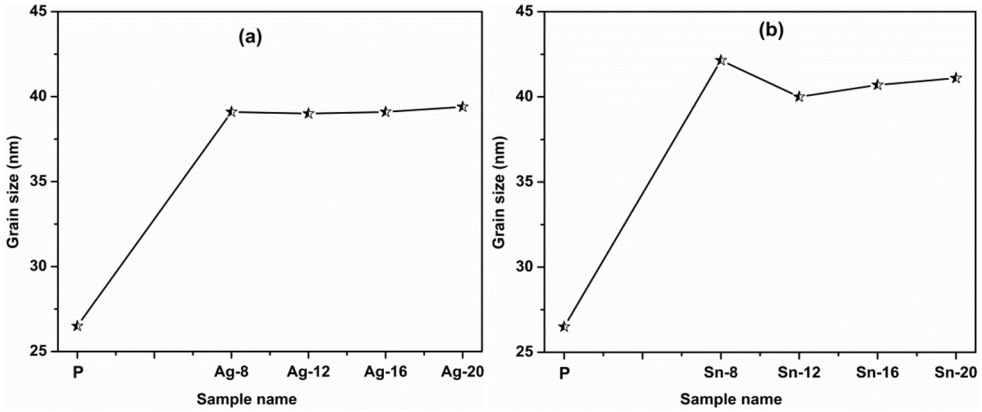

Figure 5.2. Grain size of ZnO thin films doped with (a) Ag and (b) Sn

Table 5.1. Grain size of ZnO thin films doped with Ag and Sn

Sample name	Grain size (nm)	Sample name	Grain size (nm)
P	26.5	P	26.5
P - annealed	38.6	P-annealed	38.6
Ag – 8	39.1	Sn – 8	42.1
Ag – 12	39	Sn – 12	40
Ag – 16	39.1	Sn – 16	40.7
Ag – 20	39.4	Sn – 20	41.1

5.2.2 Electrical characterization

Electrical properties of the films were analyzed by Hall effect measurement. Thickness of the films is found to be about 400 ±30nm and show a negligible variation in thickness with Ag/Sn incorporation. Electrical properties of pristine and Ag doped ZnO films are given in Table 5.2.a and that of Sn doped ZnO films are shown in Table 5.2.b. There is no change in the order of resistivity values (10^{-1} everywhere), carrier concentration and mobility of the films. It is also observed that ex-situ doping with Ag and Sn does not change the electrical properties of the films and all the films are n-type conducting.

Table 5.2.a. Electrical properties of Ag doped ZnO thin films

Sample name	Carrier Conc.(cm^{-3})	Resistivity (Ω.cm)	Mobility ($cm^2/V.s$)	Conductivity type
P	1.9×10^{18}	3.8×10^{-1}	8.3	n
Ag – 8	2.4×10^{18}	5.9×10^{-1}	4.3	n
Ag – 12	4.1×10^{18}	9.8×10^{-1}	1.5	n
Ag – 16	3.0×10^{18}	3.2×10^{-1}	6.3	n
Ag – 20	3.3×10^{18}	6.9×10^{-1}	2.7	n

Table 5.2.b. Electrical properties of Sn doped ZnO thin films

Doping Concentration	Carrier Conc.(cm^{-3})	Resistivity (Ω.cm)	Mobility ($cm^2/V.s$)	Conductivity type
Sn - 8	3.9×10^{18}	2.7×10^{-1}	5.9	n
Sn - 12	3.8×10^{18}	3.4×10^{-1}	4.9	n
Sn - 16	4.6×10^{18}	2.1×10^{-1}	6.6	n
Sn - 20	5.1×10^{18}	1.8×10^{-1}	6.9	n

5.2.3 Optical characterization

Optical transmission and absorption spectra of the films were recorded using UV-Vis-NIR spectrometer. Transmission spectra of ZnO films with Ag and Sn doping in the visible region are shown in Figure 5.3.(a) and 5.3.(b) respectively. A clear reduction in transmission with increase in doping concentrations of Ag and Sn is evident from transmission spectra. Transmission of the films is most affected in the wavelength region below 700nm. Figure 5.5.(a) and 5.5.(b) show the variation in band gap of the films with Ag and Sn doping respectively. Band gap reduction with Ag and Sn incorporation is evident from Tauc plot. Sub band levels are observed at 1.55eV and 1.05eV for Ag doped ZnO films and for ZnO thin film doped with Sn, sub band levels are observed at 1.6eV and 1.1eV. The absorption corresponding to sub band level in samples Ag-20 and Sn-20 are given as inset of the Figure 5.5.(a) and 5.5.(b) respectively.

Films turned brownish with Ag/Sn doping and are shown in Figure 5.4.(a) and 5.4.(b) respectively. Appearance of brownish color along with the reduction in transmittance with Ag/Sn doping can be attributed to the formation of sub band absorbing levels in the films on ex-situ doping.

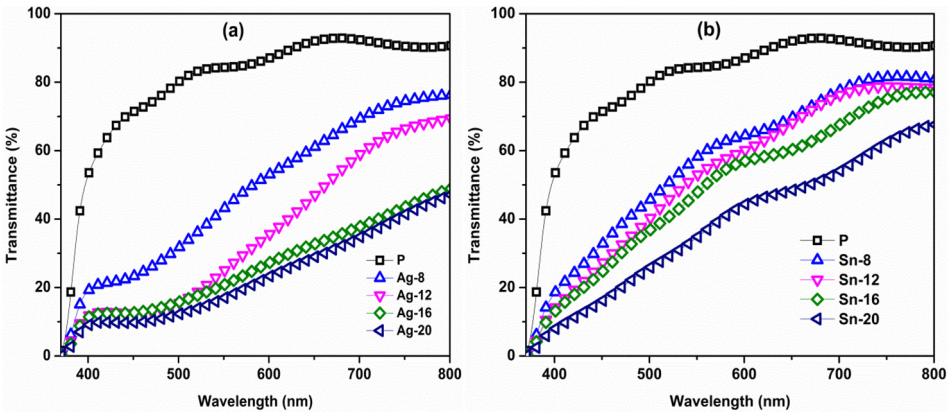

Figure 5.3. Transmission spectra of ZnO thin films doped with (a) Ag and (b) Sn

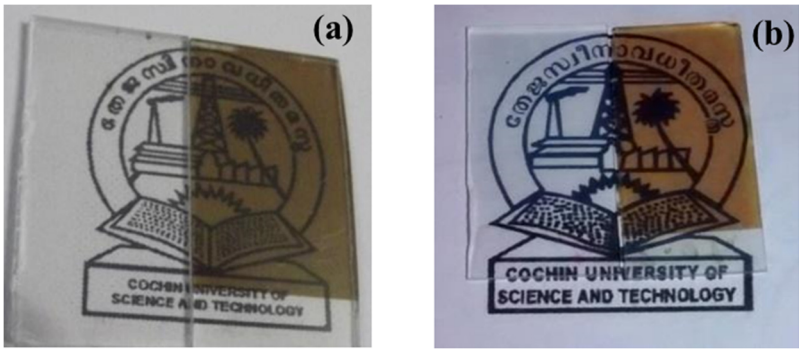

Figure 5.4. Photographic images of (a) Ag-20 and (b) Sn-20 with respect to P

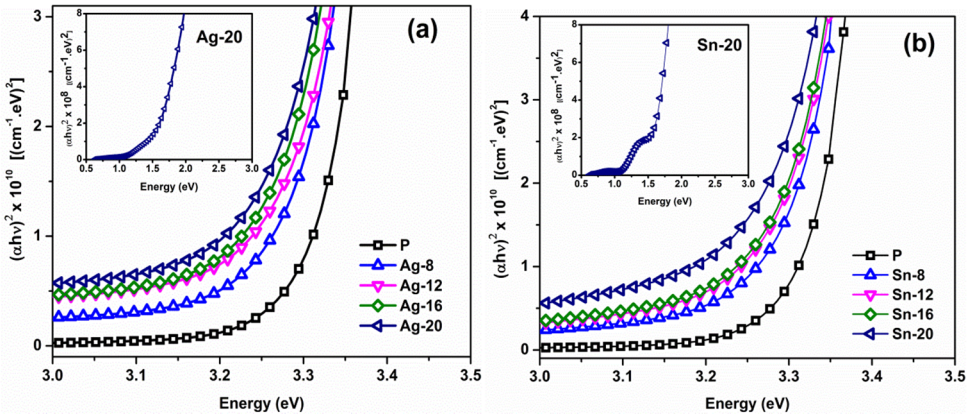

Figure 5.5. Tauc plot of ZnO films doped with (a) Ag and (b) Sn. Sub-band absorption in Ag-20 and Sn-20 are shown as inset of (a) and (b) respectively

5.2.4 Morphological characterization

Surface morphology of pristine, Ag (Ag-20) and Sn (Sn-20) doped ZnO thin film were analyzed using Zeiss sigma FESEM. It is observed that pristine ZnO thin film surface is covered with 'granules like' nanostructures having a wide range of particle size distribution. However, ex-situ doped ZnO thin films had granules with homogeneous size distribution.

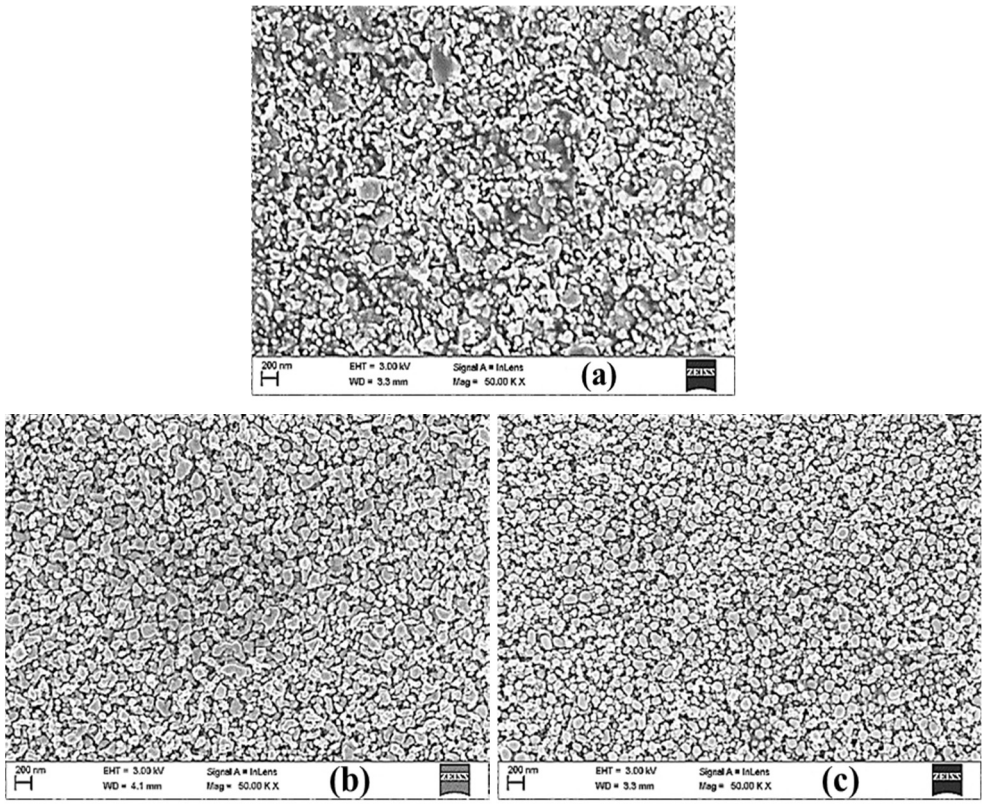

Figure 5.6. SEM micrographs of (a) P, (b) Ag-20 and (c) Sn-20

5.2.5 Compositional characterization

Compositional analysis of samples Ag-20 and Sn-20 were done by XPS depth profile measurement. This will help to understand the distribution of the dopants in the films. Any shift in peak position of the elements could be

corrected by using the C 1s peak of adventitious carbon present in the films. Figure 5.7 shows the comparison of core level peaks of Zn and O in both samples. It is observed that there is no change in binding energy for Zn and O peaks and the change in peak shape is negligible. The chemical states of Zn and O in the films remain the same irrespective of the ex-situ metal incorporation. From Zn $2p_{3/2}$ core level peak (BE = 1022.2 ±0.2eV), it is identified that Zn exists in Zn^{2+} state in the films[25].

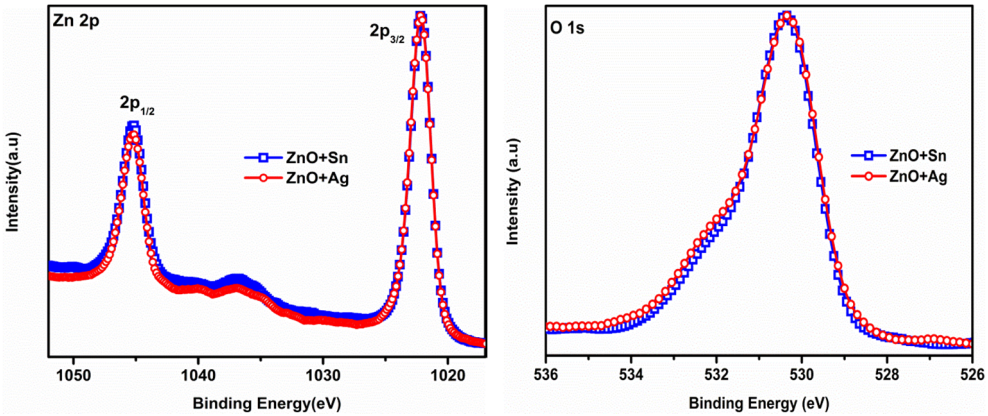

Figure 5.7. Comparison of XPS core level peaks of (a) Zn and (b) O in Ag-20 and Sn-20

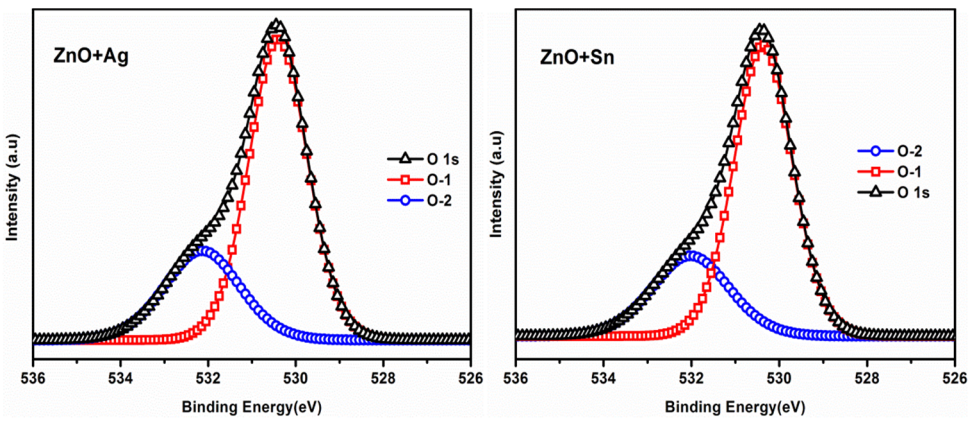

Figure 5.8. Deconvoluted components of O 1s peak in(a) Ag-20 and (b) Sn-20

The core level peak of O 1s can be deconvoluted in to two component peaks at 530.4 ±0.2eV and 531.9 ±0.2eV. The deconvoluted components of

O 1s peak are shown in Figure 5.8. The peak at lower binding energy (BE), (O-1) represents the O^{2-} oxidation state of oxygen in metal oxides and the peak at higher binding energy (O-2) represents oxygen in interstitial sites[25,26]. The relative concentration of O-1 and O-2 components is nearly 63% and 27% respectively. Oxygen in interstitial sites in oxide semiconductors can adversely affect the electrical properties of the material by acting as "killer sites". No enhancement on electrical properties even in the presence of excess metal content in the films can be attributed to the interstitial oxygen.

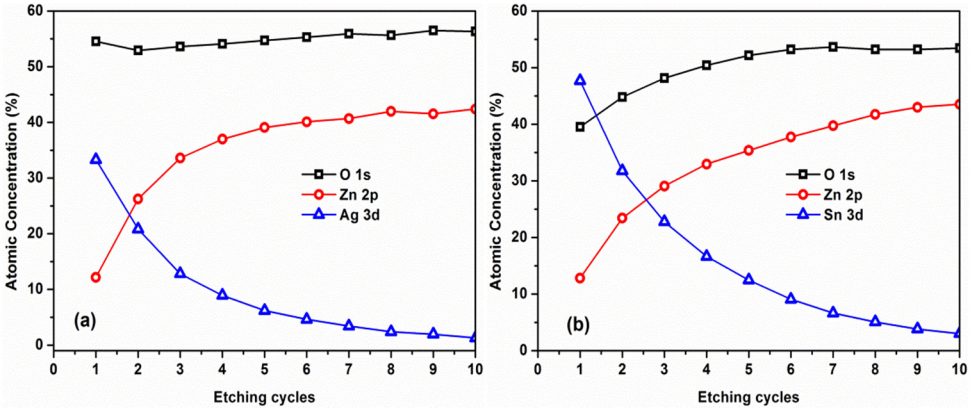

Figure 5.9. Variation in percentage of elements in (a) Ag-20 and (b) Sn-20

Figure 5.9 shows the variation in percentage of elements from the XPS depth profile of the samples Ag-20 and Sn-20. It is clear that the deposited metals got diffused into the films on vacuum annealing. The maximum concentration of incorporated metal is at the surface layer and it decreases in an exponential manner towards the bulk of the film. After a number of etching cycles by Ar ion sputtering, concentration of the dopants diminishes considerably. From Figure 5.9, it is also clear that the incorporated metals affect the concentration of Zn in the film. The higher the dopant concentration, lower the Zn concentration. Ag and Sn may be occupying the Zn position which may reduce the concentration of Zn in the sample. The concentration of O remains unchanged by metal incorporation and it remains more or less same throughout the samples.

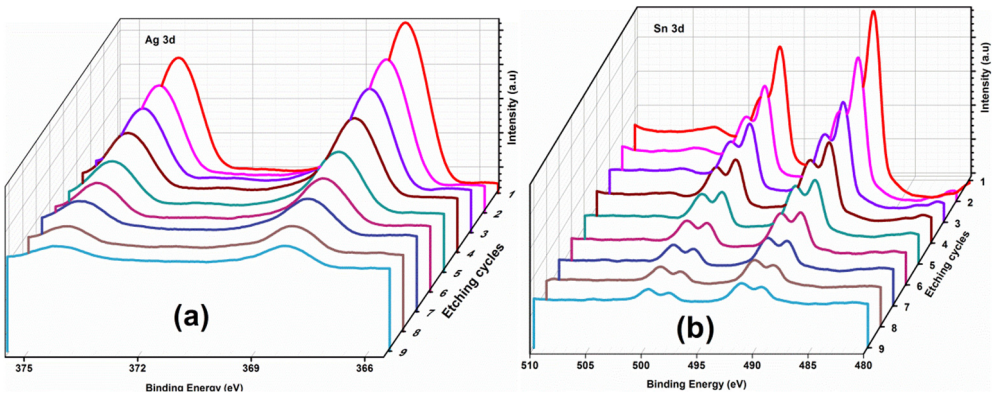

Figure 5.10. Depth profile of (a) Ag 3d and (b) Sn 3d core level peaks in Ag-20 and Sn-20

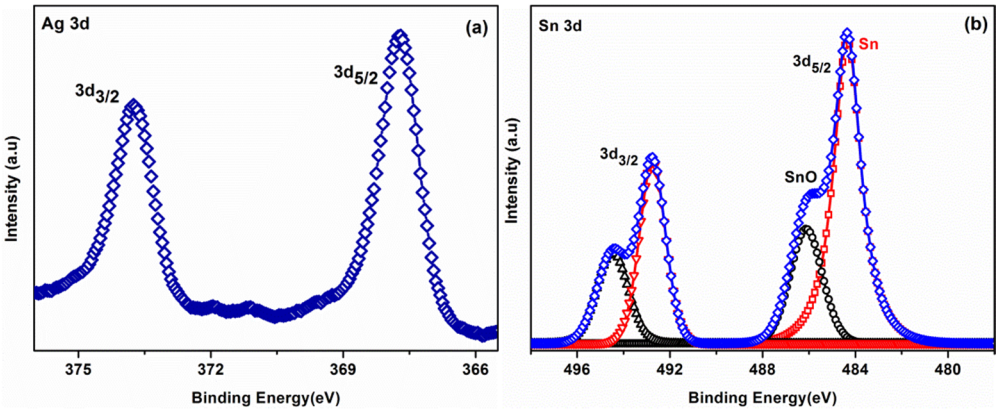

Figure 5.11. XPS core level peaks of (a) Ag 3d and (b) Sn 3d in Ag-20 and Sn-20

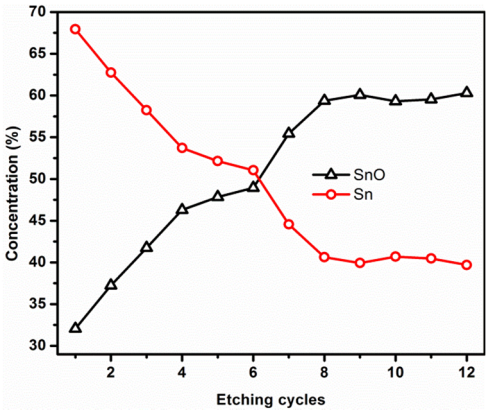

Figure 5.12. Variation of metal and metal oxide concentration of Sn in sample Sn-20

The variation in intensities of the core level peaks corresponding to the incorporated Ag and Sn are shown in Figure 5.10. The maximum intensity of the peaks is at the surface and it decreases towards the bulk of the samples. Figure 5.11 shows the core level peaks corresponding to Ag and Sn in the films. It is observed that Sn 3d peaks can be deconvoluted in to two components. The deconvoluted peaks of Sn $3d_{5/2}$ positioned at 484.2 ±0.2eV and 486.2 ±0.2eV, in which, the peak at lower BE represents the oxidation state of metallic Sn and the peak at higher BE represents oxidation state of Sn in SnO[27–29]. It is observed that the incorporated Sn exists in a metal-metal oxide mixed state in ZnO. At the surface layers, the peak corresponding to metallic Sn component is dominating. Intensity of the metallic component peak decreases and the peak corresponding to SnO state dominates along the depth of the sample (Figure 5.10.b). The variation of metal and metal oxide concentration of Sn is calculated with ion gun etching cycles and is shown in Figure 5.12.

But unlike the dopant Sn, there is no splitting for the binding energy peak corresponding Ag 3d core level peaks. However, it is difficult to find out the exact chemical state of Ag in the film as the binding energy separation between the states of Ag in metallic Ag and its oxides are less than 0.2eV and it could not be identified from the obtained spectra as the resolution is 0.2eV. Analyzing the samples using a high resolution XPS may give detailed information about the exact states of Ag present in the sample. It is observed that full width at half maximum for Ag 3d core level peaks from the sample are greater than that of metallic Ag and this can be attributed to the presence of oxides of Ag in the sample. In both cases it is found that the ex-situ doping with Ag or Sn forms their oxides in the host ZnO thin film. Formation of these low band gap oxides is the reason for the creation of sub band levels and it results in the observed color change in the films.

Conclusion

Silver and tin ex-situ doping was performed on spray deposited ZnO thin films by thermal evaporation and by subsequent annealing of the corresponding metal films. Structural, optical, electrical and compositional analysis of the films were carried out as function of thickness of deposited metal films. Electrical properties of the films show negligible variation with metal incorporation into the film. But the transmittance and band gap of the samples decrease with increase in doping and the transparent ZnO films turned to brown in color. The sub band absorption is identified from the lower energy region of the Tauc plot. Compositional analysis of the metal incorporated thin films revealed that the diffused elements exist in a metal-metal oxide mixed state in the films.

References

1 T.V. Vimalkumar, N. Poornima, K.B. Jinesh, C.S. Kartha, and K.P. Vijayakumar, Appl. Surf. Sci. **257**, 8334 (2011).

2 Ü. Özgür, Y.I. Alivov, C. Liu, a. Teke, M. a. Reshchikov, S. Doğan, V. Avrutin, S.J. Cho, and H. Morkoç, J. Appl. Phys. **98**, 1 (2005).

3 T.V. Vimalkumar, N. Poornima, C.S. Kartha, and K.P. Vijayakumar, Mater. Sci. Eng. B Solid-State Mater. Adv. Technol. **175**, 29 (2010).

4 T.V. Vimalkumar, N. Poornima, C. Sudha Kartha, K.P. Vijayakumar, T. Abe, and Y. Kashiwaba, Phys. B Condens. Matter **405**, 4957 (2010).

5 M.A. Martínez, J. Herrero, and M.T. Gutiérrez, Sol. Energy Mater. Sol. Cells **45**, 75 (1997).

6 Y. Hagiwara, T. Nakada, and A. Kunioka, Sol. Energy Mater. Sol. Cells **67**, 267 (2001).

[7] K. Matsubara, P. Fons, K. Iwata, A. Yamada, K. Sakurai, H. Tampo, and S. Niki, Thin Solid Films **431-432**, 369 (2003).

[8] J. Yoo, J. Lee, S. Kim, K. Yoon, I.J. Park, S.K. Dhungel, B. Karunagaran, D. Mangalaraj, and J. Yi, Thin Solid Films **480-481**, 213 (2005).

[9] W.J. Jeong, S.K. Kim, and G.C. Park, Thin Solid Films **506-507**, 180 (2006).

[10] W. Beyer, J. Hüpkes, and H. Stiebig, Thin Solid Films **516**, 147 (2007).

[11] S. Calnan, J. Hüpkes, B. Rech, H. Siekmann, and A.N. Tiwari, Thin Solid Films **516**, 1242 (2008).

[12] T. Tohsophon, J. Hüpkes, H. Siekmann, B. Rech, M. Schultheis, and N. Sirikulrat, Thin Solid Films **516**, 4628 (2008).

[13] Y.J. Lee, E. S. Cho, and S.J. Kwon, Vacuum **126**, 91 (2016).

[14] S. Ishizuka, K. Sakurai, A. Yamada, K. Matsubara, P. Fons, K. Iwata, S. Nakamura, Y. Kimura, T. Baba, H. Nakanishi, T. Kojima, and S. Niki, Sol. Energy Mater. Sol. Cells **87**, 541 (2005).

[15] U. Rau and M. Schmidt, Thin Solid Films **387**, 141 (2001).

[16] Y. Lare, A. Godoy, L. Cattin, K. Jondo, T. Abachi, F.R. Diaz, M. Morsli, K. Napo, M.A. del Valle, and J.C. Bernède, Appl. Surf. Sci. **255**, 6615 (2009).

[17] W.J.E. Beek, M. M.Wienk, and R. A.J.Janssen, Adv. Mater. **16**, 1009 (2004).

[18] Y. Sun, J.H. Seo, C.J. Takacs, J. Seifter, and A.J. Heeger, Adv. Mater. **23**, 1679 (2011).

[19] J. You, L. Dou, K. Yoshimura, T. Kato, K. Ohya, T. Moriarty, K. Emery, C.C. Chen, J. Gao, G. Li, and Y. Yang, Nat. Commun. **4**, 1446 (2013).

[20] E. Galoppini, J. Rochford, H. Chen, G. Saraf, Y. Lu, A. Hagfeldt, and G. Boschloo, J. Phys. Chem. B **110**, 16139 (2006).

[21] A.B.F. Martinson, J.W. Elam, J.T. Hupp, and M.J. Pellin, Nano Lett. **7**, 2183 (2007).

[22] Q. Zhang, T.P. Chou, B. Russo, S.A. Jenekhe, and G. Cao, Angew. Chemie - Int. Ed. **47**, 2402 (2008).

[23] J.B. Baxter, A.M. Walker, K. Van Ommering, and E.S. Aydil, Nanotechnology **17**, S304 (2006).

[24] S.H. Ko, D. Lee, H.W. Kang, K.H. Nam, J.Y. Yeo, S.J. Hong, C.P. Grigoropoulos, and H.J. Sung, Nano Lett. **11**, 666 (2011).

[25] M. Chen, X. Wang, Y. Yu, Z. Pei, X. Bai, C. Sun, R.. Huang, and L. Wen, Appl. Surf. Sci. **158**, 134 (2000).

[26] P.T. Hsieh, Y.C. Chen, K.S. Kao, and C.M. Wang, Appl. Phys. A Mater. Sci. Process. **90**, 317 (2008).

[27] R.I. Hegde, S.R. Sainkar, S. Badrinarayanan, and A.P.B. Sinha, J. Electron Spectros. Relat. Phenomena **24**, 19 (1981).

[28] M.A. Stranick, Surf. Sci. Spectra **2**, 45 (1993).

[29] NIST XPS Database.

Chapter

6

SPRAYED ZnO AS A CONDUCTING METAL ION DIFFUSION BARRIER LAYER OVER FLEXIBLE STEEL SUBSTRATES

Contents

6.1 Introduction

Thin film photovoltaics is one of the future alternative energy sources since it is clean, economic and environmental friendly. In conventional thin film solar cells, the substrate used is glass which increases the weight and thickness of the cell[1,2]. Glass are heavy, fragile, and hence requires extra care and support for fabrication and installation, which will eventually lead to the increase in overall expense of solar cell. Solar cell fabrication process may involve high temperature deposition steps and hence the poor thermal conductivity and expansivity of glass will result in thermal gradients and non-uniform device properties[3–6]. The above problems with solar cells can be minimized by using thin metallic foils or polymers having high temperature tolerance as substrates. Usage of flexible substrates has several advantages, such as they are not fragile and requires only minimum supporting structures. Importantly foil/flexible substrates can be used in 'roll to roll' production process[3].

Mo, Ti and stainless steel (SS) are most widely used metal substrates, among which thin foils of SS are the most attractive substrates for the production of flexible photovoltaic devices[7–9] as it can withstand high temperature processing conditions and have high radiation hardness[10]. High radiation hardness and high specific power/Kg makes them potential substrates for outer space solar cell applications also[1,11].

But the maximum efficiency of solar cells on steel substrates are lower than the efficiencies reported on rigid substrates[8,12]. Main reason for the limiting efficiency is the diffusion of detrimental substrate elements such as Fe into the absorber layer during the high temperature fabrication conditions[13,14]. To counteract the negative influence of Fe from steel substrates, barrier layers such as Cr[15], Ti or TiN[16] are mostly used. Insulating barriers like SiO_x[9,10,14] Al_2O_3[8,9] and ZnO[13] and enamel[12] were also used to suppress diffusion. All these barrier layers were deposited by employing techniques like vacuum evaporation, sputtering, and sol-gel method. However, there are no reports on the deposition of barrier layers on steel substrates through CSP.

ZnO barrier layer fabricated by C.Y. Shi *et al.* through DC sputtering was an insulating layer, and they have deposited a layer of molybdenum over the insulating ZnO layer as the back contact to use in CIGS solar cell[13]. If the barrier layer (ZnO layer) itself is conducting, then the need for Mo back contact layer could have been avoided. Reduction of a layer will result in large saving in time as well as money in solar cell production.

This chapter discusses the deposition conditions for the fabrication of an electrically conducting ZnO barrier layer to prevent Fe diffusion from steel substrates using CSP. A two-step deposition procedure is adopted. The first ZnO layer on steel substrate is deposited at a low temperature to prevent the Fe ion

diffusion followed by a higher temperature deposition of second ZnO layer to enhance the conductivity. To further reduce the sheet resistance, a second ZnO layer is doped with Al followed by "quick quenching" of the layer.

The main objective of this work is to demonstrate deposition of a conducting ZnO barrier layer instead of an insulating layer over steel substrates by an economic and scalable spray pyrolysis technique, which can be utilized for 'roll to roll' processing also. Here a CIS/InS based solar cell fabrication is also demonstrated over the steel substrate with conducting ZnO barrier layer.

6.2 Deposition of ZnO layers over flexible steel substrates

Steel sheets of thickness 0.25mm and size 50mm x 50mm were selected as substrate and were ultrasonically cleaned using acetone, and isopropyl alcohol followed by demineralized water. Then the substrates were dried in hot air current. Since substrates are flexible, a heavy mask is designed so that it will hold the substrate to the heater surface by pressing. Precursor solution (0.3M) was prepared by dissolving zinc acetate dihydrate [$Zn(CH_3COO)_2.2H_2O$] in a mixture of demineralized water and isopropyl alcohol in 1:1 ratio. Later 1.25 % of acetic acid was added to this translucent solution to get a clear solution[17].

ZnO thin films were deposited on steel substrates in two steps. To prevent the diffusion of Fe from the substrate, initial layer was deposited at a relatively lower temperature of 300 $\pm 10^0$C. At this temperature, 20ml of the precursor was sprayed on to the substrate. This layer of ZnO should act as a diffusion barrier while the next layer should be a conducting layer for using in a solar cell. Hence, the second ZnO layer was deposited at an elevated temperature of 450 $\pm 10^0$C. 30ml of the precursor solution doped with 2.56% of aluminium[18] was sprayed on to the substrate. After deposition, a quick cooling

procedure was applied by dipping it in a liquid at room temperature or below **(patent protected data).**

To further verify the effect of ZnO barrier layer, solar cells were fabricated on steel substrate using CIS and InS as absorber and buffer layers, with and without ZnO layer. The fabrication procedure for CIS/InS solar cells is reported elsewhere[19].

6.2.1 Structural characterization

X- ray diffraction data of the flexible steel substrate and ZnO layers deposited on steel substrates using CSP is shown in Figure 6.1. In addition to the peaks corresponding to the steel substrate, peaks corresponding to wurtzite hexagonal phase of ZnO (ICDD card number 79-0208) are clearly visible. The ZnO layer showed a preferential orientation along (002) plane of wurtzite hexagonal phase of ZnO.

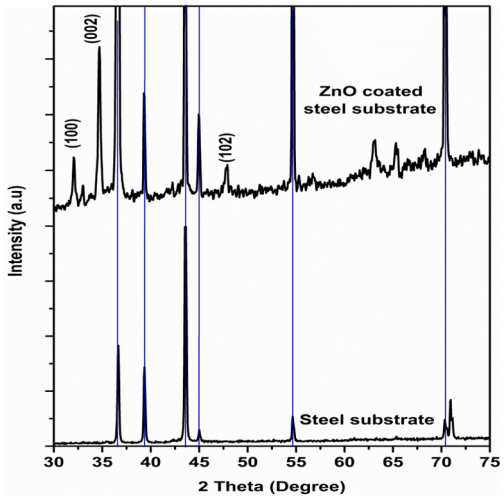

Figure 6.1. XRD pattern of steel substrate with and without ZnO layer

6.2.2 Electrical characterization

Since the substrates are flexible and magnetic in nature, thickness measurement and electrical characterization by Hall effect measurement of the

films are difficult. The sheet resistance of the substrate before any ZnO layer deposition is around 7.5 x10^{-2}Ω/sq. After coating with ZnO double layer, the sheet resistance is found to be around 2kΩ/sq. Adsorption of oxygen species increases the sheet resistance of the films. To prevent this, surface of ZnO layer has to be isolated from atmosphere immediately after deposition. Hence the deposited ZnO film was quickly removed from the heater surface and kept isolated from the atmosphere by a method discussed elsewhere[20]. The sheet resistance of this film was found to be further reduced to 500Ω/sq. For a device point of view, the sheet resistance should be well below 20Ω/sq. To achieve this, a quick quenching procedure is applied to the films by dipping it to a suitable liquid medium **(patent protected data).** The liquid temperature and sheet resistance are shown in Table 6.1 and the impact on sheet resistance is evident from the tabulated data. Spatial variation of sheet resistance of the prepared ZnO film is shown in Figure 6.2 and it is found that ZnO layer is uniform in nature with even sheet resistance over the substrate.

Table 6.1. Sheet resistance of ZnO double layer after quenching at different temperatures in different liquids

Temperature (^{0}C)	liquid 1	liquid 2
30	150Ω/sq	240Ω/sq
0	14Ω/sq	50Ω/sq

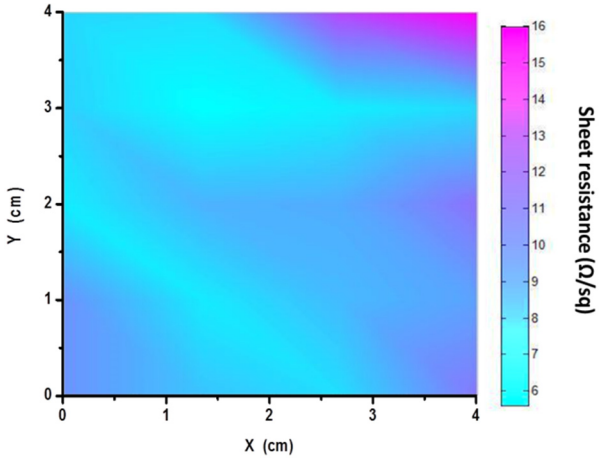

Figure 6.2. Spatial variation of resistance of ZnO double layer on steel substrate after quenching procedure

6.2.3 Morphological characterization

Surface morphology of bare steel substrates and ZnO coated substrates were analyzed using Zeiss sigma FESEM. Figure 6.3 show that the bare substrate has a non-uniform surface with large cracks and flakes, but ZnO deposited steel substrates have a uniform surface covered with nanostructures.

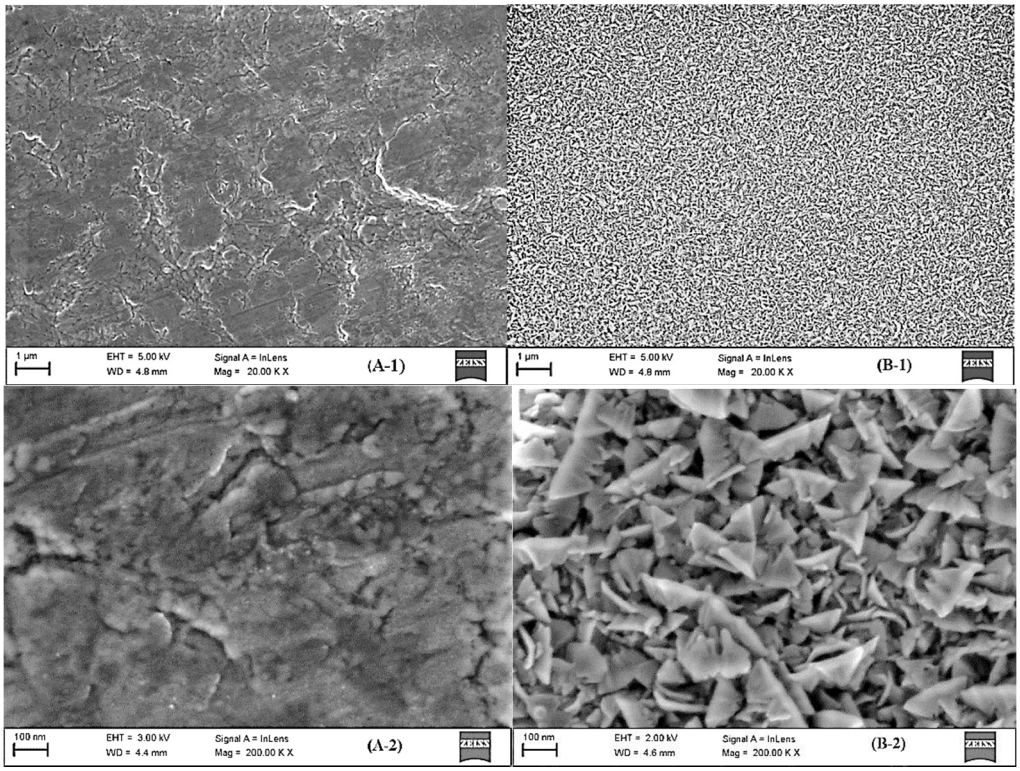

Figure 6.3. SEM micrograph of steel substrate with and without ZnO layer (A-1 and B-1 at 20K magnification and A-2 and B-2 at 200K magnification)

6.2.4 Compositional characterization

Compositional analysis of the deposited ZnO film over steel substrate was carried out by XPS depth profiling. The sample was mounted on stainless steel holders using conducting carbon tape. Argon ion sputtering is used to remove thin layers of the material after each data acquisition. The chamber was kept at a pressure

less than $3x10^{-6}$Pa and the spectrometer was calibrated by measuring the $3d_{5/2}$ core level peak of silver (368.2eV). Resolution of the analyzer is set at 150meV. Figure 6.4 shows the depth profile of ZnO layer coated over steel substrate by CSP.

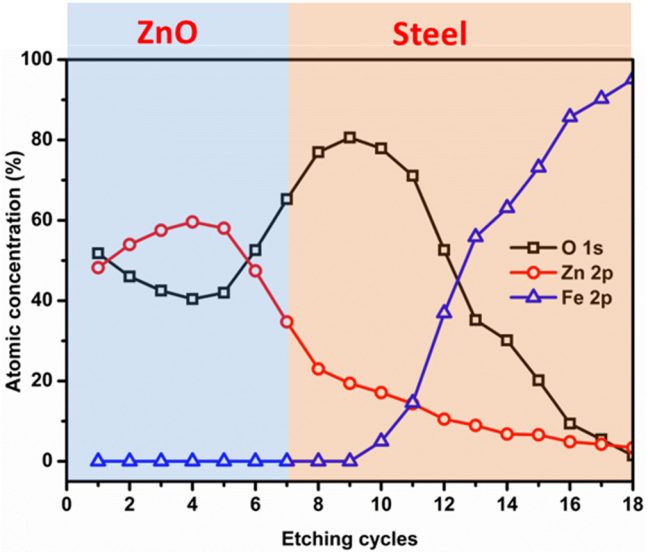

Figure 6.4. Variation in percentage of elements in ZnO coated steel substrate from XPS depth profile

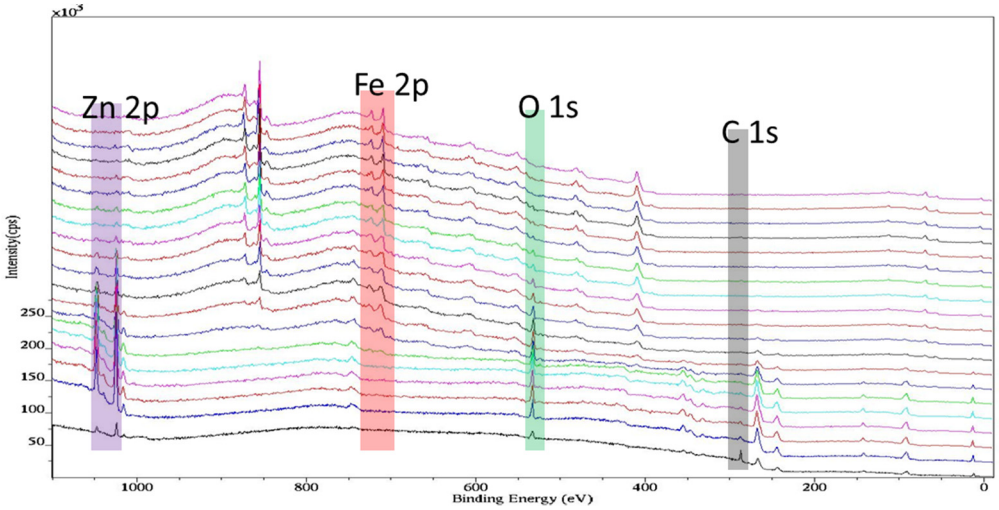

Figure 6.5. Distribution of core level peaks of elements in ZnO coated steel substrate from XPS depth profile

From the Figure 6.4, it is clear that metal ion is not diffused into ZnO layer. From the wide XPS depth profile, (spectra are shown in Figure 6.5) it is clear that peaks corresponding to zinc and oxygen are only observed at the surface. Carbon species adsorbed to the layer are removed by the first cycle of Ar ion etching. The peaks corresponding to Fe appear only after a few number of etching cycles, during which ZnO layer is completely etched out. The XPS results prove successful deposition of spray deposited ZnO layer over steel substrate to prevent Fe diffusion.

To know the extent of Fe ion diffusion in CIS absorber layer, CIS film is deposited on bare steel substrates and XPS depth profile analysis was carried out and is shown in Figure 6.6. From Figure 6.6, it is clear that the Fe ions from the substrate are well diffused into the CIS absorber layer and the atomic concentration of Fe in CIS layer varies from 1 to 3%.

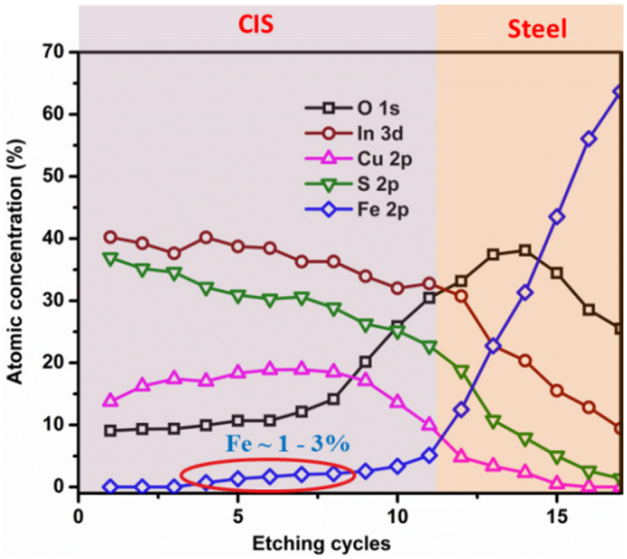

Figure 6.6. XPS depth profile of CIS absorber layer over steel substrate

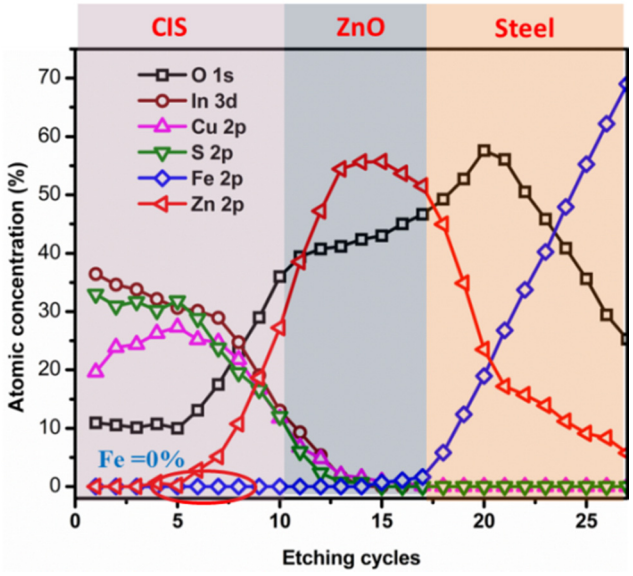

Figure 6.7. XPS depth profile of CIS layer over ZnO coated steel substrate

To see the effectiveness of the ZnO barrier layer, CIS absorber layer was deposited on the steel substrates with ZnO barrier layer and XPS depth analysis is carried out again (Figure 6.7). From Figure 6.7, it is clear that not even a trace amount of Fe is present in the absorber layer and this again proves the effectiveness of the ZnO layer as a metal ion diffusion barrier layer over steel substrate.

6.2.5. Solar cell fabrication

To show the effect of ZnO barrier layer on flexible solar cells over steel substrates, CIS/InS layers were deposited over steel substrates with and without ZnO layer. J-V characteristics of the devices deposited on steel substrates with and without ZnO barrier layer is measured and given in Figure 6.8.(a) and 6.8.(b) respectively. The device without ZnO layer shows an open circuit voltage of 375mV and a short circuit current density of 0.385mA/cm^2. The efficiency and fill factor are 0.05% and 41% respectively. On the other hand, the device deposited on ZnO coated substrates shows an improvement in efficiency.

The solar cell parameters for this solar cell are V_{oc} = 320mV, J_{sc} = 1.85mA/cm^2, η = 0.24% and FF = 40.4%. Improvement in cell parameters is due to the successful prevention of the diffusion of Fe ions into solar cell layers.

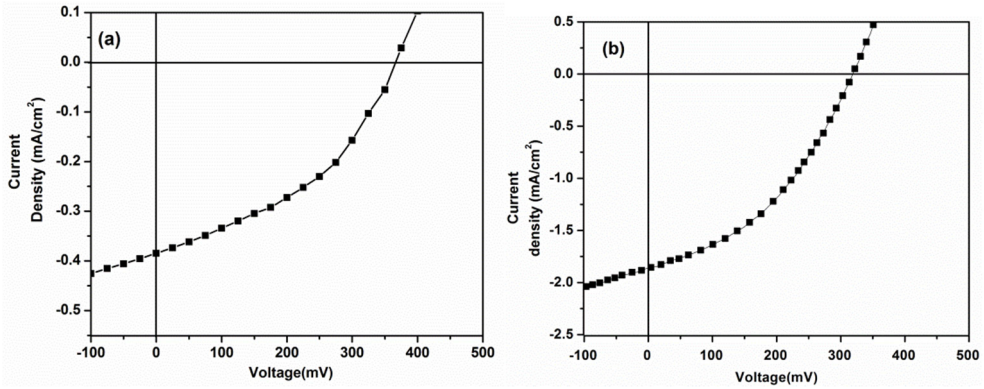

Figure 6.8. Illuminated J-V characteristics of CIS/InS solar cells over steel substrate (a) with ZnO layer and (b) without ZnO layer

Conclusion

Spray pyrolysis technique is utilized to deposit resistive as well as conducting ZnO thin films over flexible steel substrates. A double layer deposition procedure is proposed to prevent Fe ion diffusion from the substrate at high temperature deposition conditions. Films with low sheet resistance (< 14Ω/sq) are obtained for ZnO film by employing a quick quenching procedure. Successful prevention of Fe ion diffusion from the steel substrate is proved from the XPS depth analysis. Efficiency and current density of "all sprayed" CIS/InS solar cells fabricated on steel substrates with conducting ZnO barrier layer is found to be better than that of solar cells fabricated on bare steel substrates.

References

[1] M.M. Aliyu, M.A. Islam, N.R. Hamzah, M.R. Karim, M.A. Matin, K. Sopian, and N. Amin, Int. J. Photoenergy **2012**, 6 (2012).

[2] A. Seth, G.B. Lush, J.C. McClure, V.P. Singh, and D. Flood, Sol. Energy Mater. Sol. Cells **59**, 35 (1999).

[3] X. Mathew, J.P. Enriquez, A. Romeo, and A.N. Tiwari, Sol. Energy **77**, 831 (2004).

[4] G.P. Hernández, X. Mathew, J.P. Enríquez, B.E. Morales, M.M. Lira, J.A. Toledo, A.S. Juárez, and J. Campos, J. Mater. Sci. **39**, 1515 (2004).

[5] S. Chandramohan, R. Sathyamoorthy, S. Lalitha, and S. Senthilarasu, Sol. Energy Mater. Sol. Cells **90**, 686 (2006).

[6] V.P. Singh, J.C. Mcclure, G.B. Lush, W. Wang, X. Wang, G.W. Thompson, and E. Clark, **59**, 145 (1999).

[7] F. Kessler, D. Herrmann, and M. Powalla, Thin Solid Films **480**, 491 (2005).

[8] K. Herz, A. Eicke, F. Kessler, R. Wachter, and M. Powalla, Thin Solid Films **431**, 392 (2003).

[9] K. Herz, E. Kessler, R. Wachter, M. Powalla, J. Schneider, a Schulz, and U. Schumacher, Thin Solid Films **403**, 384 (2002).

[10] T. Satoh, Y. Hashimoto, S. Shimakawa, S. Hayashi, and T. Negami, Sol. Energy Mater. Sol. Cells **75**, 65 (2003).

[11] A. Romeo, D. Batzner, H. Zogg, and A. Tiwari, in *17th Eur. Photovolt. Conf. Exhib.* (2001).

[12] R. Wuerz, a Eicke, F. Kessler, S. Paetel, S. Efimenko, and C. Schlegel, Sol. Energy Mater. Sol. Cells **100**, 132 (2012).

[13] C.Y. Shi, Y. Sun, Q. He, F.Y. Li, and J.C. Zhao, Sol. Energy Mater. Sol. Cells **93**, 654 (2009).

[14] R. Wuerz, A Eicke, M. Frankenfeld, F. Kessler, M. Powalla, P. Rogin, and O. Yazdani-Assl, Thin Solid Films **517**, 2415 (2009).

[15] K.B. Kim, M. Kim, J. Baek, Y.J. Park, J.R. Lee, J.S. Kim, and C. Jeon, Electron. Mater. Lett. **10**, 247 (2014).

[16] W.S. Liu, H. C. Hu, N. W. Pu, and S. C. Liang, J. Alloys Compd. **631**, 146 (2015).

[17] T.V. Vimalkumar, N. Poornima, C.S. Kartha, and K.P. Vijayakumar, Mater. Sci. Eng. B Solid-State Mater. Adv. Technol. **175**, 29 (2010).

[18] T.V. Vimalkumar, Highly Conductive and Transparent ZnO Thin Film Using Chemical Spray Pyrolysis Technique : Effect of Doping and Deposition Parameters, Ph.D. thesis, Cochin University of Science and Technology, 2011.

[19] M.V. Santhosh, D.R. Deepu, C. Sudha Kartha, K. Rajeev Kumar, and K.P. Vijayakumar, Sol. Energy **108**, 508 (2014).

[20] T.V. Vimalkumar, N. Poornima, C. Sudha Kartha, K.. Vijayakumar, T. Abe, and Y. Kashiwaba, Phys. B Condens. Matter **405**, 4957 (2010).

Chapter

7

SUMMARY AND FUTURE PROSPECTS

Contents

7.1 Summary

Thin film solar cells are the future of green and clean energy generation. But the major concern in achieving large scale production of thin film solar cells depends on the availability and cost of indium. The major reason for higher cost of thin film solar cells is the use of ITO coated glass substrate which is very costly due to its applications in transparent electronics. Touch sensitive smart devices consumes mainly the commercially produced ITO. Hence the demand and cost of ITO is high. Moreover, it will lead to scarcity of indium. Hence developing thin film solar cells using alternative TCOs like Zinc oxide and tin oxide through low-cost deposition methods are of much interest. Thin Metal foils are also suitable and attractive substrates for thin film solar cell fabrication. Vigilant energy management methods such as use of solid state lighting, smart windows etc. along with green energy production are the key to a sustainable life.

This thesis concentrates on the development of SnO_2 based n-type TCO mainly for solar cell applications and for possible energy conservation applications like low emissivity windows. Development of intrinsic ZnO and

ZnO based p-type TCO is also discussed here. Possibility of creating sub-band absorbing levels in wide band gap ZnO by ex-situ metal doping and the fabrication of ZnO based Fe diffusion barrier layer on steel substrates is also explored.

In the first part of this study, undoped tin oxide thin films were prepared by optimizing the deposition parameters like substrate temperature, precursor concentration and spray rate. Effects of each of these parameters on the optical and electrical properties of the films were thoroughly analyzed. Tin oxide thin films with 75% transparency and 50Ω/sq sheet resistance were obtained by spray depositing the precursor ($SnCl_4.5H_2O$) solution of molarity 0.2M at a spray rate of 9ml/min over the substrate kept at 425^0C. XPS analysis of the samples prepared at different spray rates was very informative. For oxide compounds, the electrical properties are directly related to the stoichiometry of the films. It was identified that stoichiometry of oxide films can be easily controlled by varying spray rate. The films prepared at low spray rates were oxygen rich and they contain a high percentage of interstitial and chemisorbed oxygen species which will detrimentally affect the electrical properties of the films. High conductivity films were achieved by reducing this type of oxygen species by depositing the films at high spray rate.

Next aim was to improve the optical and electrical properties of tin oxide thin films by fluorine doping. Effect of two dopant sources, NH_4F and HF were studied and it was identified that NH_4F was suitable for improving the electrical and optical properties. Even though low sheet resistance of 18Ω/sq was achieved with HF dopant source, structural and optical properties of the films degraded with HF doping. At optimum doping concentration of NH_4F, sheet resistance could be brought down to less than 7Ω/sq with transmittance ranging from 77 to 95% in the visible region. Resistivity of the

film was 2.48 x$10^{-4}\Omega$.cm. The films were found to have uniform surface morphology from AFM and SEM analysis. Thickness of the film was found to be 540nm from cross sectional SEM analysis. For solar cell applications, thermal stability analysis and resistance variation mapping of the deposited FTO films were done and found that the films were uniform and thermally stable than the commercially available sputter deposited ITO. By depositing different electrodes and measuring the sheet resistance, Gold was found to be the best electrode material. These films also exhibited high reflectance in the IR region. About 95% of the incident IR waves with wavelength above 2000nm were reflected. These films can be utilized for making low emissivity windows to prevent the heat from entering or leaving the buildings.

The major aim behind the development of FTO was to fabricate all layer spray deposited solar cells. Different solar cells using the following configurations were deposited on trial basis: (1) FTO/TiO_2/InS/CIS Solar cell (efficiency 0.61%), (2) FTO/CIS/InS Solar cell (efficiency 0.94%), (3) FTO/CZTS/InS Solar cell (efficiency 1.25%) and (4) FTO/CZS/InS solar cell (efficiency 0.9%).

Other than solar cell application, the deposited FTO film was used to fabricate a low power-high temperature transparent thin film heater and the device was able to reach a high temperature of 340^0C on applying 20V.

The next step was to deposit p-type ZnO films by Ag doping. $AgNO_3$ and Ag(AC) were the dopant sources used. With Ag(AC) doping, all the films were n-type, but with $AgNO_3$ doping, the material changed its conductivity to p-type. 5% doped samples were found out as intrinsic in nature. The required oxygen rich condition for depositing p-type ZnO was achieved by reducing the spray rate. XPS analysis showed that the films are nearly stoichiometric in nature. ZnO based transparent p-i-n homojunctions were fabricated by varying

the inter layer thickness and good diode characteristics were obtained for the devices with higher inter layer thickness. Intrinsic ZnO film doped with 5% Ag was used in a CIS/CdS solar cell as window layer. Enhancement in cell parameters was observed with this intrinsic ZnO window layer.

Ex-situ doping of ZnO thin films with silver and tin was also tried. Electrical properties of the films didn't show any type of enhancement with doping. The important observation was the color change and appearance of sub-band absorbing levels with metal doping. Compositional analysis using XPS proved that the doped metals in ZnO exist in a metal-metal oxide mixed state and the appearance of sub-band energy levels are attributed to this.

Finally spray deposited ZnO layers were deposited on thin flexible steel substrates to prevent Fe ion diffusion. A two-step deposition procedure was applied. To block Fe diffusion, ZnO layer was deposited at a low temperature and for obtaining a conducting ZnO layer, Al:ZnO was deposited at a high temperature and it was followed by a quick quenching procedure. The resultant films were analyzed for uniformity by mapping the spatial variation of sheet resistance and by analyzing the surface with FE SEM. It is clear that ZnO layer was uniformly deposited over the substrate with sheet resistance less than 14Ω/sq. XPS depth profile of the steel substrates deposited with ZnO layer and CIS layer on ZnO proved that Fe diffusion can be successfully prevented by the deposited ZnO barrier layer. Trial deposition of solar cells with ZnO barrier layer showed improvement in efficiency.

7.2 Future prospects

In the present study, the efficiencies of all layer spray deposited solar cells, deposited on FTO, were comparatively lower than the devices fabricated over ITO. To improve the efficiencies of the devices, deposition parameters

for each solar cell layer has to be separately optimized. Effect of pH and ultrasonic spray on morphology and properties are to be studied for further reducing the surface roughness from 17 nm to less than 5 nm so as to reach the roughness values comparable to that of commercially available sputtered ITO. Again, deposition conditions of absorber and window layers over the FTO surface have to be modified.

Resistivity of the developed p-type ZnO was in the order of 10^1 Ω.cm. For the effective use in device applications, still lower resistivity is required. Co-doping with nitrogen can be utilized for achieving this aim. Stable p-type ZnO with enhanced conductivity can lead to the development of ZnO based optoelectronics devices.

Even though sub-band absorbing levels in ZnO films were created by ex-situ doping with Ag or Sn, fabrication of an "all layer ZnO based solar cell" is not done and this needs some more optimization work on suitable absorber layer.

Effect of Molarity on Properties of Spray Pyrolysed SnO_2:F Thin Films

D. R. Deepu, C. Sudha Kartha, K. P. Vijayakumar

Department of Physics, Cochin University of Science and Technology, Cochin – 682022, India
kpv@cusat.ac.in

Abstract. Fluorine doped tin oxide (FTO) thin films were prepared by using automated Chemical Spray Pyrolysis (CSP) machine and the effect of concentration of the precursors on the conductivity and transmittance of the films were studied. The resistivity (ρ) and mobility (μ) are in the range of 10^{-3}–10^{-4} Ω-cm and 8.2–13.5 $cm^2V^{-1}s^{-1}$respectively. The electron density lies between 3.4 x 10^{20} and 6.6x10^{20} cm^{-3}. The film transmittance varies between 70 to 80% and the films shows very good reflectivity in the IR-NIR region. Prepared films can be used as transparent electrodes in photo voltaic and optoelectronic devices.

Keywords: FTO, CSP, resistivity, mobility, transmittance
PACS: 73.61.Ga, 78.20.Ci, 78.70.Ck, 61.05.C

INTRODUCTION

The scarcity and higher cost of ITO as transparent electrodes lead the scientists to probe new low cost TCOs whose properties are comparable to that of ITO. The best alternatives were found to be ZnO:Al and SnO_2:F(FTO), in which the latter shows better thermal and chemical stability [1]. In this work we report the effect of concentration of the precursors on the properties of FTO thinfilms using automated spray Pyrolysis machine [2].

EXPERIMENTAL DETAILS

Fluorine doped Tin oxide (FTO) thin films were prepared on soda lime glass substrate by automated chemical spray Pyrolysis machine. The starting solutions were prepared from stannic chloride hydrated ($SnCl_4.5H_2O$), and ammonium fluoride (NH_4F) in methanol (CH_3OH).0.2 M and 0.25 M solutions were prepared by dissolving $SnCl_4.5H_2O$ in 100 ml methanol and NH_4F (5%) is added to this as dopant [3]. The substrates were properly cleaned and dried. The substrate temperature was set at 475^0C. Air was used as the career gas. The spray rate was set at 9ml/min. total area scanned by the spray head was $225cm^2$.

Crystallinity of the films was analyzed using Rigaku (D. Max.C) X-ray diffractometer (CuKα line; λ= 1.5405 Å). Surface morphology of the samples was studied employing scanning electron microscope (JEOL JSM-7800F). Optical transmittance of the sample at normal incidence was analyzed with the help of UV–Vis–NIR spectrophotometer (Jasco-V-570). Electrical resistivity, career concentration, and career mobility were analyzed by using Ecopia hall measurement unit (HMS-5300).

RESULTS AND DISCUSSION

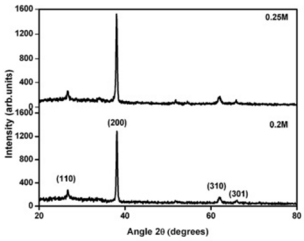

FIGURE 1. XRD patterns of FTO films

Optoelectronic Materials and Thin Films
AIP Conf. Proc. 1576, 58-59 (2014); doi: 10.1063/1.4861980

X-ray diffraction patterns of FTO thin films with change in concentrations recorded in 2θ angle in the range of 20–80◦ are depicted in Fig.1. Results from the XRD studies show that both samples exhibit polycrystalline nature with (200) as the preferred orientation. The surface and cross section SEM image of the FTO film is shown in the fig.2(a) and fig.2(b).

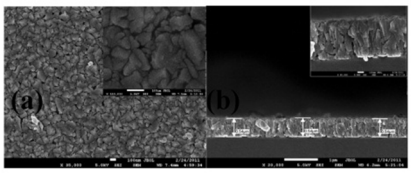

FIGURE 2. SEM micrograph for FTO film (a) Surface, (b) Cross section.

Optical transmission spectra of the films were recorded in the wavelength range 300-2500 nm. The transmittance in the visible range is above 70% for 0.25M and above 80% for 0.2M.reflection in the IR–NIR region increases with increase in molarity. The transmission spectra is depicted in fig.3

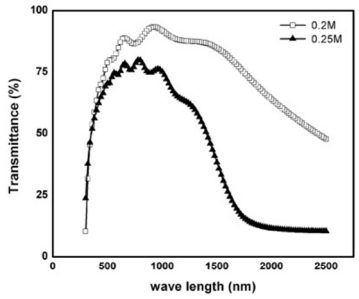

FIGURE 3. Transmission spectra of FTO thin films

Hall measurements were done after cutting the film in to a square of side 1 cm and coating silver amalgam on the four corners. The thicknesses of the samples were 540 nm for 0.25M and 390 nm for 0.2M. The electrical properties of the films are depicted in table 1.

TABLE 1. Electrical properties of FTO films

Molarity (M)	Electron density (cm-3)	Resistivity (Ωcm)	Mobility ($cm^2V^{-1}s^{-1}$)
0.25	$6.6x10^{20}$	$6.9x10^{-04}$	13.5
0.2	$3.4\ x10^{20}$	$2.2x10^{-03}$	8.2

CONCLUSION

Highly conducting device quality FTO thin films in submicron thickness can be deposited on large area for photo voltaic and optoelectronic applications. It is observed that increase in molarity reduces the resistivity considerably.

ACKNOWLEDGMENTS

All the authors would like to express their gratitude to MNRE for financial support for the work. All the authors would like to thank Dr. K. B. Jinesh for SEM analysis. One of the authors DRD would like to thank UGC for his fellowship.

REFERENCES

1. E. Elangovan, K. Ramamurthi, Journal of Optoelectronics and Advanced Materials,5,45-54 (2003).
2. T. Sebastian. PhD thesis. s.l. : Cochin University of science and technology, (2009).
3. J. Bruneaux, H. Cachet, M. Froment, A. Messad. Thin Solid Films,197,129-142 (1991).

Modification of Opto-electronic Properties of ZnO by Incorporating Metallic Tin for Buffer Layer in Thin Film Solar Cells

D.R. Deepu,[1] J. Jubimol,[1] C. Sudha Kartha,[1] Godfrey Louis,[1] K. Rajeev Kumar,[2] and K.P. Vijayakumar[1,*]

[1]*Department of Physics, Cochin University of Science and Technology, Cochin-682022, India*
[2]*Department of Instrumentation, Cochin University of Science and Technology, Cochin-682022, India*
[*] *E-mail: kpv@cusat.ac.in*

Abstract. In this report, the effect of incorporation of metallic tin (Sn) on opto-electronic properties of ZnO thin films is presented. ZnO thin films were deposited through 'automated chemical spray pyrolysis' (CSP) technique; later different quantities of 'Sn' were evaporated on it and subsequently annealed. Vacuum annealing showed a positive effect on crystallinity of films. Creation of sub band gap levels due to 'Sn' diffusion was evident from the absorption and PL spectra. The tin incorporated films showed good photo response in visible region. Tin incorporated ZnO thin films seem to satisfy the desirable criteria for buffer layer in thin film solar cells.

Keywords: ZnO, Spray pyrolysis, Resistivity, Photoluminescence, photo response.
PACS: 61.05.cp, 73.61.Ga, 78.40.Fy, 78.55.Et,

INTRODUCTION

Most of the thin film photo voltaic devices use CdS or In_2S_3 as their buffer layer [1-3]. Research is going on to find a substitute for these two compounds as Cd is toxic and In is rare and costly [4-5]. The buffer layer material should have wider band gap with low resistivity, so as to admit maximum amount of light to the junction and absorber region in solar cells [2]. Another criterion for selecting buffer layer is the lattice match between the different layers in solar cell. One promising material is ZnO [2], because of its wider band gap, and lattice match with the commonly used Al:ZnO window layer. In this report, preparation of Sn incorporated ZnO thin films for the possible application as buffer layer is discussed.

EXPERIMENTAL

Pristine ZnO films were deposited on soda lime glass using automated CSP technique. The precursor solution was prepared by dissolving Zinc acetate di hydrate ($Zn(CH_3COO)_2.2H_2O$) in a mixture of water and propanol in the ratio 1:1 [6]. The substrates were cleaned in iso-propyl alcohol in an ultrasonic bath for 10 minutes and dried properly. The substrates were preheated to 450^0C and 50 ml of the precursor solution was sprayed on to it at a rate of 7ml/minute.

Different quantities of metallic tin were evaporated over the films so as to vary the Sn concentration in the film from 0.5 to 2.5 % of number of Zn atoms in steps of 0.5 % and the films were vacuum annealed at 200^0C for 2 hours ($< 1.5x10^{-5}$ mbar). The quantity of Tin metal to be evaporated is determined from the density and volume of the films by calculating the approximate number of Zn atoms in it.

Structural studies were done using Rigaku (Model No: D. Max.C) X-ray diffractometer (CuKα line; λ= 1.5405 Å). Optical analysis of the samples were carried out by taking the absorption spectra employing UV-Vis-NIR spectrophotometer (Model No: Jasco-V-570) and room temperature Photoluminescence (PL) measurements were done using 325 nm line of Kimmon He–Cd laser [o/p power of 20 mW] with Ocean Optics USB 2000 spectrophotometer. Electrical measurements were carried out using National Instruments PXI-4130 SMU and Ecopia HMS 5300 Hall measurement system.

Solid State Physics
AIP Conf. Proc. 1665, 120019-1–120019-3; doi: 10.1063/1.4918126

RESULTS AND DISCUSSION

Structural Studies

X-Ray diffraction spectra of the films are depicted in figure 1. Prominent Peak corresponding to (002) plane of wurtzite ZnO is observed. There was no peak corresponding to the metallic tin or other oxides.

Grain size of the films was calculated from Scherrer formula (figure 2). It is observed that crystallinity and grain size of the films improves with vacuum annealing. But the incorporation of metallic tin does not show any significant influence in grain size.

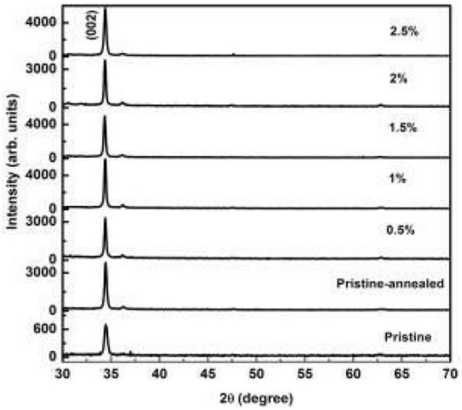

FIGURE 1. XRD pattern of pristine and Sn incorporated ZnO thin films.

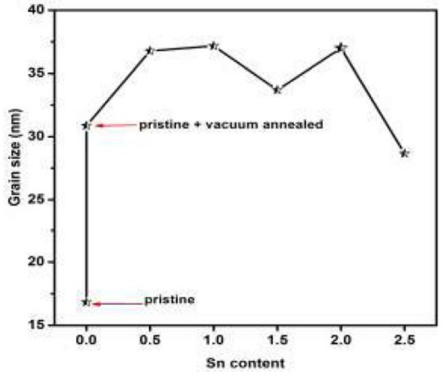

FIGURE 2. Grain size of pristine and Sn incorporated ZnO thin films.

Optical Studies

Tauc plot of pristine and Sn incorporated films is shown in the figure 3. It can be observed that with increase in Sn content, band gap of the films gradually decreases. The inset in the figure 3 shows the magnified plot in the lower energy region for 2% Sn and sub band gap absorption is evident from the spectrum. This may be the reason for the observed color variation of the films with Sn concentration.

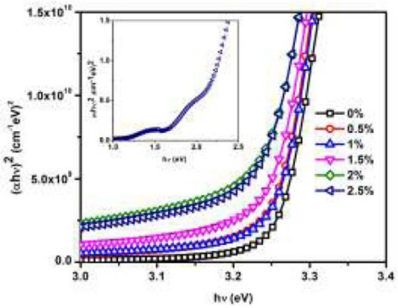

FIGURE 3. Tauc plot of ZnO films for varied Sn concentration. (The magnified plot in the lower energy region for 2% Sn is shown in the inset of this figure)

Absorption spectrum of tin doped zinc oxide reveals the presence of sub band gap absorption. Photoluminescence (PL) studies were carried out on the samples to confirm the same.

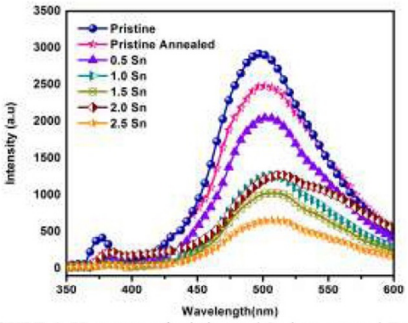

FIGURE 4. PL spectra of pristine and Sn incorporated ZnO thin films.

Figure 4. shows the PL spectra obtained for the samples. Three peaks centered at ~ 380 nm, 500 nm and 535 nm were observed. PL emission centered at ~ 380 nm, i.e. the Near Band Edge emission (NBE) and the blue - green emission (BGE) ~ 500 nm are

characteristic PL peaks of ZnO thin films [6]. The additional peak at ~ 535 nm may possibly be a consequence of 'Sn' doping in these thin films. There are reports on emission at ~ 535 nm which attribute this emission to be due to recombination of the holes with electron occupying singly ionized oxygen vacancies [7]. It is evident from the PL spectra that the intensity of green emission at ~535 nm increases with increase in concentration of 'Sn' and predominates the blue green emission for 2% Sn.

Electrical Studies

Resistivity and mobility of the films are shown in table 1. The lowest resistivity was observed for the films with 1% Sn concentration.

TABLE 1. Electrical properties of pristine and Sn incorporated ZnO thin films.

Sample Name	Resistivity (Ω.cm)	Mobility $Cm^2/V.s$
Pristine	0.18	9.8
0.5	0.12	13.6
1	0.07	11.1
1.5	0.10	10.9
2	0.26	5.8
2.5	0.15	5.4

It is important for a material to show photo response to be used in a solar cell. Photo response of ZnO film with 2% Sn was studied using two wavelengths in the visible region (532 nm and 632 nm). The film shows good photo response (Figure 5) for these wavelengths which have energies much lower than the band gap energy and this must be due to absorption through sub band gap levels.

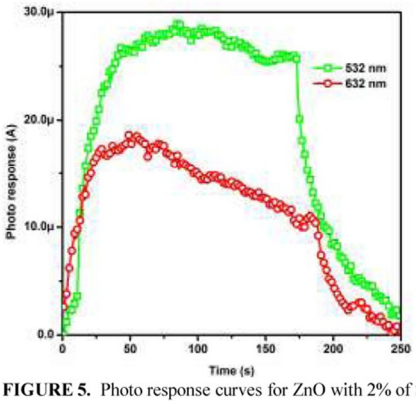

FIGURE 5. Photo response curves for ZnO with 2% of Sn.

CONCLUSION

Effect of metallic Sn content in the opto-electronic properties of spray deposited ZnO thin films was studied. Crystalline films were formed and on vacuum annealing, the crystallinity was improved. Decrease in band gap is observed with the increase in Sn concentration in the film and there were sub band gap levels were present, which was further confirmed through PL. The films showed good photo response in visible wavelengths due to the sub band gap absorption. The results thus obtained favor the role of Sn incorporated ZnO thin films as buffer layer in thin film solar cells.

ACKNOWLEDGMENTS

All the authors would like to express their gratitude to MNRE for financial support for the work. Two of the authors (DRD & JJ) would like to thank UGC and KSCSTE for their fellowships.

REFERENCES

1. I. Repins, M. A. Contreras, B. Egaas, C. DeHart, J. Scharf, C. L. Perkins, B.To and R. Noufi, Prog. Photovolt: Res. Appl. **16**, 235–239 (2008).
2. N. Naghavi, D. Abou-Ras, N. Allsop, N. Barreau, S. Bucheler, A. Ennaoui, C. H. Fischer,C. Guillen, Hariskos, J. Herrero, R. Klenk, K. Kushiya, D. Lincot, R. Menner,T. Nakada, C. Platzer Bjorkman, S. Spiering, A. N. Tiwari and T. Torndahl, Prog. Photovolt: Res. Appl. **18**, 411–433 (2010).
3. D. Hariskos, M. Ruckh, U. Rqhle, T. Walter, H. W. Schock, J. Hedstrfm and L. Stolt, Sol. Energy Mater. Sol.Cells **345**, 41–42 (1996).
4. D. Hariskos, S. Spiering and M. Powalla, Thin Solid Films **480–481**, 99–109 (2005).
5. D. R. Deepu, C. Sudha Kartha, and K. P. Vijayakumar, AIP Conf. Proc.**1576**, 58-59 (2014).
6. T.V. Vimalkumar, N. Poornima, C. Sudha Kartha and K.P. Vijayakumar, Appl. Surf. Sci. **256**, 6025–6028 (2010).
7. Seung Yong Bae, Chan Woong Na, Ja Hee Kang, and Jeunghee Park, J. Phys. Chem. B **109**, 2526-2531(2005).

Sprayed ZnO As Effective Window Layer For CIS/CdS Solar Cell

M.S. Sreejith, D.R. Deepu, C. Sudha Kartha and K. P. Vijayakumar

Department of Physics, Cochin University of Science and Technology, Cochin-22, Kerala, India.
Corresponding author's email id: kpv@cusat.in

Abstract. Thin film solar cells were fabricated using $CuInS_2$ as absorber layer and CdS as buffer layer. $CuInS_2$ and CdS layers are deposited using chemical spray pyrolysis and chemical bath deposition respectively. Proper movement and collection of generated carriers really affect the performance of the cell. Introduction of a very thin layer of silver doped ZnO (ZnO:Ag) window layer between the buffer layer and ITO improves performance of the cell, with open circuit voltage of 409mV, short circuit current density of 2.89 mA/cm^2, fill factor of 44.3% and conversion efficiency of 0.52%.

Keywords: Semiconductors, Spray coating techniques, Solar cell
PACS: 81.05.Hd, 81.15.Rs, 88.40.hj, 88.40.jn

INTRODUCTION

Chemical spray pyrolysis and chemical bath deposition are the most cost efficient methods for thin film deposition. In the present work cells were fabricated successfully with these techniques. Materials selected for cell fabrication are CdS and $CuInS_2$(CIS). CIS was the absorber layer having absorption coefficient of 10^4 cm^{-1} and band gap of 1.5eV. $CuInS_2$ was deposited using Chemical spray pyrolysis(CSP) and buffer layer CdS was prepared using CBD method. Ito and Nakabayashi has reported cell, fabricated using sulphurisation method with cell structure CdS/CIS [1]. Ogawa, Ito and Yoshitaka also reported cells with the same cell structure and depositing technique [2]. A. Mere and M. Krunks have reported cell with cell structure ZnO/CdS/CIS, deposited using spray pyrolysis and chemical bath deposition [3].

Our aim was to fabricate a cell with these economically viable deposition techniques. The material chosen were CdS and $CuInS_2$. In the present paper we report the improvement of CdS/$CuInS_2$ cell deposited using chemical methods on introducing Silver doped ZnO film as window layer.

EXPERIMENTAL

We used automated CSP machine for depositing the absorber layer and CBD method for depositing the buffer layer. Glass plates coated with ITO were used as the substrate. Aqueous solution containing cuprous chloride (0.012M), indium chloride (0.012M) and thiourea (0.012M) was sprayed at a rate of 3ml/min onto the substrate kept at 573K using compressed air (pressure~1.5bar) as the carrier gas. Concentration of thiourea was 5 times the stoichiometric requirement (0.05 M) to compensate for the loss of sulphur during pyrolysis [4]. Cadmium sulphate (0.0125M), ammonia solution (35%), sodium hydroxide (0.025M) and thiourea (0.1M) are used for depositing CdS buffer layer, through CBD technique. Bath was set at 353K. Window layer of ZnO:Ag was deposited by spraying aqueous solution of ZnO(0.05M) with small percentage of Ag, at 5 ml/min spray rate and 750K temperature. Silver electrodes having an area of 0.01 cm^2 were given over CdS layer using vacuum evaporation.

RESULTS AND DISCUSSION

At first, we prepared CdS/CIS bilayer on ITO coated glass substrate. Silver was deposited over this using physical vapour deposition to act as the top electrode. ITO was the bottom electrode. The cell parameters obtained were Voc=0.387V, J_{sc}=1.23mA/cm^2, FF =26.7%, η= 0.138%. Series resistance (R_s) and shunt resistance (R_{sh}) were found to be 232Ωcm^2 and 395Ωcm^2 respectively. These parasitic resistances of the devices were calculated from the slope of the illuminated J-V characteristics at V=0 (for Rs) and J=0 (for Rsh) [5]. The J value is very

small because most of the light generated carriers are not collected properly at ITO. There may be some mismatch between the energy bands of CdS (Eg = 2.4eV) and ITO (Eg = 3.8eV) which results in the low current value of the fabricated device. Here we are able to improve the performance by introducing a very thin window layer of ZnO:Ag between ITO and CdS buffer layer. The conduction band of ZnO (Eg =3.3eV) lies within the conduction band energies of CdS and ITO which enables the device for the efficient collection of electrons.

The J-V curves under illumination, for the cells with and without ZnO window layer are shown in Figure 1. The device parameters obtained for modified cell were V_{oc}=0.409V, J_{sc}=2.89mA/cm^2, FF=44.3%, η= 0.52%, R_s=35Ωcm^2 and R_{sh}=469Ωcm^2.

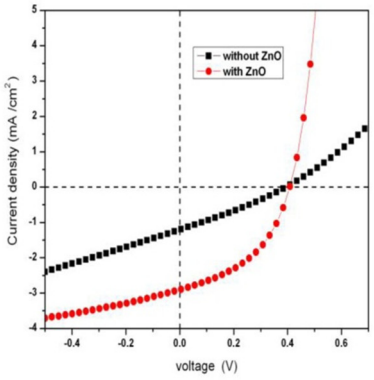

Figure 1. J-V curves under illumination, for the cell without and with ZnO window layers.

CONCLUSION

We have successfully fabricated ITO/ZnO/CdS/$CuInS_2$ solar cells by combining the cost efficient techniques like automated spray pyrolysis and chemical bath setup. It is observed that on introducing a thin ZnO:Ag window layer between ITO and CdS buffer layer cell performance was enhanced considerably. The best device under this study has the following cell parameters V_{oc}= 0.408V, J_{sc}= 2.89mA/cm^2, FF = 44.3%, η= 0.52%, R_s= 35Ωcm^2 and R_{sh}= 469 Ωcm^2.

ACKNOWLEDGEMENTS

All the authors would like to thank Ministry of New and Renewable Energy (MNRE) for providing financial support for this work.

REFERENCES

1. K. Ito, T. Nakabayashi, T. Miyazawa, Y. Hashimoto, Solar Energy Materials and Solar Cells, **49** (1997) 375-381.
2. K. Ito, Yoshikata Ogawa, J. Appl. Phys. **33** (1994) L1775-L1777.
3. A. Mere, O. Kijatkina, H. Rebane, J. Krustok, M. Krunks, Journal of Physics and Chemistry of Solids **64** (2003) 2025–2029.
4. Tina Sebastian, PhD thesis, Cochin University of Science and Technology (2009).
5. N. Moritake, Y. Fukui, M. Oonuki, K. Tanaka, H. Uchiki, Phys.Stat. Sol. C **6** (2009) 1233.

IOP Publishing Semiconductor Science and Technology
Semicond. Sci. Technol. **29** (2014) 115026 (7pp) doi:10.1088/0268-1242/29/11/115026

Spray pyrolysed microporous TiO_2 thin films by optimisation of substrate temperature for 'all sprayed' solar cells

M V Santhosh[1], D R Deepu[1], R Geethu[1], K Rajeev Kumar[2], C Sudha Kartha[1] and K P Vijayakumar[1]

[1] Department of Physics, Cochin University of Science and Technology, Cochin-22, Kerala, India
[2] Department of Instrumentation, Cochin University of Science and Technology, Cochin-22, Kerala, India

E-mail: kpv@cusat.ac.in

Received 3 May 2014, revised 22 August 2014
Accepted for publication 4 September 2014
Published 2 October 2014

Abstract

Titanium dioxide thin films were deposited on glass substrate at temperatures ranging from 300 °C to 500 °C by a simple, cost effective spray pyrolysis method using commercially available TiO_2 powder (Degussa P25). Analyses using scanning electron microscopy (SEM) and atomic force microscopy (AFM) reveal the microporous nature of the films at 350 °C. X-ray diffraction (XRD) and Raman studies reveal that these films are amorphous in nature. The films were subsequently annealed at 500 °C for 2 h, resulting in crystallisation (the tetragonal anatase phase). XPS analysis was effectively used to study the chemical composition of the samples. Finally, optimized microporous TiO_2 thin films were used for the fabrication of an 'all-sprayed' solar cell utilizing well-established $CuInS_2$ as the absorber layer. The best device under this study has an open-circuit voltage of 409 mV and a short-circuit current density of 3.90 mA cm^{-2}. The efficiency and fill factor were 0.61% and 38%, respectively.

Keywords: chemical spray pyrolysis (CSP), thin films, atomic force microscopy (AFM), scanning electron microscopy (SEM), x ray photon spectroscopy (XPS), microporous

(Some figures may appear in colour only in the online journal)

1. Introduction

TiO_2 thin films have attracted attention because of their ease of preparation using simple, cost-effective chemical methods such as chemical spray pyrolysis (CSP) [1, 2]. These films have widespread applications in the fields of antireflection coatings [3], solar cells [4], optical fibres [5], gas sensors [6], ceramic membranes [7], waveguides [8], photocatalysts [9], etc. These applications arise because of their n-type conductivity and micro- or nanostructures in thin film forms. A variety of physical and chemical approaches for thin film fabrication, such as magnetron sputtering [10], electron beam evaporation [11, 12], chemical vapour deposition [13, 14], the sol–gel process [15], spray pyrolysis [16] and ink-jet printing [17], have been used to prepare TiO_2 thin films. In this work, CSP was used for the preparation of TiO_2 thin films. For spray pyrolysis, most works deal with organometallic Ti compound precursors such as Ti tetra–ethoxide, Ti iso-propoxide, Ti acetyl acetonate and Ti isobutoxide [18]. In addition to organometallic Ti compound precursors, peroxo-polytitanic acid prepared from Ti-metal powder was also used as a precursor for spray deposition [19, 1]. In our case, commercially available TiO_2 powder (Degussa P25-DP25) with high chemical purity was used for the TiO_2 film deposition. DP25 is a mixture of anatase and rutile crystallites and was generally used as a photocatalyst [20, 21].

In the present work, microporous anatase phase TiO_2 was isolated from DP25 by selective dissolution with a hydrogen peroxide-ammonia mixture. Micro- or nanostructured anatase TiO_2 films are generally used as the electron conducting layer for solar cell applications [22]. It was observed that substrate temperature plays a crucial role in the morphology of the deposited films. The initial work in this paper deals with the optimisation of substrate temperature for microstructured

anatase phase films. Our major aim is to realise an 'all-sprayed' solar cell using these microstructured TiO_2 films with a minimum absorber layer thickness. The thickness of the absorber layer was kept low (~200 nm) in order to promote the effective charge carrier separation by reducing the transport path for the excited charge carriers within the absorber layer [23]. Also, the infiltration of the absorber layer into the porous TiO_2 layer by the CSP method enhances the effective path length of light in the absorbing material, which leads to high light absorption. For the realisation of the 'all-sprayed' solar cells using the microstructured TiO_2, an FTO/TiO_2/In_2S_3/$CuInS_2$/Ag structure was followed. Many workers reported the fabrication of solar cells using this structure; however, in most cases, the back contact materials [fluorine-doped tin oxide (FTO) or tin-doped indium oxide (ITO)] were prepared through either sputtering or evaporation [22, 24]. In our work, spray-pyrolysed FTO films serves as the back contact. $CuInS_2$ was used as the absorber layer because of its band gap of 1.5 eV, which is optimum for the photovoltaic application. A thin layer of In_2S_3 (~50 nm) sprayed between the TiO_2 and $CuInS_2$ layers serves as a buffer layer, which suppresses the back recombination of injected carriers [22].

2. Experimental details

An automated CSP unit was employed for the film fabrication [25]. Here, an air blast type of atomization was made possible using a stainless steel surgical needle. Compressed and filtered air were used as the carrier gas. The substrates for the film deposition were placed on a hot plate in air, which can provide a uniform surface temperature. The distance between the atomizer and hot plate was optimised for pinhole-free, uniform films that have good adhesion to the substrate. The TiO_2 thin films were prepared using commercial TiO_2 powder (Degussa P25, supplied by Evonik industries, Japan, with TiO_2 weight percentage 99.5) on ultrasonically cleaned soda lime glass substrate. Initially, a precursor solution of 0.125 M peroxo-titanic acid was prepared by dissolving the powder in a solution of hydrogen peroxide (H_2O_2) and ammonium hydroxide (NH_4OH) taken in the ratio 8:2. The precursor solution was made to 0.025 M using distilled water. The spray rate was maintained at 6 ml min^{-1}, and the substrate temperature was varied from 300 °C to 500 °C in steps of 50 °C. The samples prepared at 300 °C, 350 °C, 400 °C, 450 °C and 500 °C were named Ti-300, Ti-350, Ti-400, Ti-450 and Ti-500, respectively, with thicknesses around 510 nm, 500 nm, 480 nm, 450 nm and 380 nm. For the device fabrication, fluorine-doped tin oxide (FTO) thin films (with a sheet resistance of 20 $\Omega/\square$) were deposited on glass substrates kept at 425 °C by the CSP method. Stannic chloride ($SnCl_4$) was used as the precursor solution. Fluorine doping was made possible using an ammonium fluoride (NH_4F) solution. The TiO_2 films after the optimisation of the substrate temperature was sprayed over the FTO layer. Optimized In_2S_3 and $CuInS_2$ thin films were sprayed over the FTO layer in a sequence, as mentioned in our previous work [26]. Indium chloride ($InCl_3$, 0.03 M) and thiourea [$CS(NH_2)_2$, 0.3 M] were the precursors for the In_2S_3 films. For the $CuInS_2$ deposition, the precursor solutions were copper chloride ($CuCl_2.2H_2O$, 0.0175 M), indium chloride ($InCl_3$, 0.0125 M) and thiourea [$CS(NH_2)_2$, 0.0625 M] [27]. The substrate temperature and spray rate were maintained at 350 °C and 4 ml min^{-1} for both the $CuInS_2$ and In_2S_3 layers. The front contact was through vacuum evaporated silver over the cell structure ($area = 0.03\ cm^2$).

An SU6600 variable pressure field emission scanning electron microscope (FESEM) (Hitachi, Japan) was used for structural analysis. The Nanosurf EasyScan 2 AFM System was used for the morphological analysis of the films. The prepared TiO_2 samples were also characterized using a Rigaku (model D/Max-C) x- ray diffractometer employing a CuKα line and a Ni filter operated at 30 kV and 20 mA. Raman analysis of the prepared samples was done using the Horiba Jobin Yvon LabRAM HR system at a spatial resolution of 2 mm in a backscattering configuration. The 514.5 nm line of an Argon ion laser was used for excitation. The chemical compositions of the films were evaluated using the XPS technique (Shimadzu XPS unit, model: AMICUS). The photovoltaic response of the fabricated solar cell was studied using a class AAA solar simulator (PET, model SS50AAA).

3. Results and discussion

The evolution of the films' surfaces with the deposition temperature was studied using the SEM. At a lower temperature, it was observed that the adhesion of TiO_2 over the substrate was very poor, making the films nonuniform. From 300 °C and above, the films had adhesion and were continuous. The samples deposited at 300 °C were composed of nonuniformly arranged aggregates (figure 1(a)). As the temperature increased to 350 °C, the aggregates arranged themselves into open, porous structures [with a size in the range of 2–6 microns], as shown in the figure 1(b). The SEM analysis of the samples prepared at higher substrate temperatures of 400 °C, 450 °C and 500 °C (figures 1(c)–(e)) show that they are not microporous in nature, but possess good adhesion and homogeneity over the substrate. The AFM analysis (not shown) indicates that the RMS roughness of the samples decreases with an increase in the substrate temperature. For the Ti-350 samples, the RMS roughness was 180 nm, which decreases to 30 nm for Ti-500 samples. The highly interconnected porous structure is unique to the samples prepared at a substrate temperature of 350 °C; hence, the study reveals that the porosity of the films strongly depends on the substrate temperature.

As the substrate temperature increases, the evaporation rate of the constituents in the precursor solution also increases. Hence, the composition of the deposited films has a strong dependence on the substrate temperature [2]. The EDAX measurements prove that the atomic concentration of Ti decreases as the substrate temperature increases. As a result, the thickness of the films decreases drastically. Above 500 °C, the film's surface seems to be discontinuous. The

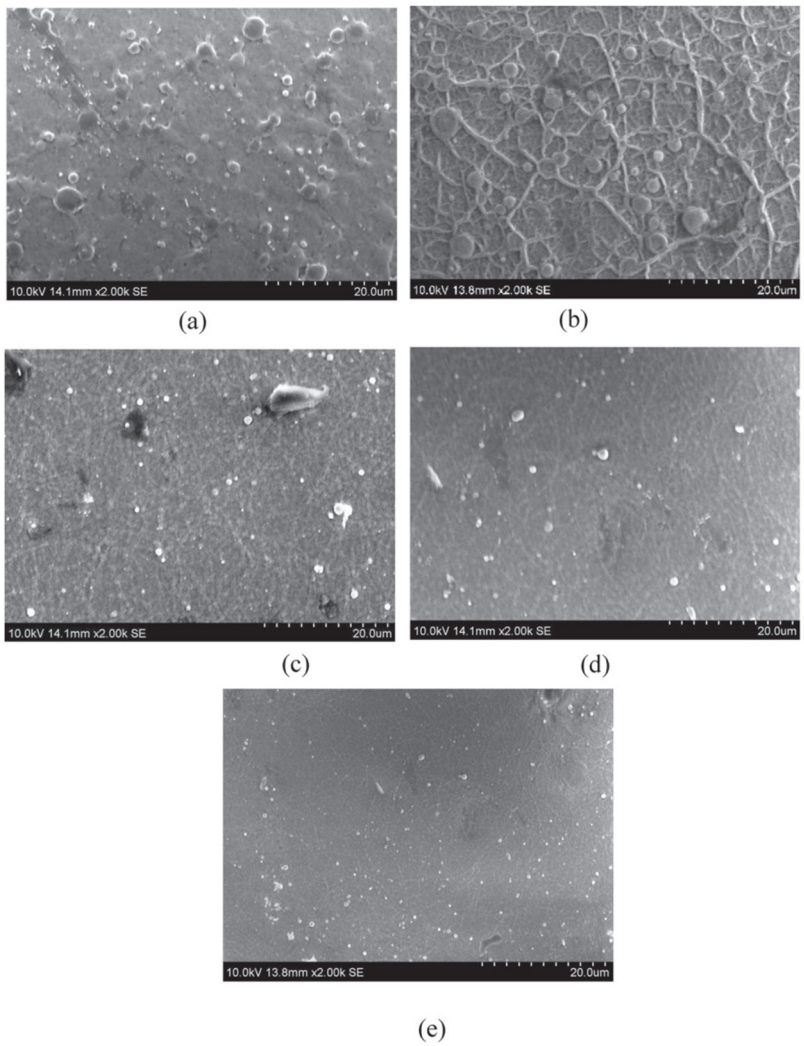

Figure 1. SEM pictures of TiO_2 samples (a) Ti-300, (b) Ti-350, (c) Ti-400, (d) Ti-450, (e) Ti-500.

atomic concentrations of Ti and O with the substrate temperature are depicted in figure 2.

The SEM analysis clearly indicates the microporous nature of the TiO_2 films at 350 °C, and an EDAX analysis shows that the films are nearly stoichiometric. The results of the SEM and EDAX analyses show that the Ti-350 samples can be good candidates for solar cell applications. Moreover, the In_2S_3 buffer layer and $CuInS_2$ absorber layer were also prepared at 350 °C. This is very important as far as device fabrication at an industrial level is concerned since there is no need to change the substrate temperature for each layer fabrication. Thus, the cell fabrication in this study was just a one stretch process. Only the Ti-350 samples were selected for the remaining studies in this paper.

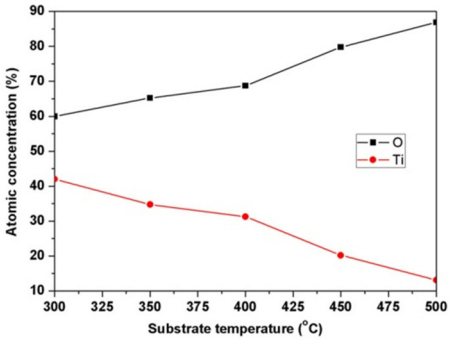

Figure 2. Atomic concentration of titanium and oxygen in TiO_2 films versus the substrate temperature (obtained from the EDAX analysis).

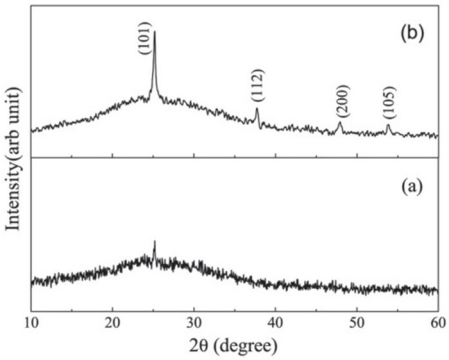

Figure 4. XRD spectrum of the Ti-350 samples (a) before air annealing, (b) after air annealing at 500 °C.

The AFM analysis was also done on the Ti-350 samples. Both the 3D view and colour map view of the sample surfaces are shown in figure 3. The two-dimensional AFM images are in good correlation with the SEM micrographs. From the 3D AFM analysis, the average surface roughness was observed to be 180 nm. For the FTO coated glass substrate, the average surface roughness value is 20 nm.

Both the AFM and SEM analyses reveal the porous nature of the films prepared at 350 °C. However, they were almost amorphous in nature, as revealed by the XRD analysis. In order to improve the crystallinity of the samples for device applications, air annealing was carried out for 2 h at 500 °C. Even after annealing, the films were microporous in nature with no significant changes in pore size. After annealing, the sample showed different strong XRD peaks, which confirmed the polycrystalline nature of the film, as depicted in figure 4. All of the diffraction peaks of the films are indexed to (101), (112), (200) and (105), with preferential orientation along the (101) plane, which is characteristic of the tetragonal anatase phase [28]. The crystallite size (deduced from the well-known Scherrer formula [29]) is estimated to be 40 nm. The full width at half maximum (β) of the XRD peak is related to microstrain (ε) and crystallite size (t), according to the Williamson–Hall equation as:

$$\beta \cos\theta = \frac{k\lambda}{t} + 4\varepsilon \sin\theta \qquad (1)$$

where θ is the Bragg angle, k is the shape factor (0.9) and λ is the wavelength of the x-rays [30]. Equation (1) represents a straight line with the y intercept as $k\lambda/t$ and the slope as ε. The calculated values of the microstrain and grain size were 2.5×10^{-3} and 46 nm, respectively (figure 5). The grain size obtained using the Scherrer formula correlate well with that obtained from the Williamson–Hall plot.

Figure 6 shows the Raman scattering spectrum of the 'as-prepared' and 'annealed' samples. Before annealing, only the peak at 144 cm^{-1} existed, and this low frequency 'Eg mode' is the peculiarity of the 'anatase phase.' Upon annealing, the sample exhibited Raman peaks at 144, 398, 518 and

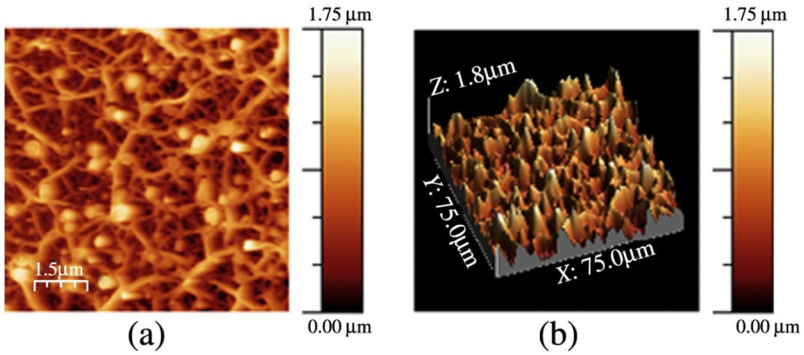

Figures 3. (a) 2D and (b) 3D AFM image of the Ti-350 samples.

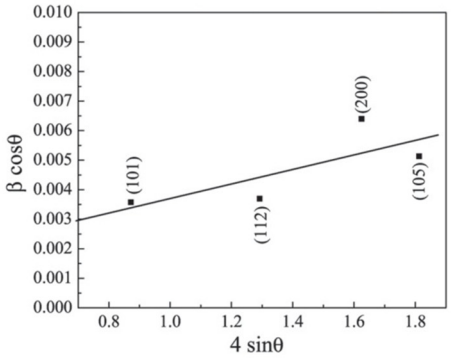

Figure 5. Williamson–Hall plot of the Ti-350 samples.

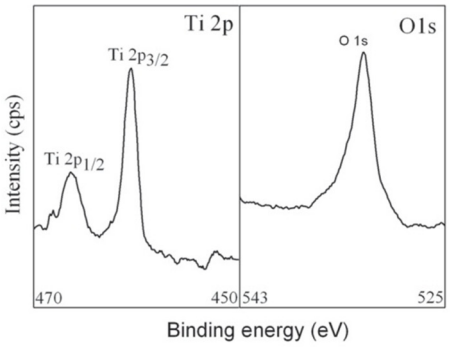

Figure 7. XPS analysis of the Ti 2p and O1s states in the Ti-350 films.

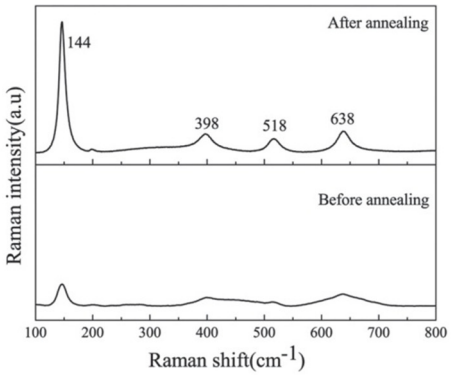

Figure 6. Raman spectrum of the Ti-350 films before and after air annealing.

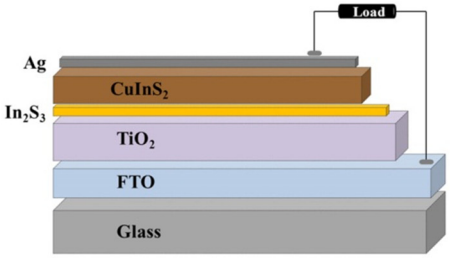

Figure 8. Schematic diagram of the fabricate device.

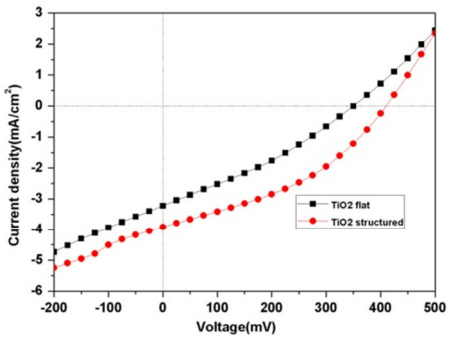

Figure 9. *J–V* characteristics of solar cells fabricated using structured and flat TiO_2 films

638 cm^{-1}, which are also assigned to the characteristic Raman modes of 'anatase phase' TiO_2 films [4]. The full width at half maximum (FWHM) of the peaks decreases upon annealing, indicating structural improvement; this is in good agreement with the XRD results [31]. Thus, the Raman analysis also confirmed the crystalline anatase phase of the Ti-350 samples.

To analyse the chemical state in the films, 'XPS depth profile' measurements were performed. Ten cycles of Argon ion etching were carried out in these films. The XPS measurements show the oxygen to titanium ratio as 63:37. This was comparable to the value, 65:35, obtained from the EDAX analysis. Figure 7 represents the binding energy versus intensity spectra for the Ti 2p and O 1s states in the samples after etching. The presence of the Ti $2p_{3/2}$ peak at 460.46 eV indicates the presence of Ti^{4+} oxidation states. The binding energy peak at 466.44 eV indicates the Ti $2p_{½}$ peak. The doublet separation between the $2p_{3/2}$ peak and Ti $2p_{½}$ peak was 5.92 eV, which is in good agreement with the reported value of 5.7 eV for anatase phase TiO_2 thin films deposited by MOCVD [32]. The O1s binding energy is at 532.15 eV; this indicates the bonding of oxygen to the tetravalent Ti ions [33].

Table 1. Photovoltaic parameters of the S-400 and S-350 cells.

Cell name	V_{oc} (mV)	J_{sc} (mA cm^{-2})	FF (%)	η (%)	R_s (Ω cm^2)	R_{sh} (Ω cm^2)
S-400 (Flat)	350	3.22	31	0.35	75	141
S-350 (Structured)	409	3.90	38	0.61	45	196

3.1. Fabrication of 'all-sprayed' FTO/TiO_2/In_2S_3/$CuInS_2$/Ag solar cells

In order to explore the effect of the microporous structure on cell performance, solar cells were fabricated using both the microporous (Ti-350) and flat structured (Ti-400) TiO_2 thin films, and they were named S-350 and S-400. In both cases, the thickness of the $CuInS_2$ absorber layer and In_2S_3 buffer layer were kept constant. The thicknesses of the FTO, TiO_2, $CuInS_2$, In_2S_3 and Ag layers were around 300 nm, 350 nm, 200 nm, 50 nm and 50 nm, respectively. A schematic diagram of the fabricated device is shown in figure 8.

Figure 9 shows illuminated J–V characteristics of S-350 and S-400 solar cells. The S-400 cells show an open circuit voltage (V_{oc}) of 350 mV and a short circuit current density J_{sc}) of 3.22 mA cm^{-2}. The efficiency (η) and fill factor (FF) were 0.35% and 31%. On the other hand, the S-350 cells show an improvement in the device parameters. It has $V_{oc} = 409$ mV, $J_{sc} = 3.90$ mA cm^{-2}, $\eta = 0.61\%$ and $FF = 38\%$. In this case, the thin absorber layer was sprayed over the microporous structured TiO_2 thin films that have an enhanced surface area compared to the flat structured samples. Hence, the thickness of the absorber layer may be comparable with the depletion layer extension, and it may be the reason for the improvement of the device parameters [34].

The performance parameters of the devices can also be explained on the basis of its parasitic resistances [series (R_s) and shunt (R_{sh})]. R_s and R_{sh} were calculated from the slope of the illuminated J–V characteristics at $V = 0$ (for R_s) and $J = 0$ (for R_{sh}) [35]. When comparing the performance parameters (shown in table 1) of two cells on the basis of R_s and R_{sh}, the better one should have a low value for R_s and a high value for R_{sh}. For the S-400 cells, R_{sh} was 141 Ω cm^2, and it increased to 196 Ω cm^2 for the S-350 cells. This increase in R_{sh} may be responsible for the effective charge carrier separation there by reducing the alternate path for the light-generated carriers [36]. As a consequence of this process, the V_{oc} for the S-350 cells was 409 mV, which is a better value compared to that of 350 mV for the S-400 cells. The series resistance value for the S-350 cells was 45 Ω cm^2, and that of the S-400 cells was 72 Ω cm^2. The increase in the value of J_{sc} for the S-350 cells may be attributed to the decrease in the series resistance. Since V_{oc} and J_{sc} are enhanced for the S-350 cells, the efficiency and fill factor of these cells also improve.

4. Conclusion

A simple and cost-effective CSP method was successfully used to prepare microporous TiO_2 thin films using the commercially available TiO_2 powder, DP25. It was observed that the microporous structure of the sprayed TiO_2 thin films have a strong dependence on the substrate temperature, and the optimised temperature was 350 °C. The microporous nature of the film was confirmed using both SEM and AFM analysis, and they show a reasonably good correlation. The as-prepared films were amorphous in nature. Air annealing of these samples for 2 h at 500 °C results in a crystalline anatase phase for the TiO_2 thin films. We demonstrated the modified structural properties of the films upon post-deposition annealing by XRD and Raman analyses. Also, the solar cells fabricated using microstructured TiO_2 thin films show better device parameters compared to flat structures. The performance parameters of the best cell fabricated is quite low. However, for the present work, only the CSP method was employed for all of the layers of the cell. CSP already proved to be a simple, cost-effective candidate for large area deposition. In this aspect, the result is quite promising. Also, the electrical properties of TiO_2 and FTO layers can be further improved for better device parameters. Moreover, the application of a suitable carrier transport layer (metal/TCO) over the present cell structure will ensure better electrical conduction and may enhance the device's parameters appreciably.

Acknowledgements

The authors would like to thank the Ministry of New and Renewable Energy (MNRE) for funding the project and MVS for the fellowship.

References

[1] Rogers K D, Lane D W, Painter J D and Chapman A 2004 Structural characterisation of sprayed TiO_2 films for extremely thin absorber layer solar cells *Thin Solid Films* **446** 97–102

[2] Deshmukh H P, Shinde P S and Patil P S 2006 Structural, optical and electrical characterization of spray-deposited TiO_2 thin films *Mater. Sci. Eng.* B **130** 220–7

[3] Bange K, Otterman C R, Anderson O, Jeschkowski U, Laube M and Feile R 1991 Investigations of TiO_2 films deposited by different techniques *Thin Solid Films* **197** 279–85

[4] Krunks M, Katerski A, Dedova T, Oja A I and Mere A 2008 Nanostructured solar cell based on spray pyrolysis deposited ZnO nanorod array *Sol. Energy Mater. Sol.* C **92** 1016–9

[5] Peill N J and Hoffmann M R 1995 Development and optimization of a TiO_2-coated fiber-optic cable reactor: photocatalytic degradation of 4-chlorophenol *Environ. Sci. Technol.* **29** 2974–81

[6] Tang H, Prasad K, Sanjines R and Levy F 1995 TiO_2 anatase thin films as gas sensors *Sensors Actuators* B **26** 71–5

[7] Kim J, Shan W, Davies S H R, Baumann M J, Masten S J and Tarabara V V 2009 Interactions of aqueous NOM with nanoscale TiO_2: implications for ceramic membrane filtration-ozonation hybrid process *Environ. Sci. Technol.* **43** 5488–94

[8] Zhang Z, Dan-Feng L and Zhi-Mei Q 2012 Application of porous TiO_2 thin films as wavelength-interrogated waveguide resonance sensors for bio/chemical detection *J. Phys. Chem.* C **116** 3342–8

[9] Parka H, Park Y, Kim W and Choi W 2013 Surface modification of TiO_2 photocatalyst for environmental applications *J. Photochem. Photobiol.* C **15** 1–20

[10] Kikuchi H, Kitano M, Takeuchi M, Matsuoka M, Anpo M and Kamat P V 2006 Extending the photoresponse of TiO_2 to the visible light region: photoelectrochemical behavior of TiO_2 thin films prepared by the radio frequency magnetron sputtering deposition method *J. Phys. Chem.* B **110** 5537–41

[11] Rao K N, Murthy M A and Mohan S 1989 Optical properties of electron-beam-evaporated TiO_2 films *Thin Solid Film* **176** 181–6

[12] Barros A D, Albertin K F, Miyoshi J, Doi I and Diniz J A 2010 Thin titanium oxide films deposited by e-beam evaporation with additional rapid thermal oxidation and annealing for ISFET applications *Microelectron. Eng.* **87** 443–6

[13] Zhang Q and Griffin G L 1995 Gas-phase kinetics for TiO_2 CVD: hot-wall reactor results *Thin Solid Films* **263** 65–71

[14] Boschloo G K, Goosens A and Schoonman J 1997 Photoelectrochemical study of thin anatase TiO_2 films prepared by metallorganic chemical vapor deposition *J. Electrochem. Soc.* **144** 1311–7

[15] Wen T, Gao J and Shen J 2001 Preparation and characterization of TiO_2 thin films by the sol-gel process *J. Mater. Sci.* **36** 5923–6

[16] Xu W W, Kershaw R, Dwight K and Wold A 1990 Preparation and characterization of TiO_2 films by a novel spray pyrolysis method *Mater. Res. Bull.* **25** 1385–92

[17] Kim S J and Mckean D E 1998 Aqueous TiO_2 suspension preparation and novel application of ink-jet printing technique for ceramics patterning *J. Mater. Sci. Lett.* **17** 141–4

[18] Natarajan C, Fukunaga N and Nogami G 1998 Titanium dioxide thin film deposited by spray pyrolysis of aqueous solution *Thin Solid Films* **322** 6–8

[19] Aoki A and Nogami G 1996 Fabrication of anatase thin films from peroxo-polytitanic acid by spray pyrolysis *J. Electrochem. Soc.* **143** L191–3

[20] Zhao C, Krall A, Zhao H, Zhang Q and Li Y 2012 Ultrasonic spray pyrolysis synthesis of Ag/TiO_2 nanocomposite photocatalysts for simultaneous H_2 production and CO_2 reduction *Int. J. Hydrog. Energy* **37** 9967–76

[21] Hurum D C, Agrios A G and Gray K A 2003 Explaining the enhanced photocatalytic activity of Degussa P25 mixed-Phase TiO_2 using EPR *J. Phys. Chem.* B **107** 4545–9

[22] Nanu M, Schoonman J and Goossens A 2005 Solar-energy conversion in $TiO_2/CuInS_2$ nanocomposites *Adv. Funct. Mater.* **15** 95–100

[23] Ernst K, Belaidi A and Konenkamp K 2003 Solar cell with extremely thin absorber on highly structured substrate *Semicond. Sci. Technol.* **18** 475–9

[24] Goossens A and Hofhuis J 2009 Spray-deposited $CuInS_2$ solar cells *Nanotechnology* **19** 424018

[25] Sebastian T, Jayakrishnan R, Kartha C S and Vijayakumar K P 2009 Characterization of spray pyrolysed $CuInS_2$ thin films *Open Surf. Sci. J.* **1** 1–6

[26] Santhosh M V, Kartha C S and Vijayakumar K P 2011 Improvement of device parameters of $CuInS_2/In_2S_3$ junction deposition using automated spray machine *AIP Conf. Proc.* **1349** 673–4

[27] John T T, Kartha C S, Vijayakumar K P, Abe T and Kashiwaba Y 2006 *Appl. Phys.* A **82** 703–7

[28] Tang H, Prasad K, Sanjines R, Schmid P E and Levy F 1994 Electrical and optical properties of TiO_2 anatase thin films *J. Appl. Phys.* **75** 2042–7

[29] Bhuvanesh N S P and Gopalakrishnan J 1997 Solid-state chemistry of early transition-metal oxides containing d^0 and d^1 cations *J. Mater. Chem.* **7** 2297–306

[30] Mote V D, Purushotham Y and Dole B N 2012 Williamson-Hall analysis in estimation of lattice strain in nanometer-sized ZnO particles *J. Theor. Appl. Phys.* **6** 6

[31] Oja I, Mere A, Krunks M, Nisumaa M, Solterbeck C H and Es-Souni M 2006 Structural and electrical characterization of TiO_2 films grown by spray pyrolysis *Thin Solid Films* **515** 674–7

[32] Babelon P, Dequiedt A S, Mostefa-Sba H, Bourgeois S, Sibillot P and Sacilotti M 1998 SEM and XPS studies of titanium dioxide thin films grown by MOCVD *Thin Solid Films* **322** 63–7

[33] Stefanov P, Shipochka M, Stefchev P, Raicheva Z, Lazarova V and Spassov L 2008 XPS characterization of TiO_2 layers deposited on quartz plates *J. Phys.: Conf. Ser.* **100** 012039

[34] Kaiser I, Ernst K, Fischer C-H, Konenkamp R, Rost C, Sieber I and Lux-steiner M C 2001 Theta-solar cell with $CuInS_2$: a photovoltaic cell concept using extremely thin absorber *Sol. Energy Mater. Sol. Cells* **67** 89–96

[35] Moritake N, Fukui Y, Oonuki M, Tanaka K and Uchiki H 2009 Preparation of Cu_2ZnSnS_4 thin film solar cells under non-vacuum condition *Phys. Stat. Sol.* C **6** 1233–6

[36] Priyanka, Lal M and Singh S N 2007 A new method of determination of series and shunt resistances of silicon solar cells *Sol. Energy Mater. Sol. Cells* **91** 137–42

Available online at www.sciencedirect.com
ScienceDirect
Solar Energy 108 (2014) 508–514
SOLAR ENERGY
www.elsevier.com/locate/solener

All sprayed ITO-free $CuInS_2/In_2S_3$ solar cells

M.V. Santhosh [a], D.R. Deepu [a], C. Sudha Kartha [a], K. Rajeev Kumar [b], K.P. Vijayakumar [a,*]

[a] Department of Physics, Cochin University of Science and Technology, Cochin 682022, India
[b] Department of Instrumentation, Cochin University of Science and Technology, Cochin 682022, India

Received 14 April 2014; received in revised form 3 July 2014; accepted 7 July 2014
Available online 24 August 2014

Communicated by: Associate Editor Takhir Razykov

Abstract

$CuInS_2$, In_2S_3 and fluorine doped tin oxide (FTO) thin films were prepared by simple, cost effective Chemical Spray Pyrolysis (CSP) method and effect of [Cu]/[In] ratio on the structural, optical, electrical and morphological properties of $CuInS_2$ thin films were investigated. X-ray diffraction analysis shows that grain size of $CuInS_2$ samples increases with increase in [Cu]/[In] ratio in the spray solution. It could be figured out that Cu_xS binary phases are absent in the films. Optical studies reveals that the band gap of the films decreases on increasing the [Cu]/[In] ratio. Type of conductivity and resistivity of $CuInS_2$ films were estimated from Hall measurement system. On increasing [Cu]/[In] ratio resistivity decreases. Surface morphology of the films deposited at different spray rates were analyzed using Atomic Force Microscopy (AFM) and results shows that there should be an optimum spray rate for device fabrication and was fixed at 4 ml/min. Surface structure and uniformity were confirmed by employing Scanning Electron Microscopy (SEM). Composition and p-type conductivity of $CuInS_2$ samples were analyzed through Energy Dispersive X-ray analysis (EDX). Finally the optimized $CuInS_2$ films were used for device fabrication. The best device in this study has open circuit voltage of 457 mV and short circuit current density of 5.45 mA/cm^2. Efficiency and fill factor were 0.94% and 38% respectively.

Keywords: Chemical Spray Pyrolysis; Solar cells; $CuInS_2$; In_2S_3

1. Introduction

Copper indium sulphide ($CuInS_2$) is one of the I-III-VI_2 compound semiconductors which have theoretically the highest conversion efficiency among the chalcopyrite based solar cells (Parameshwari et al., 2012; Klaer et al., 1998). Direct band gap of 1.55 eV, high absorption coefficient ($\sim 10^5$ cm^{-1}) and non-toxicity of the constituents are the important attributes of $CuInS_2$ films to be used as an absorber layer in thin film solar cells (Qiu et al., 2006). Indium sulphide (In_2S_3) has been observed to be an efficient alternative to toxic CdS buffer layer for $CuInS_2$ based solar cells (Trigo et al., 2008; Kilani et al., 2011). Fluorine doped tin oxide (FTO) films are promising candidate as transparent conducting oxides (TCO) for thin film solar cells due the high transparency and conductivity among easily available TCOs (Elangovan and Ramamurthi, 2005). For the simplicity and versatile implementation of thin film solar cells, the entire layers essential for their fabrication i.e., absorber layer, buffer layer and transparent conducting oxides must be prepared by the same deposition technique. More over the deposition technique should also be cost effective to ensure low economic payback time affordable to common people. In the present work, we fabricated $CuInS_2$ absorber layer, In_2S_3 buffer layer and fluorine doped tin oxide TCO layers essential for the fabrication of FTO/$CuInS_2$/In_2S_3 solar cell by simple, cost effective

* Corresponding author. Tel.: +91 9562019287, +91 9847322577.
E-mail address: kpv@cusat.ac.in (K.P. Vijayakumar).

http://dx.doi.org/10.1016/j.solener.2014.07.001
0038-092X/

Chemical Spray Pyrolysis (CSP) method. Solar cells having efficiencies up to 9.5% has been reported using sprayed $CuInS_2/In_2S_3$ heterojunction (John et al., 2005), but in most cases the back contact materials used was either tin doped indium oxide (ITO) or molybdenum (Mo) prepared by sputtering or vacuum evaporation (Klenk et al., 2005; Braunger et al., 1996). This work used sprayed FTO samples for device fabrication. Prior to the fabrication of the device we optimized sprayed $CuInS_2$ thin films structurally, electrically and morphologically to implement as an absorber layer in FTO/$CuInS_2$/In_2S_3 solar cells. Finally the optimized $CuInS_2$ absorber layer was used for the fabrication of all sprayed solar cells.

2. Experimental details

FTO thin films (sheet resistance of 25 Ω per square) were deposited on ultrasonically cleaned soda lime glass substrates kept at 425 °C by automated Chemical Spray Pyrolysis machine. The precursor solution used was stannic chloride ($SnCl_4$). Ammonium fluoride (NH_4F) was added in the spray solution for doping with fluorine (Elangovan and Ramamurthi, 2005; Shewale et al., 2010). $CuInS_2$ thin films were deposited on FTO coated glass substrate also by CSP machine (John et al., 2005). Aqueous solutions of $CuCl_2$, $InCl_3$ and thiourea were used as the precursors for Cu, In and S (Cherian et al., 2012). It was observed that the deposition rates of $CuInS_2$ over FTO films are very low. Therefore it will take a long time to deposit the necessary thickness of $CuInS_2$ absorber layer over FTO films. For a particular volume, thickness of spray deposited $CuInS_2$ layer can be increased by increasing the [Cu]/[In] ratio in the precursor solution (Hussain et al., 2012). For that [Cu]/[In] ratio in the precursor solution was varied as 0.8, 1, 1.2 and 1.4. Above [Cu]/[In] ratio 1.4 the solution gets precipitated. [S]/[In] ratios in all these films were maintained as 5. Deposition temperature and spray volume for $CuInS_2$ thin films were fixed at 350 °C and 80 ml (Sebastian et al., 2009). Spray rate was optimized at 4 ml/min as explained in Section 3.5. Trials shows that as [Cu]/[In] ratio increases, the deposition rate over the FTO layer increases. In order to characterize these films structurally, optically and electrically, ultrasonically cleaned soda lime glass plates were also placed along with FTO in each spray and the deposited films were named as Cu-0.8, Cu-1, Cu-1.2 and Cu-1.4. Finally In_2S_3 buffer layer was deposited by spraying 35 ml of aqueous solution containing indium and sulfur precursors in the ratio 1.2:12 (Santhosh et al., 2011; Mathew et al., 2010). For electrical contact at the top, silver electrode (thickness ~50 nm) was vacuum evaporated at a pressure of 2×10^{-5} mBar.

$CuInS_2$, In_2S_3 and FTO samples were structurally characterized using Rigaku (D. Max. C) X-ray diffractometer employing Cu Kα line and Ni filter operated at 30 kV and 20 mA. Thicknesses of the films were measured using the Stylus profilometer (Dektak-6 M). Optical absorbance of the samples at normal incidence was studied employing UV–VIS–NIR spectrophotometer (JASCO V-570 model). Using Van der pauw four probe technique, Hall effect measurement system (HMS 5300, Ecopia) was employed to characterize the electrical transport properties of the $CuInS_2$ thin films at room temperature. 'Nanosurf easyScan 2' AFM System was used for the morphological analysis of the films. Surface features of $CuInS_2$ thin films were explored using Scanning Electron Microscopy (SEM) (JEOL, JSM-840, operated at 20 kV). Composition analysis of the deposited films was done using Energy Dispersive X-ray (EDAX) analysis which is attached with SEM. Photovoltaic response of the heterojunction was studied using class AAA solar simulator (PET, model SS50AAA).

3. Results and discussion

3.1. Structural characterization

XRD profiles of each layer of the fabricated device are shown in Fig. 1.

From Fig. 1(a) it is clear that FTO films were crystalline in nature with preferential orientation along (200) plane. XRD analysis of samples Cu-0.8, Cu-1, Cu-1.2, Cu-1.4 prove the tetragonal structure of $CuInS_2$ (JCPDS data card 270159) with preferential orientation along (112) plane (Fig. 1(b)). One of the main challenges regarding $CuInS_2$ based solar cells is the formation of binary phases such as Cu_xS, which affects the performance of the device. From XRD analysis, the films deposited during CSP do not show any peak corresponding to binary phases even though [Cu]/[In] ratio was varied from 0.8 to 1.4 (John et al., 2005). Hence KCN etching (which is a difficult process due to toxicity of KCN) and optimized 3-stage growth process usually employed to remove these secondary phases can be avoided (Ogawa et al., 1996; Calderon et al., 2010). Grain sizes of the deposited films were calculated using Scherer's formula. As [Cu]/[In] ratio increases grain size also improves and for [Cu]/[In] ratio 1.4 the films possess a grain size of 32 nm. Thickness and grain size for samples Cu-0.8, Cu-1, Cu-1.2 and Cu-1.4 are tabulated in Table 1. It is very important to mention that this increase in grain size is appreciable for a good quality absorber layer as it improves electrical transport properties in thin film solar cells (Bergmann, 1999). Variation of grain size with [Cu]/[In] ratio is shown in Fig. 2. In_2S_3 film showed (Fig. 1(c)) preferential orientation of (220) plane which is the characteristics of β-In_2S_3 thin films.

3.2. Optical properties

Optical absorption spectra of the $CuInS_2$ samples with different [Cu]/[In] ratios are depicted in Fig. 3(a). Absorption coefficient (α) is related to the energy gap (E_g) according to the equation

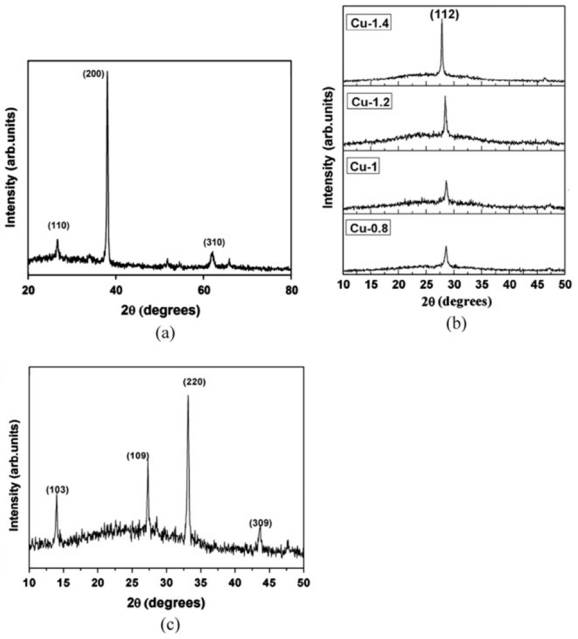

Fig. 1. XRD analysis of (a) FTO (b) $CuInS_2$ samples deposited by varying [Cu]/[In] ratio as 0.8, 1, 1.2, 1.4 and (c) In_2S_3 samples.

Table 1
Thickness and grain size for $CuInS_2$ samples with different [Cu]/[In] ratio.

[Cu]/[In] ratio	Thickness (nm)	Grain size (nm)
0.8	415	19
1	450	22
1.2	495	24
1.4	525	32

$$\alpha h\nu = A(h\nu - E_g)^n$$

where A is a constant, h the plank's constant, ν the frequency of incident beam and n is equal to ½ for direct allowed band gap. E_g can be obtained from the graph of $(\alpha h\nu)^2$ versus $h\nu$ which is illustrated in Fig. 3(b). It is observed that the band gap decreases from 1.45 to 1.35 eV as [Cu]/[In] ratio in the film increases from 0.8 to 1.4. Defects in $CuInS_2$ films are responsible for carrier degeneracy and may produce gap-states near the band edge (Zhang et al., 1997). This may be a possible reason for the decrease in band gap.

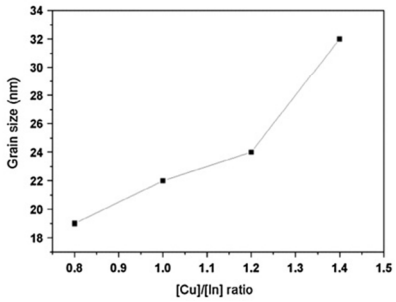

Fig. 2. Grain size of the deposited films Vs [Cu]/[In] ratio in the precursor solution.

3.3. Electrical characterization

Electrical characterization of the films (performed using Hall Effect measurement at room temperature) are tabulated in Table 2.

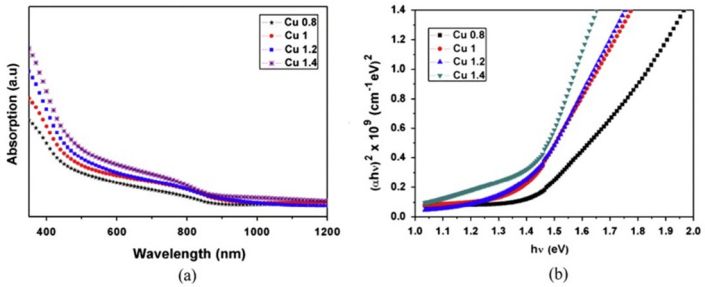

Fig. 3. (a) UV visible absorption spectra and (b) $(\alpha h\nu)^2$ versus hν graph of films prepared with different [Cu]/[In] ratio in precursor solution.

Samples Cu-0.8 are having excess indium and possess poor crystallinity compared to other samples; as a result the resistivity is high (Shi et al., 2006). As [Cu]/[In] ratio increases, the resistivity decreases. This result correlates with the increase in grain size of the deposited films. Bulk concentration of carriers enhanced by four orders when [Cu]/[In] ratio was varied from 0.8 to 1.4. Thus films deposited at [Cu]/[In] ratio 1.4 was superior to others in terms of structural and electrical properties. Hence we chose $CuInS_2$ films having [Cu]/[In] ratio 1.4 as the absorber layer for the device fabrication.

3.4. Compositional analysis

Using EDAX measurements attached with SEM the non-stoichiometry parameter $(\Delta y = [2S/(Cu + 3In)] - 1)$ was evaluated for films Cu-0.8, Cu-1, Cu-1.2, and Cu-1.4 (Table 3). For all films $\Delta y > 0$, indicates p-type conductivity of the films (Xu et al., 2011). The Δy values calculated from EDAX analysis and results from Hall measurements are in good agreement. As [Cu]/[In] ratio increases probability of existence of defect states such as copper in indium sites (Cu_{In}) and indium vacancies (V_{In}) increases (Goossens and Hofhuis, 2008). Probability of existence of indium vacancy is very low since Cu_xS binary phase is absent in the film. Hence copper in indium sites (Cu_{In}) defect states act as shallow acceptor levels. As a result, the samples become more p-type on increasing [Cu]/[In] ratio in the precursor solution. From EDAX analysis the atomic percentage of copper (Cu), indium (In) and sulfur (S), was 24%, 22% and 54% respectively.

Table 2
Electrical characterization of Cu-0.8, Cu-1, Cu-1.2 and Cu-1.4 samples.

[Cu]/[In] ratio	Bulk concentration (cm^{-3})	Resistivity (Ω cm)	Mobility (cm^2/VS)	Conductivity type
0.8	1.29×10^{15}	100.93	48	p-type
1	5.92×10^{16}	10.55	10	p-type
1.2	4.56×10^{17}	9.86	1.39	p-type
1.4	3.45×10^{19}	0.27	0.066	p-type

Table 3
Non-stoichiometry parameters and conductivity type from EDAX measurement for $CuInS_2$ films with different [Cu]/[In] ratios.

Sample name	Δy	Conductivity type
Cu-0.8	0.04	p
Cu-1	0.06	p
Cu-1.2	0.13	p
Cu-1.4	0.20	P

SEM analysis of the $CuInS_2$ films prepared on glass plates using optimized spaying conditions (i.e. [Cu]/[In] ratio 1.4 and spray rate 4 ml/min) are shown in Fig. 4. Films were free from pinhole and crack. Moreover growths of the films were observed to be uniform, densely packed and well covered to the glass substrate.

3.5. Morphological characterization

For device fabrication, $CuInS_2$ films having very low surface roughness is preferred. Otherwise the deposition of In_2S_3 buffer layer over the highly rough surface of

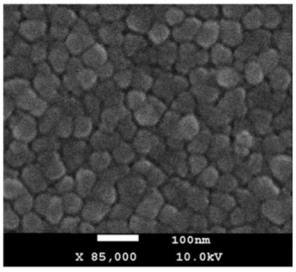

Fig. 4. SEM analysis of optimized $CuInS_2$ samples (Cu-1.4).

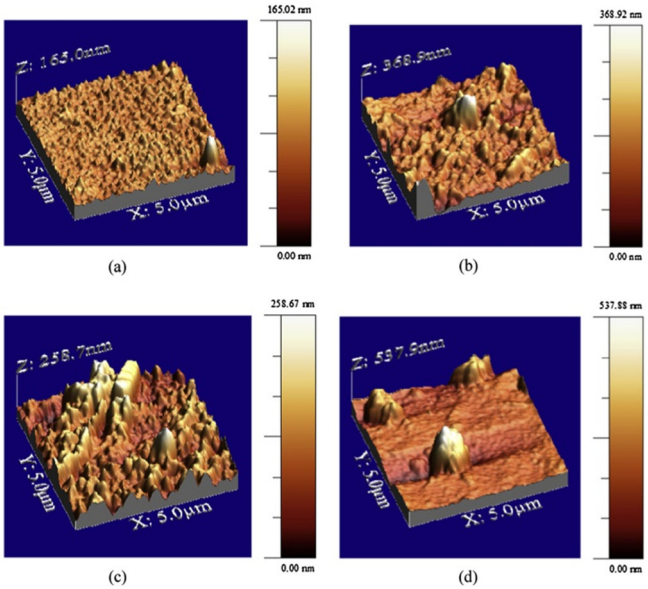

Fig. 5. AFM analysis of $CuInS_2$ samples at different spay rates (a) 2 ml/min, (b) 4 ml/min, (c) 6 ml/min, and (d) 8 ml/min.

$CuInS_2$ films increases the probability of 'shorting' the device. In CSP technique, spray rate is an important parameter that manipulates this surface roughness. In order to optimize the spray rate, $CuInS_2$ films having [Cu]/[In] ratio 1.4 were deposited with spray rates 2, 4, 6 and 8 ml/min over FTO films. AFM analysis of these films are shown in Fig. 5. It was observed that for very low spray rate i.e. at 2 ml/min, temperature deviation of the heater surface is very small since the quantity of solution hitting the heater surface per minute is small. Hence the comparatively high surface temperature increases the probability of re-evaporation and hence films have low thickness. The deposited films have smoother surface (surface roughness 11 nm); however resistivity is high due to low thickness. Films having required thickness can be deposited at 2 ml/min but it will take long time to complete the spray. As a result we have to go for higher spray rate. But at higher spray rates (i.e., at 8 ml/min) temperature deviation of the heater surface is high and the films have comparatively high thickness. The films have low resistivity but possess higher surface roughness (61 nm). Hence for device fabrication, films prepared at intermediate spray rate are preferred. Films sprayed at 4 ml/min have an intermediate surface roughness of 40 nm and resistivity of $4.5 \times 10^{-1}\ \Omega$ cm. Hence films having [Cu]/[In] ratio 1.4 and sprayed at 4 ml/min were used for device fabrication.

3.6. FTO/$CuInS_2$/In_2S_3 solar cell fabrication

Using the optimized $CuInS_2$ (Cu-1.4) thin films, FTO/$CuInS_2$/In_2S_3/Ag solar cells were fabricated. Area of silver electrode deposited using vacuum evaporation is 0.03 cm^2. Silver was observed to be a suitable top electrode for $CuInS_2$/In_2S_3 hetero junction as it improves the crystallinity of In_2S_3 thin films (John et al., 2005). The cell structure is as shown in Fig. 6. In thin film solar cells the overall

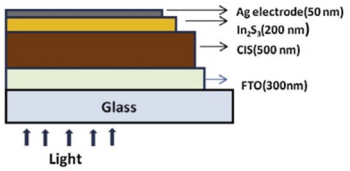

Fig. 6. Structure of the fabricated device.

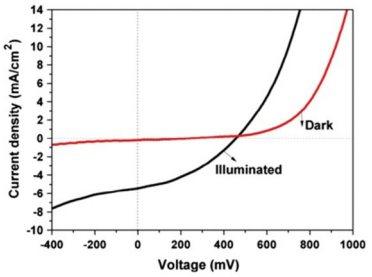

Fig. 7. J–V characteristics of FTO/$CuInS_2$/In_2S_3 solar cells.

device performance has an inevitable dependence on the thickness of individual layers. Using automated CSP machine, thickness of individual layers can be easily varied. Optimized thickness of SnO_2:F transparent conducting oxide, $CuInS_2$ absorber layer and In_2S_3 buffer layer in this study were 300, 500 and 200 nm respectively.

Fig. 7 shows the photovoltaic response of the device under an illumination of 100 mW/cm^2. The optimized device has open circuit voltage (V_{oc}) of 457 mV, short circuit current density (J_{sc}) of 5.45 mA/cm^2. Efficiency and fill factor were 0.94% and 38% respectively. Parasitic resistances [series (R_s) and shunt (R_{sh})] of the devices were calculated from the slope of the illuminated J–V characteristics at $V = 0$ (for R_s) and $J = 0$ (for R_{sh}) (Moritake et al., 2009) as 40 Ω cm^2 and 250 Ω cm^2 respectively.

4. Conclusions

Versatile and cost effective Chemical Spray Pyrolysis technique was successfully employed for the fabrication of all sprayed FTO/$CuInS_2$/In_2S_3/Ag solar cells. Structural and electrical properties of $CuInS_2$ absorber layer was optimized for a good quality absorber layer by adjusting the [Cu]/[In] ratio in the precursor solution. Moreover it was observed that even though we varied [Cu]/[In] ratio from 0.8 to 1.4, Cu_xS binary phases were absent and hence we could avoid usual KCN etching. Due to the existence of shallow acceptor levels (Cu_{In} defect states), $CuInS_2$ samples become more p-type on increasing [Cu]/[In] ratio in the precursor solution. This is confirmed by both Hall effect measurements and EDAX analysis. The device fabricated in this work shows an efficiency of 0.94% which is the best value reported so far for all sprayed FTO/$CuInS_2$/In_2S_3/Ag solar cells without the application of a TCO layer and anti-reflection coating. Even though the efficiency at the initial stage is rather low, the "all sprayed" solar cells fulfill the demands like low toxicity, easy adaptability for large scale production and cost effectiveness prevailing in photovoltaic industry.

Acknowledgements

Authors would like to thank Ministry of New and Renewable Energy (MNRE) for funding the project and one of the authors (M.V.S.) is grateful to MNRE for the fellowship.

References

Bergmann, R.B., 1999. Crystalline Si thin-film solar cells: a review. Appl. Phys. A 69, 187–194.
Braunger, D., Hariskos, D., Walter, T., Schock, H.W., 1996. An 11.4% efficient polycrystalline thin film solar cell based on $CuInS_2$ with a Cd-free buffer layer. Solid Energy Mater. Solid Cell. 40, 97–102.
Calderon, C., Bartolo-Perez, P., Clavijo, J., Oyola, J.S., Gordillo, G., 2010. Morphological characterization and AES depth profile analysis of $CuInS_2$ thin films. Solid Energy Mater. Solid Cell. 94, 17–21.
Cherian, A.S., Jinesh, K.B., Kashiwaba, Y., Abe, T., Balamurugan, A.K., Dash, S., Tyagi, A.K., Kartha, C.S., Vijayakumar, K.P., 2012. Double layer $CuInS_2$ absorber using spray pyrolysis: a better candidate for $CuInS_2$/In_2S_3 thin film solar cells. Sol. Energy 86, 1872–1879.
Elangovan, E., Ramamurthi, K., 2005. Studies on micro-structural and electrical properties of spray-deposited fluorine-doped tin oxide thin films from low-cost precursor. Thin Solid Films 476, 231–236.
Goossens, Albert, Hofhuis, Joris, 2008. Spray-deposited $CuInS_2$ solar cells. Nanotechnology 19, 424018.
Hussain, K.M.A., Podder, J., Saha, D.K., Ichimura, M., 2012. Structural, electrical and optical characterization of $CuInS_2$ thin films deposited by spray pyrolysis. Indian J. Pure Appl. Phys. 50, 117–122.
John, Teny Theresa, Mathew, Meril, Sudha Kartha, C., Vijayakumar, K.P., Abe, T., Kashiwaba, Y., 2005. $CuInS_2$/In_2S_3 thin film solar cell using spray pyrolysis technique having 9.5% efficiency. Solid Energy Mater. Solid Cell. 89, 27–36.
Kilani, M., Yahmadi, B., Kamoun Turki, N., Castagne, M., 2011. Effect of Al doping and deposition runs on structural and optical properties of In_2S_3 thin films grown by CBD. J. Mater. Sci. 46, 6293–6300.
Klaer, J., Bruns, J., Henninger, R., Siemer, K., Klenl, R.R., Ellmer, R.R., Braunig, D., 1998. Efficient $CuInS_2$ thin-film solar cells prepared by a sequential process. Semicond. Sci. Technol. 13, 1456–1458.
Klenk, R., Klaer, J., Scheer, R., Lux-Steiner, M.Ch., Luck, I., Meyer, N., Ruhle, U., 2005. Solar cells based on $CuInS_2$ – an overview. Thin Solid Films 480–481, 509–514.
Mathew, M., Gopinatha, M., Kartha, C.S., Vijayakumar, K.P., Kashiwaba, Y., Abe, T., 2010. Tin doping in spray pyrolysed indium sulfide thin films for solar cell applications. Sol. Energy 84, 888–897.
Moritake, Noriko, Fukui, Yuki, Oonuki, Masatoshi, Uchiki, Hisao, Tanaka, Kunihiko, 2009. Preparation of Cu_2ZnSnS_4 thin film solar cells under non-vacuum condition. Phys. State Solid C 6, 1233.
Ogawa, Y., Jager-Waldau, A., Hua, T.H., Hashimoto, Y., Ito, K., 1996. Influence of KCN treatment on $CuInS_2$ thin films. Appl. Surf. Sci. 92, 232–236.
Parameshwari, P.M., Bhat, Shashidhar, Gopalakrishna Naik, K., 2012. Structural, electrical and optical studies on spray deposited cadmium sulphide and copper indium disulphide thin film. Arch. Phys. Res. 3 (6), 441–451.
Qiu, Jijun, Jin, Zhengguo, WeiBing, Wu, Xiao, Liu-Xin, 2006. Characterization of $CuInS_2$ thin films prepared by ion layer gas reaction method. Thin Solid Films 510, 1–5.
Santhosh, M.V., Sudha Kartha, C., Vijayakumar, K.P., 2011. Improvement of device parameters of $CuInS_2$/In_2S_3 junction deposition using automated spray machine. AIP Conf. Proc. 1349, 673–674.
Sebastian, T., Gopinatha, M., Kartha, C.S., Vijayakumar, K.P., Abe, T., Kashiwaba, Y., 2009. Role of substrate temperature in controlling properties of sprayed $CuInS_2$ absorbers. Sol. Energy 83, 1683–1688.
Shewale, P.S., Patil, S.I., Uplane, M.D., 2010. Preparation of fluorine-doped tin oxide films at low substrate temperature by an advanced

spray pyrolysis technique and their characterization. Semicond. Sci. Technol. 25, 115008–115013.
Shi, Yong, Jin, Zhengguo, Li, Chunyan, An, Hesong, Qiu, Jijun, 2006. Effect of [Cu]/[In] ratio on properties of $CuInS_2$ thin films prepared by successive ionic layer absorption and reaction method. Appl. Surf. Sci. 252, 3737–3743.
Trigo, J.F., Asenjo, B., Herrero, J., Gutierrez, M.T., 2008. Optical characterization of In_2S_3 solar cell buffer layers grown by chemical bath and physical vapor deposition. Solid Energy Mater. Solid Cell. 92, 1145–1148.
Xu, X.H., Wang, F., Liu, J.J., Park, K.C., Fujishige, M., 2011. A novel one-step electrodeposition to prepare single-phase $CuInS_2$ thin films for solar cells. Solid Energy Mater. Solid Cell. 95, 791–796.
Zhang, S.B., Wei, Su-Huai, Zunger, Alex, 1997. Stabilization of ternary compounds via ordered arrays of defect pairs. Phys. Rev. Lett. 78, 4059–4062.